

INFORMATION TO USERS

This manuscript has been reproduced from the microfilm master. UMI films the text directly from the original or copy submitted. Thus, some thesis and dissertation copies are in typewriter face, while others may be from any type of computer printer.

The quality of this reproduction is dependent upon the quality of the copy submitted. Broken or indistinct print, colored or poor quality illustrations and photographs, print bleedthrough, substandard margins, and improper alignment can adversely affect reproduction.

In the unlikely event that the author did not send UMI a complete manuscript and there are missing pages, these will be noted. Also, if unauthorized copyright material had to be removed, a note will indicate the deletion.

Oversize materials (e.g., maps, drawings, charts) are reproduced by sectioning the original, beginning at the upper left-hand corner and continuing from left to right in equal sections with small overlaps.

Photographs included in the original manuscript have been reproduced xerographically in this copy. Higher quality 6" x 9" black and white photographic prints are available for any photographs or illustrations appearing in this copy for an additional charge. Contact UMI directly to order.

ProQuest Information and Learning
300 North Zeeb Road, Ann Arbor, MI 48106-1346 USA
800-521-0600

UMI[®]

A SEQUENTIAL INVERSE APPROACH FOR HYDRAULIC TOMOGRAPHY AND
ELECTRICAL RESISTIVITY TOMOGRAPHY: AN EFFECTIVE METHOD FOR
SITE CHARACTERIZATION

by

Shuyun Liu

A Dissertation Submitted to the Faculty of the
DEPARTMENT OF HYDROLOGY AND WATER RESOURCES

In Partial Fulfillment of the Requirements
For the Degree of

DOCTOR OF PHILOSOPHY
WITH A MAJOR IN HYDROLOGY

In the Graduate College

THE UNIVERSITY OF ARIZONA

2001

UMI Number: 3031351



UMI Microform 3031351

Copyright 2002 by Bell & Howell Information and Learning Company.

All rights reserved. This microform edition is protected against
unauthorized copying under Title 17, United States Code.

Bell & Howell Information and Learning Company
300 North Zeeb Road
P.O. Box 1346
Ann Arbor, MI 48106-1346

THE UNIVERSITY OF ARIZONA ©
GRADUATE COLLEGE

As members of the Final Examination Committee, we certify that we have read the dissertation prepared by Shuyun Liu entitled A Sequential Inverse Approach for Hydraulic Tomography and Electrical Resistivity Tomography: An Effective Method for Site Characterization

and recommend that it be accepted as fulfilling the dissertation requirement for the Degree of Doctor of Philosophy

T.-C. Jim Yeh

Tian-Cheng Yeh

8 May 01
Date

A. W. Warrick

A. W. Warrick

8 May 01
Date

Donald Myers

Donald Myers

8 May 01
Date

Peter J. Wierenga

Peter J. Wierenga

May 8, 01
Date

Mark L. Brusseau

Mark L. Brusseau

8 May 01
Date

Final approval and acceptance of this dissertation is contingent upon the candidate's submission of the final copy of the dissertation to the Graduate College.

I hereby certify that I have read this dissertation prepared under my direction and recommend that it be accepted as fulfilling the dissertation requirement.

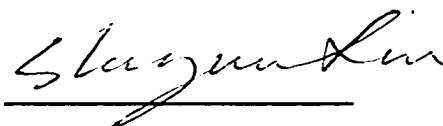
Tian-Cheng Yeh
Dissertation Director T.-C. Jim Yeh

8/16/01
Date

STATEMENT BY AUTHOR

This dissertation has been submitted in partial fulfillment of requirements for an advanced degree at The University of Arizona and is deposited in the University Library to be made available to borrowers under rules of the Library.

Brief quotations from this dissertation are allowable without special permission, provided that accurate acknowledgement of source is made. Requests for permission for extended quotation from or reproduction of this manuscript in whole or in part may be granted by the head of the major department or the Dean of the Graduate College when in his or her judgement the proposed use of the material is in the interests of scholarship. In all other instances, however, permission must be obtained from the author.

SIGNED: 

ACKNOWLEDGEMENTS

I would like to show my deep appreciation to my dissertation advisor, Dr. T. – C. Jim Yeh, for his continuous financial support, excellent academic guidance, and encouragement. When I came to the Department of Hydrology and Water Resources in 1996, I didn't have any financial aid. After one semester's struggling, I started to have doubt to continue my doctoral program considering my critical financial status. Right at this critical time, Dr. Yeh talked to me and accepted me as his doctoral students. Since then, I have learned a lot from him including inverse modeling and stochastic analysis. In addition, I have learned from him the ways to be a good scientist: be aggressive, be creative and be opinionated.

I would like to thank my other committee members: Dr. A. W. Warrick, Dr. Donald Myers, Dr. Mark Brusseau and Dr. Peter Wierenga for their valuable time and good comments on this dissertation. I would also like to thank all my course-work instructors, from whom I have learned a lot of background knowledge essential to my research.

I am grateful to the John Harshbarger's family for their generous donation and to the faculty of the Dept. of Hydrology & Water Resources for granting me the 2000-2001 John and Margaret Harshbarger Doctoral Fellowship. The award of this fellowship has been very timely, as I was at a crucial stage in my research and welcome this financial support. I am grateful to Terrie Thompson, the academic advisor of our department, for her help and excellent advisory during my doctoral program.

I would like to thank my officemates at room 250: Bailing Li, Debra Hughson, Zhiming Lu, Hsin-chia Chao, Vargas Guzman, Chuanjun Li and Dale Rucker. I have had numerous discussions with them, which made my study more enjoyable. I also want to thank Yunjung Hyun, Feyzan Misirli, Sofie Pasilis and Fan Li, we went to so many classes together and had so much fun.

I would like to thank my brother for his love and great encouragement, without his inspiration I would never come to the States to pursue this doctoral degree. I am grateful to my parents for their love and confidence on me. I saved the most important acknowledgement for last. I want to thank my husband for his love and understanding. To support me to pursue this doctoral degree, he gave up everything he has successfully achieved in China and came here to be with me and started everything from the beginning. Only with his love and encouragement, my student life could be so smooth and this dissertation could come out in time.

DEDICATION

To my brother: Xuehou Liu

TABLE OF CONTENTS

ABSTRACT	7
CHAPTER 1 INTRODUCTION	9
Research Problem	9
Literature Review	10
Characterization of Aquifer Heterogeneity: Hydraulic Tomography	10
Monitoring Water Movement In Vadose Zone: Electrical Resistivity Tomography	15
Explanation of Dissertation Format	20
CHAPTER 2 PRESENT STUDY	21
Summary	21
Concluding Remarks of the Dissertation	27
REFERENCES	30
APPENDIX A: HYDRAULIC TOMOGRAPHY: DEVELOPMENT OF A NEW AQUIFER TEST METHOD	33
APPENDIX B: EFFECTIVENESS OF HYDRAULIC TOMOGRAPHY: SANDBOX EXPERIMENTS	73
APPENDIX C: UNCERTAINTIES IN INTERPRETATION OF ELECTRICAL RESISTIVITY SURVEY IN SUBSURFACE HYDROLOGICAL APPLICATIONS...	105
APPENDIX D: A HYDRO-GEOPHYSICAL INVERSE APPROACH FOR ELECTRICAL RESISTIVITY TOMOGRAPHY: AN EFFECTIVE TOOL FOR MONITORING WATER MOVEMENT IN VADOSE ZONE	144

ABSTRACT

Hydraulic tomography (i.e., a sequential aquifer test) has recently been proposed as a method for characterizing aquifer heterogeneity. In this study a sequential inverse approach is developed to interpret results of hydraulic tomography. The approach uses an iterative geostatistical inverse method to yield the effective hydraulic conductivity of an aquifer, conditioned on each set of head/discharge data. To efficiently include all the head/discharge data sets, a sequential conditioning method is employed.

Two-dimensional numerical experiments were conducted to investigate the optimal sampling scheme for the hydraulic tomography. The effects of measurement errors and uncertainties in statistical parameters required by the inverse model were also investigated. The robustness of this inverse approach was demonstrated through its application to a hypothetical, three-dimensional, heterogeneous aquifer.

Two sandbox experiments were conducted to evaluate the performance of the sequential geostatistical inverse approach under realistic conditions. One sandbox was packed with layered sands to represent a stratified aquifer while the other with discontinuous sand bodies of different shapes and sizes to represent a more complex and realistic heterogeneous aquifer. The tomography was found ineffective if abundant head measurements were collected at closely spaced intervals in a highly stratified aquifer. While it was found beneficial when head measurements were limited and the geological structure was discontinuous.

The sequential inverse approach for hydraulic tomography was extended for electrical resistivity tomography. Numerical experiments were conducted to demonstrate

the robustness of this approach for delineating the resistivity distribution in the subsurface and to investigate effectiveness of different sampling arrays of the ERT: the surface, the down-hole, and the combination of the surface and down-hole array. Orientation of bedding was found to dictate the effectiveness of the ERT layout.

Samples were collected to quantify spatial variability of the resistivity-moisture relationship in the field. Numerical experiments then illustrated how the spatially varying relationship exacerbated the level of uncertainty in the interpretation of change of moisture content based on the estimated change in resistivity. A sequential inverse approach was then developed to estimate water content with less uncertainty by considering the spatial variability of the resistivity-moisture relationship and incorporating point moisture measurements and ERT data sets.

CHAPTER 1 INTRODUCTION

Research Problem

Hydrological properties of the subsurface exhibit strong spatial variability at various scales due to the heterogeneous nature of geological formations. Detailed and accurate knowledge of these heterogeneous properties plays a key role in predicting groundwater flow and contaminant movement in the subsurface. Consequently, increasing concern over soil and groundwater contamination stimulates research on quantitative characterization of aquifers and vadose zones.

Direct measurement of hydraulic properties of small-scale samples at a large number of locations is time-consuming, labor-intensive and hence costly. To circumvent these difficulties and to efficiently gain information of the spatial distribution of hydraulic conductivity, the geophysical tomography concept has been employed, and resulted in hydraulic tomography, a sequential aquifer test method. Hydraulic tomography can yield many useful sets of aquifer response data that can be used to identify the heterogeneity, however, a reliable and efficient inverse methodology is needed to interpret these data sets. Classical inverse methodologies such as the minimum-output-error based approaches are known to have many numerical difficulties, they also confront an insurmountable computational burden when they are used to delineate three-dimensional aquifer heterogeneity. On the other hand, the linear assumption embedded in cokriging limits its application in aquifer characterization when the degree of aquifer heterogeneity is large. Better inverse approaches are needed to

interpret the abundant data sets from hydraulic tomography in order to reveal the aquifer heterogeneity at greater details.

Similarly, electrical resistivity tomography (ERT) has been used to image the electrical properties of the vadose zone and the resistivity change is then used to reflect water content change in the vadose zone by assuming some constant empirical relationship between resistivity and moisture content. However, field data indicates that the resistivity-moisture relationship exhibits strong spatial variability. Neglecting the spatial variability results in misleading interpretation of water movement based on the resistivity change. In addition, unsaturated hydraulic conductivity is a function of water content instead of water content change. Thus effective characterization of the vadose zone requires a novel inverse methodology that can directly estimate water content with less uncertainty and less numerical difficulty by conditioning on available moisture measurements and ERT data sets and accounting for the spatial variability of the resistivity-moisture relationship.

Literature Review

Characterization of Aquifer Heterogeneity: Hydraulic Tomography

Aquifer systems are essentially heterogeneous and this heterogeneity plays an extremely important role in flow and contaminant movement in the aquifer system. As a consequence, accurate predictions of water and solute distributions and movement in geological formations require detailed knowledge of the spatial distribution of the hydraulic properties of the formations (Yeh, 1992 and 1998). Conventional aquifer tests

(also known as pumping tests) assume aquifer homogeneity and yield effective hydraulic conductivity and the storage coefficient for an equivalent homogeneous aquifer. These hydraulic parameters are average properties of the aquifer over a large volume (Butler and Liu, 1993) and do not provide information on the spatial distribution of hydraulic conductivity within the volume. On the other hand, measurement of hydraulic conductivity of small-scale samples at a large number of locations is time consuming, costly, and impractical.

To circumvent these difficulties and to efficiently characterize the spatial distribution of hydraulic conductivity, the tomography concept widely used in medical and geophysical imaging during the last two decades has recently been employed (Gottlieb and Dietrich, 1995; Butler et al., 1999). Specifically, fully screened wells are segregated into many vertical intervals using packers. Water is pumped from or injected into an aquifer at one of the intervals to create a steady flow condition. Hydraulic head responses of the aquifer at other intervals are then monitored, yielding a set of head/discharge (or recharge) data. By sequentially pumping (or injecting) water at one interval and monitoring the steady-state head response at others, many head/discharge (or recharge) data sets are obtained. Such a sequential aquifer test is referred to as hydraulic tomography. This new field method has significant advantages over traditional pumping tests. For instance, hydraulic tomography can provide detailed information about vertical and lateral pressure head responses induced by pumping at a given location. Furthermore, by changing the position of the pump in the well, many sets of aquifer responses to pumping at different locations can be obtained. Such a large number of

data sets may minimize the non-uniqueness issue of the inverse problem and may reveal the details of a heterogeneous hydraulic conductivity field.

Several researchers (Scarascia and Ponzini, 1972; Sagar et al., 1975; Giudici et al., 1995; and Snodgrass and Kitanidis, 1998) have investigated the use of data corresponding to different flow situations to improve the uniqueness of the inverse solution or to reduce uncertainties in the identification of flow model parameters. Until recently, very few researchers have investigated the use of hydraulic tomography. For example, Gottlieb and Dietrich (1995) proposed a method of hydraulic tomography for identifying the permeability distribution in a hypothetical, two-dimensional saturated soil. They used two boreholes to create hydraulic dipoles. The positions of source and sink were varied over both boreholes. Pore-water pressure changes along the vertical were monitored in monitoring wells at other locations. They subsequently applied a least-squares based inverse approach to the pressure data to produce an image of the spatial distribution of hydraulic conductivity. Butler et al. (1999) applied this hydraulic tomography concept to networks of multilevel sampling wells. They developed new techniques for measuring drawdown data at a scale that were previously unobtainable. These new techniques greatly facilitate the implementation of hydraulic tomography in the field.

Hydraulic tomography can yield many useful sets of secondary information, namely head responses, which can be used to identify heterogeneity of the aquifer. Still, a reliable and efficient inverse methodology is required to decipher the information so that a reliable image of the hydraulic conductivity field can be obtained. Classical

inverse methodologies are known to have many difficulties (Yeh, 1986). They also confront an insurmountable computational burden when they are used to estimate detailed hydraulic properties in three-dimensional geological formations (Kitanidis, 1997). Consequently, few classical inverse models have been used to identify small-scale heterogeneity in three-dimensional geological media. More importantly, the abundance of hydraulic head information generated by hydraulic tomography presents an even greater challenge for classical inverse methodologies.

In the past few decades, cokriging has been used to estimate hydraulic conductivity fields from scattered measurements of pressure head in saturated flow problems (Kitanidis and Vomvoris, 1983; Hoeksema and Kitanidis, 1984). However, cokriging is a linear estimator and its application is limited to mildly nonlinear systems, such as groundwater flow in geological formations of mild heterogeneity (variance of natural log of conductivity, $\sigma^2_{\ln k}=0.1$). When the degree of aquifer heterogeneity is large ($\sigma^2_{\ln k}>1$) and the linear assumption becomes inadequate, cokriging cannot provide a good estimate of the conditional mean conductivity field (Yeh et al., 1996). In other words, it cannot take full advantage of the head information to obtain an optimal estimate of the hydraulic properties.

To overcome this shortcoming, Yeh et al. (1995 and 1996), and Zhang and Yeh (1997) developed an iterative geostatistical technique in which a linear estimator was successively used to incorporate the non-linear relationship between hydraulic properties and pressure head. This method is referred to as a successive linear estimator (SLE). They demonstrated that with the same amount of information, the SLE revealed a more

detailed conductivity field than cokriging. Hughson and Yeh (1998 and 2000) showed that the SLE is computationally efficient compared to the classical inverse method. They extended it to the inverse problem in three-dimensional, variably saturated, heterogeneous porous media, which had not been done before. In their study, pressure head and moisture content measurements at 42 locations (7 wells x 6 depths) in a three-dimensional porous medium were collected at three different times during an infiltration event. This secondary information was then used to estimate saturated hydraulic conductivity, K_s , α and n parameters of the Mualem-van Genuchten unsaturated hydraulic property model (van Genuchten, 1980) at 500 locations in the porous medium.

In the first manuscript (Appendix A), we develop a sequential inverse technique for hydraulic tomography to process the large amount of data to characterize aquifer heterogeneity which is based on the SLE. While demonstrating the robustness of the inverse method, we also investigate the effect of monitoring intervals, pumping intervals, and the number of pumping locations on the final estimate of hydraulic conductivity. Guidelines for optimal design of a hydraulic tomography test are subsequently established. To further verify our results, Monte Carlo inverse simulations are performed, and the effects of measurement errors and uncertainties in the statistical parameters required by the inverse model are investigated. Finally, an example is used to illustrate the effectiveness and robustness of this sequential approach for hydraulic tomography under three-dimensional, steady flow conditions.

Hydraulic tomography has been tested using numerical experiments (Gottlieb and Dietrich, 1995; Yeh and Liu, 2000) but not laboratory or field experiments. In numerical

experiments, the effects of conceptual model errors are absent because synthetic tomography data are generated from the same model used in the inversion. Model inputs are also assumed error-free. Conversely, in field experiments, the effects of conceptual model errors are unknown. Model inputs, such as boundary conditions, pumping rates, the mean, variance, and correlation scales, are always subject to uncertainty. Further, the pressure head/discharge data inevitably contain unknown measurement errors. Field experiments are, thus, the most appropriate test for hydraulic tomography.

Nevertheless, field experiments are so costly that well-controlled sandbox experiments are a reasonable alternative. In the second manuscript (Appendix B), we test the effectiveness of our sequential inverse approach (Yeh and Liu, 2000) with two sandbox experiments. The first experiment represents a stratified aquifer system, while the other represents a more complex and realistic heterogeneous aquifer. In addition, numerical experiments are conducted to diagnose anomalies in the inverse results from the sandbox experiments, and to explore conditions under which the hydraulic tomography can be effective.

Monitoring Water Movement in Vadose Zone: Electrical Resistivity Tomography

The dc resistivity survey is an inexpensive and widely used technique for investigation of near surface resistivity anomalies and it recently has become popular for the investigation of subsurface pollution problems (NRC, 2000). In principle, it measures the voltage generated by transmission of current between electrodes implanted at the ground surface. Apparent (bulk or effective) resistivity is then calculated and used to interpret subsurface structures.

The conventional resistivity survey includes vertical sounding and profiling (Sharma, 1997). Vertical sounding is used to provide a resistivity map as a function of depth. In a sounding, voltage probes are fixed at a center location in between two source electrodes and voltages are measured at a variety of source electrode separation distances (i.e., the Schlumberger array). The depth of investigation increases with increases in separation distances. In the classical interpretation of the sounding survey, the apparent resistivity for a given source electrode separation distance is determined using the voltage measurement and an analytical model that assumes resistivity homogeneity of the subsurface. Because of the homogeneity assumption, the calculated resistivity represents a spatially averaged resistivity value over a volume of geological media that varies with the distance between the source electrodes. The greater the distance between the source electrodes, the greater volume the apparent resistivity represents. As a result, sounding is most suitable for the cases where the geological formation is made of only a few layers with significant resistivity contrast or where a relatively uniform formation embeds some simple objects of resistivity distinctly different from the surrounding media. For more complex heterogeneity patterns, deciphering signals from the survey becomes more difficult, subjective, non-unique and highly uncertain due to the averaging nature of the apparent resistivity.

Profiling is used to detect lateral changes in resistivity. In profiling, the spacing between current electrodes and between two voltage probes is fixed, and the relative position of the electrodes and probes array is also fixed in space, but the entire array is moved laterally (i.e., the Wenner array). At a given array position, measurements of

current and voltage are used to determine the apparent resistivity, by using an analytical formula that assumes subsurface homogeneity. Again, the estimated apparent resistivity is a volume-averaged property. As a consequence, the estimated resistivity field is generally very smooth unless a distinct resistivity anomaly exists in the subsurface.

Because the homogeneity assumption is embedded in the formulas for calculating apparent resistivity and the potential field is smooth due to its highly diffusive nature, conventional interpretations of resistivity survey data have been virtually ineffective in environmental hydrology or pollution applications, where resistivity anomalies are subtle, complex, and multi-scale. To overcome these difficulties, contemporary resistivity surveys collect extensive current and electrical potential data sets in multi-dimensions. Without assuming subsurface homogeneity, a mathematical computer model is employed to invert the data sets to estimate the resistivity field, using the minimum output error (MOE) criterion (e.g., Ellis and Oldenburg, 1994; Li and Oldenburg, 1994; Zhang et al., 1995; and Daily et al., 1992). However, the general uniqueness and resolution of the three-dimensional resistivity inversion have not been investigated sufficiently thus far (NRC, 2000).

While the physical process is different, the governing equation for electrical currents and potential fields created in the resistivity survey is analogous to that for steady flow in saturated porous media. The mathematical solution to the inversion of a resistivity survey is, thus, similar to that of a groundwater hydrological survey.

In the third manuscript (Appendix C), we extend the inverse methodology developed by Yeh and Liu (2000) to the three-dimensional, electrical resistivity

tomography (ERT) problem. This method allows the use of prior information on the resistivity fabric, and point measurements of voltage and resistivity, if any, to be included in the interpretation of the result of the ERT. Numerical simulations are carried out to illustrate the robustness of the approach and discuss pros and cons of surface and down-hole resistivity surveys. We sampled twenty-seven cores in a field, conducted laboratory measurements to determine the relationship between resistivity and moisture content of the core samples, and analyzed the spatial variability of the resistivity-moisture content relationship. Subsequently, impacts of the spatial variability on the estimated changes in moisture content in the vadose zone, based on ERT, are explored and discussed.

As discussed above, the ERT survey has found its way into subsurface hydrological applications. This is attributed to the fact that resistivity can be related to water content with some empirical relationships, i.e. the power law (Knight, 1991). During an infiltration event, water content of geological media is generally the only element that undergoes dramatic changes. Therefore, tracking the resistivity difference at different time has often been regarded as a useful tool to detect the temporal changes of water content in the vadose zone (Daily et al., 1992). To do this, current/potential data sets are collected using ERT surveys before and after infiltration. With the help of inverse models, the images of resistivity distribution before and after infiltration are obtained and then the change in resistivity is computed accordingly. By assuming a constant deterministic relationship between resistivity and water content, the change in resistivity is converted to the change in water content.

However, the resistivity-moisture relationship exhibits strong spatial variability in the field (Yeh, et al., 2001). Therefore, ignoring the spatial variability while using the simplified assumption exacerbates the level of uncertainty in the interpretation of change of moisture content based on the estimated change in resistivity. Regardless of the uncertainties in the interpretation of the change of moisture content, this change in moisture content only provides qualitative information of water movement in the vadose zone. The exact water content distribution remains unknown. Since unsaturated hydraulic conductivity is a function of water content instead of water content change, the converted change of moisture content can not be directly used in hydrological inversions. A novel inverse methodology that considers the spatial variability of the resistivity-moisture relationship and is able to directly estimate the water content distribution with less uncertainty is needed for better characterization of the vadose zone.

In the fourth manuscript (appendix D), we adopt the sequential inverse approach for hydraulic tomography (Yeh and Liu, 2000) to the ERT survey. In this method, we do not simply estimate resistivities, instead, we simultaneously estimate ρ_o, θ and m , which are functions of resistivity. This method allows processing of a large number of current/voltage data yielded by ERT survey, incorporates the point measurements of moisture content, and estimates the actual water content distribution. More importantly, this model considers the spatial variability of the resistivity-water content relationship. Three-dimensional numerical experiments are carried out to illustrate the robustness of our sequential inverse approach in delineating water content distribution at time of 50,000 minutes after an infiltration event. Meanwhile, change in resistivity due to

infiltration is also obtained to track the change of moisture content. The converted change in water content is then compared to the true change in water content, thus to evaluate the effect of the spatial variability of the resistivity-moisture relationship.

Explanation of Dissertation Format

This dissertation consists of two chapters (“Introduction” and “Present Study”), and four manuscripts (appendices A-D). The first manuscript (appendix A) was published in Water Resources Research, Vol. 36, No. 8, Pages 2095-2105, August 2000. The second manuscript (appendix B) was accepted by Water Resources Research in December, 2000. Appendix C has been submitted for peer review and appendix D is to be submitted for peer review. I am responsible for developing and testing the sequential inverse model for hydraulic tomography and ERT, and responsible for planning and performing all the simulations presented in each manuscript and modifying /adding new source codes to the existing code (NU_LI) to fulfill my research purposes.

My advisor, Dr. T. –C. Jim Yeh, helped me to decide the research topic presented in this dissertation, and he has provided valuable insight and guidance in model conceptualization, and result interpretation.

The sandbox experiments data were obtained by Ryan Gardiner, and the field electrical resistivity data were provided by Kristine Baker from the Sandia-Tech Vadose zone (STVZ) project. R. Glass, J.R. Brainard, D. Alumbaugh and D. LaBrecque are investigators of the STVZ project, and they provided useful background information of the infiltration site and the project.

CHAPTER 2 PRESENT STUDY

The approaches, results and conclusions of this study are presented in the four manuscripts appended to this dissertation. The following is a summary of the most important findings in this dissertation, which are contributions to the understanding of subsurface heterogeneity characterization.

Summary

Characterization of subsurface heterogeneity is of fundamental importance to the study of groundwater flow and contaminant transport in aquifers and vadose zones. Conventional aquifer test methods assume aquifer homogeneity and yield effective hydraulic conductivity and the storage coefficient for an equivalent homogeneous aquifer. These hydraulic parameters are average properties of the aquifer over a large volume and do not provide information on the spatial distribution of the hydraulic conductivity within the volume. On the other hand, measurement of hydraulic conductivity of small-scale samples at a large number of locations is time-consuming, costly and therefore impractical.

Since pressure head measurements are less expensive and can be obtained with relative ease, a cost-effective methodology is needed to yield abundant pressure head data sets to help decipher aquifer heterogeneity. Hydraulic tomography is such an effective tool. During a hydraulic tomography experiment, water is sequentially pumped from or injected into an aquifer at different vertical portions or intervals of the aquifer. During

each pumping or injection, hydraulic head responses of the aquifer at other intervals are monitored, yielding a set of head/discharge (or recharge) data. By sequentially pumping (or injecting) water at one interval and monitoring the steady-state head responses at others, many head/discharge (recharge) data sets are obtained.

In the present study, a sequential inverse approach is developed to interpret results of hydraulic tomography. The approach uses an iterative geostatistical inverse method to yield the effective hydraulic conductivity of an aquifer, conditioned on each set of head/discharge data. To efficiently include all the head/discharge data sets, a sequential conditioning method is employed. It uses the estimated hydraulic conductivity field and covariances, conditioned on the previous head/discharge data set, as prior information for the next stage of estimations using a new set of pumping data.

The proposed sequential inverse approach has several advantages. It incorporates the spatial structure of hydraulic conductivity through its input parameters such as mean, variance and correlation structure; it incorporates point measurements such as conductivity measurements and pressure head measurements and preserves these measurement values during the inversion and thus tailors our estimates based on these site-specific information; it considers the non-linear relationship between hydraulic conductivity and pressure head and manages to take full advantage of the secondary information (pressure head); it is able to process abundant data sets yielded by hydraulic tomography since it processes pressure data sets in a sequential manner. Results of numerical experiments show that the sequential inverse approach, using data obtained by hydraulic tomography, is a promising tool for characterizing aquifer heterogeneity. By

sequentially using the secondary information, the size of the covariance matrix in our inverse approach remains small so that the matrix equations can be solved with ease. Thus, inversion of the large amount of secondary information collected during hydraulic tomography becomes feasible. Compared to the results yielded from the Monte Carlo simulations, the residual variance produced from our sequential approach reflects the pattern of the conditional variance.

Results of our numerical experiments also show that the hydraulic tomography can be most effective if the horizontal separation distance between wells is set to be half of the horizontal correlation scale of hydraulic conductivity. The vertical interval between two pressure monitoring locations should be no more than half of the vertical correlation scale of hydraulic conductivity. The optimal number of pumping locations is equal to the ratio of the aquifer depth to the vertical correlation scale of hydraulic conductivity. The pumping rate has no effect on the estimate.

Our analysis shows that the uncertainty in the input variance for our inverse model has no influence on the estimates. Similarly, uncertainty in correlation scales of hydraulic conductivity has no significant effect on the estimate unless the correlation scales are extremely under-estimated or over-estimated. Abundant secondary information (such as pressure head) in space can greatly reduce the effect caused by inaccurate knowledge of the correlation structure. If there are large measurement errors associated with pressure head, our inverse approach yields a smoother estimate than that obtained from the error-free data, reflecting the fact that less information is extracted

from the measurements. Consequently, accurate measurements of the secondary information (i.e. pressure head) are needed to make hydraulic tomography successful.

Hydraulic tomography appears to be a promising field technique for providing abundant secondary information for characterizing aquifer heterogeneity. Using our sequential inverse model, hydraulic tomography can reveal more detailed aquifer heterogeneity than classical aquifer tests.

In numerical experiments, effects of conceptual model errors are absent because synthetic tomography data are generated from the same model used in the inversion. Model inputs are also assumed error-free. Conversely, in field experiments, the effects of conceptual model errors are unknown. Model inputs, such as boundary conditions, pumping rates, the mean, variance, and correlation scales, are always subject to uncertainty. Further, the pressure head/discharge data inevitably contain unknown measurement errors. Field experiments are, thus, the most appropriate test for hydraulic tomography.

Nevertheless, field experiments are so costly that well-controlled sandbox experiments are a reasonable alternative. In the present study, we tested the effectiveness of our sequential inverse approach under realistic conditions with two sandbox experiments. One sandbox was packed with layers of sands to represent a stratified aquifer while the other with discontinuous sand bodies of different shapes and sizes to represent a more complex and realistic heterogeneous aquifer. Parallel to the sandbox experiments, numerical experiments were conducted to assess the effects of measurement

errors and uncertainties associated with laboratory data, and to diagnose the hydraulic conductivity estimates obtained from sandbox experiments.

For both sandbox experiments, our inverse model was able to reproduce the major heterogeneous patterns. The results show that our approach works well under realistic conditions, in spite of measurement errors and uncertainties associated with the pressure head/discharge data sets and other input parameters required by our model. Our analyses also indicate that hydraulic tomography does not improve the conductivity estimate significantly if abundant head measurements are available. This is especially true for a stratified aquifer system represented in sandbox 1. Hydraulic tomography can be useful and effective when pressure head measurements are not available at a large number of sample locations, and when aquifer heterogeneity exhibits highly discontinuous and non-uniform nature as presented in sandbox 2.

Our well-controlled sandbox experiments tested the effectiveness of our inverse method for realistic problems where measurements are inherently imperfect. Our successful laboratory verifications of the inverse approach is a step towards applications of our inverse model to field-scale problems.

A resistivity survey is an inexpensive and widely used technique for investigation of near surface resistivity anomalies and it recently has been popular for the investigation of the subsurface pollution problems. In addition, resistivity is related to moisture content through some empirical relationship, for instance, the power law. During an infiltration event, water content of geological media is generally the only element that undergoes dramatic changes. Therefore, tracking the change in resistivity has often been

regarded as a useful means to delineate the change of the water content in the vadose zone.

While the physical process is different, the governing equation for electrical currents and potential fields created in the resistivity survey is analogous to that for steady flow in saturated porous media. The mathematical solution for the inversion of a resistivity is, thus, similar to that of a groundwater hydrological survey. In the present study, the inverse methodology for hydraulic tomography is extended to the three-dimensional, electrical resistivity tomography (ERT). This sequential inverse approach is computationally efficient, allows fine-grid discretization of the solution domain, and permits sequential inclusion of different data sets. Further more, the conditional variance in the inverse model quantifies uncertainty in the estimate.

Through numerical experiments based on our inverse approach, we showed that geological bedding dictates effectiveness of the sampling array of ERT: sampling perpendicular to bedding (down-hole array) increase resolution of the resistivity estimate due to the long correlation of resistivity in the direction parallel the bedding. On the other hand, the long correlation scale of resistivity along the bedding and the short correlation scale of resistivity perpendicular to bedding restrict the effectiveness of the surface array (sampling parallel to bedding) to a shallow depth.

Conducting ERT surveys before and after infiltration events and then applying the sequential inverse approach to the ERT data sets, we can obtain the detailed resistivity distributions before and after infiltration. The resistivity change is then computed accordingly and used to interpret water movement in the vadose zone by

assuming a constant relationship between resistivity change and water content change. However, great variability of the resistivity-moisture relationship was found to exist in our field samples. Both the theoretical analysis and numerical experiments suggested that such a spatially varying relationship exacerbates the level of uncertainty in the interpretation of change of moisture content based on the estimated change in resistivity.

In addition to the great uncertainty resulted from the interpretation of the estimated change in resistivity, the change of water content only provides qualitative information of the water movement in the vadose zone, the actual water content distribution remains unknown. Since the unsaturated hydraulic conductivity is a function of water content instead of water content change, the converted change of water content cannot be directly used by hydraulic inversions to better characterize the vadose zone. Therefore, in the present study, a sequential conditioning approach that considers the spatial variability of the resistivity-moisture relationship, incorporates point moisture measurements, and efficiently utilizes the large number of voltage data sets yielded by ERT is developed to directly estimate the water content distribution. By applying our inverse approach to the ERT surveys conducted at different times, the 3-D development of water plume in the vadose zone with time can be monitored with less uncertainty, and this information is significantly beneficial to the quantitative characterization of the vadose zone.

Concluding Remarks of the dissertation

This study makes several contributions to the methods for quantitative characterization of aquifer heterogeneity and to the cost-effective and more accurate method of monitoring water movement in the vadose zone. These new findings have applications to advanced site characterization and enhanced remediation of contaminated sites where heterogeneity is present.

Hydraulic tomography is a cost-effective tool that can yield abundant pressure head measurements that give the site-specific information of aquifer systems. The sequential inverse approach makes it mathematically feasible and computationally efficient to process such a large number of data sets and yields a greater detail of hydraulic conductivity distribution for a three-dimensional aquifer. Numerical experiments demonstrate the robustness of the inverse approach, establish the guidelines of optimal network design. Sandbox experiments verify the effectiveness of the sequential inverse approach under realistic conditions where all the input data of the inverse model are inherently imperfect. These successful laboratory verifications of the inverse approach is a step towards applications of our inverse model to field-scale problems.

Electrical resistivity surveys have been widely used to detect the subsurface resistivity anomalies and has recently become popular for the investigation of water movement in vadose zone. The sequential inverse approach for hydraulic tomography is adapted for interpreting electrical resistivity tomography with higher efficiency and less uncertainty. However, the interpretation of water movement using estimated resistivity change involves great uncertainty by assuming a constant resistivity-moisture content

relationship. Our theoretical analysis and field data reveal that the resistivity-moisture content relationship exhibits strong spatial variability. Neglecting the spatial variability may result in a misleading interpretation of water movement in vadose zone. The sequential inverse approach for electrical resistivity tomography is extended to directly estimate water content distribution. This inverse model considers the spatial variability of the resistivity-moisture content relationship, incorporates point moisture content measurements and resistivity data and quantifies the uncertainty associated with our estimate through conditional variance. Our inverse model provides valuable information, the water content distribution, for hydraulic inversion in vadose zone and thus makes it possible to enhance the vadose zone characterization by integrating geological, hydrological and geophysical data sets.

REFERENCES

- Butler, J.J., Jr. and W.Z. Liu, Pumping tests in nonuniform aquifers: the radially asymmetric case, *Water Resour. Res.*, 29(2), 259-269, 1993.
- Butler, J.J., Jr., C.D. McElwee and G.C. Bohling, Pumping tests in networks of multilevel sampling wells: methodology and implications for hydraulic tomography, *Water Resour. Res.*, To appear, 1999.
- Daily, W., A. Ramirez, D. LaBrecque and J. Nitao, Electrical resistivity tomography of vadose water movement, *Water Resour. Res.*, 28(5), 1429-1442, 1992.
- Ellis, R. G., and S. W. Oldenburg, The pole-pole 3-d dc resistivity inverse problem: a conjugate gradient approach, *Geophysical journal international* 119,187-194, 1994.
- Giudici M., Morossi G., Parravicini G., and Ponzini G., A new method for the identification of distributed transmissivities, *Water Resour. Res.*, 31, 1969-1988, 1995.
- Gottlieb, J., and P. Dietrich, Identification of the permeability distribution in soil by hydraulic tomography, *Inverse Problems*, 11, 353-360,1995.
- Hoeksema, R. J., and P. K. Kitanidis, An application of the geostatistical approach to the inverse problem in two-dimensional groundwater modeling, *Water Resour. Res.*, 20(7), 1003-1020, 1984.
- Hughson, D. L., and T.-C. J. Yeh, A geostatistically based inverse model for three-dimensional variably saturated flow, *Stochastic Hydrol. Hydraul.* 12(5), 285-298, 1998.
- Hughson, D. L., and T.-C. J. Yeh, An inverse model for three-dimensional flow in variably saturated porous media, *Water Resour. Res.*, 36(4), 829-839, 2000.
- Knight, R., Hysteresis in the electrical resistivity of partially saturated sandstones, *Geophysics*, Vol. 56, No. 12: 2139-2147, 1991.
- Kitanidis, P. K., and E. G. Vomvoris, A geostatistical approach to the inverse problem in groundwater modeling and one-dimensional simulations, *Water Resour. Res.*, 19(3), 677-690, 1983.
- Kitanidis, P. K., Comment on “ A reassessment of the groundwater inverse problem” by D. Mclaughlin and L. R. Townley, *Water Resour. Res.*, 33(9), 2199-2202, 1997.
- Li, Y., and D. W. Oldenburg, Inversion of 3D dc-resistivity data using an approximate inverse mapping, *Geophysical journal international* 116, 527-537, 1994.

NRC, *Seeing into the earth: noninvasive characterization of the shallow subsurface for environmental and engineering application*, Board on earth sciences and resources, water science and technology board, Commission on Geoscience, Environment, and Resources National Research council, National academy press, Washington D.C, 2000.

Sagar B., Yakowitz S., and Duckstein L., A direct method for the identification of the parameters of dynamic nonhomogeneous aquifers, *Water Resour. Res.*, 11, 563-570, 1975.

Scarascia S., and Ponzini G., An approximate solution for the inverse problem in hydraulics, *UEnergia Elettrica*, 49, 518-531, 1972.

Sharma, P. V., *Environmental and engineering geophysics*, Cambridge University Press, Cambridge, UK, 1997

Snodgrass M. F., and Kitanidis P.K., Transmissivity identification through multi-directional aquifer stimulation, *Stochastic Hydrol. Hydraul.*, 12, 299-316, 1998.

van Genuchten, M. T., A closed-form equation for predicting the hydraulic conductivity of unsaturated soils. *Soil Sci. Soc. Am. J.* 44, 892-898, 1980.

Yeh, W. W-G., Review of parameter identification procedures in groundwater hydrology: the inverse problem, *Water Resour. Res.*, 22(1), 95-108, 1986.

Yeh, T.-C. J., Stochastic modeling of groundwater flow and solute transport in aquifers, *J. of Hydrologic Processes*, Vol. 6, 369-395, 1992.

Yeh, T.-C. J., Scale issues of heterogeneity in vadose-zone hydrology, in *Scale Dependence and Scale Invariance in Hydrology*, edited by G. Sposito, Cambridge Press, 1998.

Yeh, T.-C. J., A.L. Gutjahr, and M. Jin, An iterative cokriging-like technique for groundwater flow modeling, *Ground Water*, 33(1), 33-41, 1995.

Yeh, T.-C. J., and J. Zhang, A geostatistical inverse method for variably saturated flow in the vadose zone, *Water Resour. Res.*, 32(9), 2757-2766, 1996.

Yeh, T.-C., M. Jin, and S. Hanna, An iterative stochastic inverse method: conditional effective transmissivity and hydraulic head fields, *Water Resour. Res.*, 32(1), 85-92, 1996.

Yeh, T. -C. J., and S. Liu, Hydraulic tomography: development of a new aquifer test method, *Water Resour. Res.*, 36(8), 2095-2105, 2000.

Yeh, T. -C. J., and S. Liu, K. Baker, R. Glass, J. R. Brainard, D. Alumbaugh, D. LaBrecque, Uncertainties in interpretation of electrical resistivity surveys in subsurface hydrological applications, submitted to *Water Resour. Res.*, 2001.

Zhang, J., R. I. Mackie, and T. Madden, 3-D resistivity forward modeling and inversion using conjugate gradients. *Geophysics* 60, 1313-1325, 1995.

Zhang, J., and T.-C. J. Yeh, An iterative geostatistical inverse method for steady flow in the vadose zone, *Water Resour. Res.*, 33(1), 63-71, 1997.

APPENDIX A

HYDRAULIC TOMOGRAPHY: DEVELOPMENT OF A NEW AQUIFER TEST METHOD

T.-C. Jim Yeh and Shuyun Liu

Department of Hydrology and Water Resources

John W. Harshbarger Building

The University of Arizona,

Tucson, Arizona 85721.

published in

Water Resources Research, Vol., 36, No. 8, Pages 2095-2105

August 2000

Abstract

Hydraulic tomography (i.e., a sequential aquifer test) has recently been proposed as a method for characterizing aquifer heterogeneity. During a hydraulic tomography experiment, water is sequentially pumped from or injected into an aquifer at different vertical portions or intervals of the aquifer. During each pumping or injection, hydraulic head responses of the aquifer at other intervals are monitored, yielding a set of head/discharge (or recharge) data. By sequentially pumping (or injecting) water at one interval and monitoring the steady-state head responses at others, many head/discharge (recharge) data sets are obtained.

In this study a sequential inverse approach is developed to interpret results of hydraulic tomography. The approach uses an iterative geostatistical inverse method to yield the effective hydraulic conductivity of an aquifer, conditioned on each set of head/discharge data. To efficiently include all the head/discharge data sets, a sequential conditioning method is employed. It uses the estimated hydraulic conductivity field and covariances, conditioned on the previous head/discharge data set, as prior information for next estimations using a new set of pumping data.

This inverse approach was first applied to hypothetical, two-dimensional, heterogeneous aquifers to investigate the optimal sampling scheme for the hydraulic tomography, i.e., the design of well spacing, pumping and monitoring locations. The effects of measurement errors and uncertainties in statistical parameters required by the inverse model were also investigated. Finally, the robustness of this inverse approach was demonstrated through its application to a hypothetical, three-dimensional, heterogeneous aquifer.

1. Introduction

Accurate predictions of water and solute distributions and movement in geological formations require detailed knowledge of the spatial distribution of the hydraulic properties of the formations (Yeh, 1992 and 1998). Conventional aquifer tests (also known as pumping tests) assume aquifer homogeneity and yield effective hydraulic conductivity and the storage coefficient for an equivalent homogeneous aquifer. These hydraulic parameters are average properties of the aquifer over a large volume (Butler and Liu, 1993) and do not provide information of spatial distribution of the hydraulic conductivity within the volume. On the other hand, measurement of hydraulic conductivity of small-scale samples at a large number of locations is time consuming, costly, and impractical.

To circumvent these difficulties and to efficiently gain information of the spatial distribution of hydraulic conductivity, the tomography concept widely used in medical and geophysical imaging during the last two decades has recently been employed (Gottlieb and Dietrich, 1995; Butler et al., 1999). Specifically, fully screened wells are segregated into many vertical intervals using packers. Water is pumped from or injected into an aquifer at one of the intervals to create a steady flow condition. Hydraulic head responses of the aquifer at other intervals are then monitored, yielding a set of head/discharge (or recharge) data. By sequentially pumping (or injecting) water at one interval and monitoring the steady-state head response at others, many head/discharge (or recharge) data sets are obtained. Such a sequential aquifer test is referred to as hydraulic

tomography. This new field method has significant advantages over traditional pumping tests. For instance, hydraulic tomography can provide detailed information about vertical and lateral pressure head responses induced by pumping at a given location. Furthermore, by changing the position of the pump in the well, many sets of aquifer responses to pumping at different locations can be obtained. Such a large number of data sets may reduce the non-uniqueness issue of the inverse problem and may reveal the details of a heterogeneous hydraulic conductivity field.

Several researchers have recently investigated this idea of hydraulic tomography. For example, Gottlieb and Dietrich (1995) proposed a method of hydraulic tomography for identifying the permeability distribution in a hypothetical, two-dimensional saturated soil. In their study, they used two boreholes to create hydraulic dipoles. The positions of source and sink are varied over both boreholes. Pore-water pressure changes along the vertical were monitored in monitoring wells at other locations. They subsequently applied a least-squares based inverse approach to the pressure data to produce an image of the spatial distribution of hydraulic conductivity. Butler et al. (1999) applied this hydraulic tomography concept to networks of multilevel sampling wells. They developed new techniques for measuring drawdown data at a scale that had previously been unobtainable. These new techniques greatly facilitate the implementation of hydraulic tomography in the field.

Hydraulic tomography can yield many useful sets of secondary information, namely head responses, which can be used to identify heterogeneity of the aquifer. Still,

a reliable and efficient inverse methodology is required to decipher the information so that a reliable image of the hydraulic conductivity field can be obtained. Classical inverse methodologies are known to have many difficulties (Yeh, 1986). They also confront an insurmountable computational burden when they are applied to estimate detailed hydraulic properties in three-dimensional geological formations (Kitanidis, 1997). Consequently, few classical inverse models have been applied to identify small-scale heterogeneity in three-dimensional geological media. More importantly, the abundance of hydraulic head information generated by hydraulic tomography presents an even greater challenge for the classical inverse methodologies.

In the past few decades, cokriging has been used to estimate hydraulic conductivity fields from scattered measurements of pressure head in saturated flow problems (Kitanidis and Vomvoris, 1983; Hoeksema and Kitanidis, 1984). However, cokriging is a linear estimator and its application is limited to mildly nonlinear systems, such as groundwater flow in geological formations of mild heterogeneity (variance of natural log of conductivity, $\sigma^2_{\ln k}=0.1$). When the degree of aquifer heterogeneity is large ($\sigma^2_{\ln k}>1$) and the linear assumption becomes inadequate, cokriging cannot provide a good estimate of the conditional mean conductivity field (Yeh et al., 1996). In other words, it cannot take full advantage of the head information to obtain an optimal estimate of the hydraulic properties.

To overcome this shortcoming, Yeh et al. (1995 and 1996), and Zhang and Yeh (1997) developed an iterative geostatistical technique in which a linear estimator was used successively to incorporate the non-linear relationship between hydraulic properties

and pressure head. This method is referred to as a successive linear estimator (SLE). They demonstrated that with the same amount of information, the SLE revealed a more detailed conductivity field than cokriging. Hughson and Yeh (1998 and 2000) showed that the SLE is computationally efficient compared to the classical inverse method. They extended it to the inverse problem in three-dimensional, variably saturated, heterogeneous porous media, which had not been attempted before. In their study, pressure head and moisture content measurements at 42 locations (7 wells x 6 depths) in a three-dimensional porous medium were collected at three different times during an infiltration event. This secondary information was then used to estimate saturated hydraulic conductivity, K_s , and α parameter of the Mualem-van Genuchten unsaturated hydraulic property model (van Genuchten, 1980) at 500 locations in the porous medium.

In this paper, based on the SLE we develop a sequential inverse technique for hydraulic tomography to process the large amount of data to characterize aquifer heterogeneity. While demonstrating the robustness of the inverse method, we also investigate the effect of monitoring intervals, pumping intervals, and the number of pumping locations on the final estimate of hydraulic conductivity. Guidelines for optimal design of a hydraulic tomography test are subsequently established. To further verify our results, Monte Carlo inverse simulations are performed, and the effects of measurement errors and uncertainties in statistical parameters required by the inverse model are investigated. Finally, an example is used to illustrate effectiveness and robustness of this sequential approach for hydraulic tomography under three-dimensional, steady flow conditions.

2. Methodology

2.1. Equation of flow in three-dimensional saturated media:

In this study, we assume that the steady-state flow field, created by the hydraulic tomography in three-dimensional, saturated, heterogeneous, porous media can be described by the following equation:

$$\nabla \bullet (K(x)\nabla \phi) + Q(x) = 0 \quad (1)$$

with boundary conditions

$$\phi|_{\Gamma_1} = \phi^* \quad \text{and} \quad (K(x)\nabla \phi) \bullet \mathbf{n}|_{\Gamma_2} = q \quad (2)$$

where ϕ is total head [m], \mathbf{x} is the location vector ($\mathbf{x} = \{x_1, x_2, x_3\}$, [m]), and x_3 represents the vertical coordinate and is positive upward), Q is the pumping rate [$\text{m}^3/\text{hr} - \text{m}^3$] at the selected interval during the tomography experiment, and $K(\mathbf{x})$ is the saturated hydraulic conductivity field in [m/hr]. In (2), prescribed total head on the Dirichlet boundary, Γ_1 , is denoted by ϕ^* [m]. Specified flux, q in [m/hr], is given on the Neumann boundary conditions, Γ_2 , and \mathbf{n} is a unit vector normal to the union of Γ_1 and Γ_2 .

2.2. Sequential inverse algorithm:

To deal with aquifer heterogeneity, the natural log of hydraulic conductivity, $\ln K(x)$, of an aquifer is treated as a stationary stochastic process with an unconditional mean, $\langle \ln K \rangle = F$ ($\langle \rangle$ denotes the expected value) and the unconditional perturbation, f . The corresponding steady hydraulic head distribution due to pumping in an interval in the

hydraulic tomography is then presented by $\phi(x) = H(x) + h(x)$, where $H = \langle \phi \rangle$ and h is the unconditional head perturbation. Suppose that we have used well-log data and core samples to determine n_f conductivity values, $f_i^* = (\ln K_i^* - F)$ where $i = 1, 2, \dots, n_f$ (we will refer to these data sets as primary information). Additionally, we have estimated the mean and correlation structure of the conductivity field. Also assume that, during a hydraulic tomography experiment, we have collected m sets of n_h observed head values, ϕ_j^* , where $j = n_f + 1, n_f + 2, \dots, n_f + m \times n_h$ during m sequential pumping tests. These head data sets are referred to as secondary information. We then seek an inverse model that can produce head and conductivity fields that preserve the observed head and conductivity values at sample locations, and satisfy their underlying statistical properties (i.e., mean and covariance, etc.) and the governing flow equation. In the conditional probability concept, such a head or conductivity field is a conditional realization of ϕ or $\ln K$ field among many possible realizations of the ensemble. Consequently, a conditional conductivity field can be expressed as the sum of conditional mean conductivity and its conditional perturbation, $K_c(x) = \langle K_c(x) \rangle + k_c(x)$. Similarly, the conditional head field can be written as $\phi_c = \langle \phi_c(x) \rangle + h_c(x)$ (the subscript c denotes conditional). While many possible realizations of such conditional $\ln K$ and ϕ fields exist, the conditional mean fields, i.e., $\langle K_c(x) \rangle$ and $\langle \phi_c(x) \rangle$, are unique. One way to derive these conditional mean fields is to solve the inverse problem in terms of the conditional mean flow equation. The conditional mean equation can be formulated by substituting the conditional stochastic variables into the governing groundwater flow

equation (1) and taking the expected value. The conditional mean flow equation then takes the form:

$$\nabla \bullet [\langle K_c(x) \rangle \nabla \langle \phi_c(x) \rangle] + \langle \nabla \bullet [k_c(x) \nabla h_c(x)] \rangle + Q(x) = 0 \quad (3)$$

We assume the pumping rate $Q(x)$ is deterministic. Notice that the true conditional mean K and ϕ fields do not satisfy the continuity equation (3) unless the second term in (3) is zero. The second term, $\langle \nabla \bullet (k_c \nabla h_c) \rangle$, becomes zero only under two conditions: 1) all the conductivity values in the aquifer are specified (i.e., $k_c(x) = 0$); or 2) all the head values in the domain are known (measured) so that $h_c(x)$ is zero everywhere. In practice, these two conditions will never be met and we are currently unaware of a means by which to correctly evaluate this term. Accordingly, we will assume that this term is proportional to the conditional mean gradient such that we can rewrite the mean equation as:

$$\nabla \bullet [\langle K_{eff}(x) \rangle \nabla \langle \phi_c(x) \rangle] + Q(x) = 0 \quad (4)$$

This conditional mean equation has the same form as (1) but it is expressed in terms of the conditional effective conductivity and conditional mean hydraulic head field. The conditional effective conductivity, $\langle K_{eff} \rangle$, is a parameter that combines the conditional mean conductivity $\langle K_c \rangle$ and the ratio of the second term to the conditional mean gradient.

Based on the concept of conditional mean equation, we essentially seek an inverse approach to derive the conditional effective hydraulic conductivity that will produce a

conditional mean head field in (4). To do this, we used the SLE, which starts with the classical cokriging technique using observed f_i^* and h_j^* collected in one pumping test in the tomography to construct a cokriged, mean-removed log conductivity map. That is,

$$f_k(x_o) = \sum_{i=1}^{n_f} \lambda_{io} f_i^*(x_i) + \sum_{j=n_f+1}^{n_f+n_h} \mu_{jo} h_j^*(x_j) \quad (5)$$

where $f_k(x_o)$ is the cokriged f value at location x_o . Then, conductivity $K_k(x_o)$ becomes $\exp [F + f_k(x_o)]$. λ_{io} and μ_{jo} are the cokriging weights associated with x_o , which can be evaluated as follows:

$$\begin{aligned} \sum_{i=1}^{n_f} \lambda_{io} R_{ff}(x_\ell, x_i) + \sum_{j=n_f+1}^{n_f+n_h} \mu_{jo} R_{fh}(x_\ell, x_j) &= R_{ff}(x_o, x_\ell) \quad \ell = 1, 2, \dots, n_f \\ \sum_{i=1}^{n_f} \lambda_{io} R_{hf}(x_\ell, x_i) + \sum_{j=n_f+1}^{n_f+n_h} \mu_{jo} R_{hh}(x_\ell, x_j) &= R_{hf}(x_o, x_\ell) \quad \ell = n_f + 1, n_f + 2, \dots, n_f + n_h \end{aligned} \quad (6)$$

where R_{ff} , R_{hh} , and R_{fh} , are covariances of f and h , and the cross-covariance of f and h , respectively. The covariance R_{hh} , and the cross-covariance R_{fh} in (6) are derived from the first-order numerical approximation (similar to equations (9) - (11)) because of its flexibility for cases that involve bounded domains and nonstationary problems.

As mentioned in introduction, the information of hydraulic head may not be fully utilized because of the nonlinear relationship between f and h and the linear assumption embedded in cokriging. To circumvent this problem, a successive linear estimator is used. That is,

$$\hat{Y}_c^{(r+1)}(x_o) = \hat{Y}_c^{(r)}(x_o) + \sum_{j=n_f+1}^{n_f+n_h} \omega_{jo}^{(r)} [\phi_j^*(x_j) - \phi_j^{(r)}(x_j)] \quad (7)$$

where ω_{jo} is the weighting coefficient for the estimate at location x_o with respect to the head measurement at location x_j , and r is the iteration index. $\hat{Y}_c^{(0)}$ is an estimate of the conditional mean of $\ln K$, which is equal to the cokriged log conductivity field, $f_k + F$, at $r = 0$. The residual about the mean estimate at an iteration r is y^r (i.e., $y^r = \ln K - \hat{Y}_c^{(r)}$). In (7), $\phi_j^{(r)}$ is the head at the j^{th} location of the solution to (4) at iteration r and ϕ_j^* is the observed head at location j (i.e., $\phi_j^* = H_j + h_j^*$). The values of ω 's are determined by solving the following system of equations:

$$\sum_{j=n_f+1}^{n_f+n_h} \omega_{jo}^{(r)} \varepsilon_{hh}^{(r)}(x_\ell, x_j) + \theta \delta_{ii} = \varepsilon_{hy}^{(r)}(x_o, x_\ell) \quad \ell = n_f+1, n_f+2, \dots, n_f+n_h \quad (8)$$

where ε_{hh} and ε_{hy} , are the error covariance (or conditional covariance function) and error cross-covariance (or conditional cross-covariance), respectively, at each iteration. θ is a stabilizing term and δ_{ii} is an identity matrix. During the iteration, the stabilizing term is added to the diagonal terms of the left-hand side matrix of equation (8) to numerically condition the matrix, and thus to assure a stable solution. A larger term can result in a slower convergence rate, and a smaller θ value may lead to numerical instability. In our approach, this stabilizing term is determined dynamically as the product of a constant weighting factor and the maximum value of the diagonal terms of ε_{hh} at each iteration.

The solution to (8) requires knowledge of ε_{hy} and ε_{hh} , which is approximated at each iteration. Based on the first-order analysis for a finite element groundwater flow

model (Dettinger and Wilson, 1981), hydraulic head at the r^{th} iteration can be written as a first-order Taylor series:

$$\phi = \hat{\phi}_c^{(r)} + h^{(r)} = G(\hat{Y}_c^{(r)} + y^{(r)}) \approx G(\hat{Y}_c^{(r)}) + \left. \frac{\partial G(\hat{Y}_c^{(r)})}{\partial \ln K} \right|_{\hat{Y}_c^{(r)}} y^{(r)} \quad (9)$$

where $G(\hat{Y}_c^{(r)})$ represents the resulting head of the conditional mean equation (4) evaluated with parameters $\hat{Y}_c^{(r)}$. The first-order approximation of the residual $h^{(r)}$ can then be written as

$$h^{(r)} \approx \left. \frac{\partial G(\hat{Y}_c^{(r)})}{\partial \ln K} \right|_{\hat{Y}_c^{(r)}} y^{(r)} = J^{(r)} y^{(r)} \quad (10)$$

where J can be evaluated using an adjoint state sensitivity method (Sykes et al., 1985; Sun and Yeh, 1992; Li and Yeh, 1998) subject to boundary conditions. Using (11), we then derive the approximate covariance of $h^{(r)}$ and cross-covariances between $y^{(r)}$ and $h^{(r)}$.

$$\begin{aligned} \mathcal{E}_{hh}^{(r)} &= J^{(r)} \mathcal{E}_{yy}^{(r)} J^{T(r)} \\ \mathcal{E}_{hy}^{(r)} &= J^{(r)} \mathcal{E}_{yy}^{(r)} \end{aligned} \quad (11)$$

where J is the sensitivity matrix of $n_h \times N$, and superscript T stands for the transpose. \mathcal{E}_{yy} is the covariance of y , which is given by

$$\mathcal{E}_{yy}^{(l)}(x_o, x_k) = R_{ff}(x_o, x_k) - \sum_{i=1}^{n_f} \lambda_{io} R_{ff}(x_i, x_k) - \sum_{j=n_f+1}^{n_f+n_h} \mu_{jo} R_{fh}(x_j, x_k) \quad (12)$$

at iteration $r = 0$, where $k = 1, 2, \dots, N$, and λ and μ are cokriging coefficients. Equation (12) is the cokriging variance if $x_o = x_k$. For $r \geq 1$, the covariances are evaluated according to

$$\mathcal{E}_{yy}^{(r+1)}(x_o, x_k) = \mathcal{E}_{yy}^{(r)}(x_o, x_k) - \sum_{i=n_f+1}^{n_f+n_h} \omega_{io}^{(r)} \mathcal{E}_{yh}^{(r)}(x_i, x_k) \quad (13)$$

These covariances are approximate conditional covariances. The accuracy of this approximation was investigated by Hanna and Yeh (1998) and will be discussed in section 5.

After updating $Y_c(x)$, the mean flow equation (4) is solved again with the newly updated $Y_c(x)$ for a new head field, ϕ . Then, the change of σ_f^2 (the variance of the estimated conductivity field) and the change of the biggest head misfit among all the monitoring locations between two successive iterations are evaluated. If both changes are smaller than prescribed tolerances, the iteration stops. If not, new ε_{hy} and ε_{hh} are evaluated using (11). Equation (8) is then solved to obtain a new set of weights which are used in (7) with $(\phi^* - \phi^{(n)})$ to obtain a new estimate of $Y_c(x)$.

The above discussion describes the SLE for only one set of primary and secondary information during a hydraulic tomography experiment. This algorithm can also simultaneously include all of the head data collected during all the pumping operations in the sequence. Nevertheless, the system of equations in (6) and (8) can become extremely large and ill conditioned, and stable solutions to the equations can become difficult to obtain (Hughson and Yeh, 2000).

To avoid this problem, the head data sets are used sequentially. Specifically, our method starts the iterative process with the available conductivity measurements and the head data set collected from one of the pumping operations. Once the estimated field converges to the given criteria, the newly estimated conductivity field, \hat{Y}_c , is the effective conductivity conditioned on head data due to pumping at the first location, and the residual conductivity covariance is the corresponding conditional conductivity

covariance. Subsequently, the conditional effective conductivity is used to evaluate the conditional mean head and sensitivity matrix, associated with pumping at the next location. Based on (11), the sensitivity matrix in conjunction with the conditional conductivity covariance then yields the head covariance and cross-covariance of head and conductivity that reflect pumping at the next location, which are subsequently employed in (8) to derive the new weights (Li and Yeh, 1999). With the conditional mean heads, new weights, and the observed heads, equation (7) yields the conductivity estimate, representing the first estimate based on the information from the pumping at the new location. The iterative process is then employed to include the nonlinear relationship between head and conductivity. The same procedure is used for the next pumping location. In essence, our sequential approach uses the estimated hydraulic conductivity field and covariances, conditioned on previous sets of head measurements, as prior information for the next estimation based on a new set of pumping data. It continues until all the data sets are fully utilized. Such a sequential approach allows accumulation of high-density secondary information obtained from hydraulic tomography, while maintaining the covariance matrix at a manageable size that can be solved with the least numerical difficulties. Vargas-Guzman and Yeh (1999) provided a theoretical proof to show that such a sequential approach is identical to the simultaneous approach for linear systems.

3. Design Criteria for Hydraulic Tomography

The design of the monitoring network, the pumping location, the number of pumping tests, and the pumping rate can influence the effectiveness of hydraulic tomography. In this section, the “optimum” design of hydraulic tomography is investigated by applying our sequential geostatistical inverse model to a two-dimensional, vertical, hypothetical aquifer. The hydraulic tomography experiment considered consists of two fully screened wells, separated into many vertical intervals by packers, in a confined aquifer. Water is pumped from the aquifer at one of the vertical intervals and after steady-state flow is established, head responses of the aquifer are monitored at the other intervals. The same procedure is then repeated at different pumping locations.

3.1. Aquifer description and evaluation criteria:

The hypothetical confined aquifer was assumed to be 20 m x 20 m, and was discretized into 400 elements of one meter square. Each element was assigned a conductivity value using a random field generator (Gutjahr, 1989). This generated conductivity field had a geometric mean of 0.44 m/hr and an exponential correlation structure with a variance of 0.63 for $\ln K$. The correlation structure was anisotropic: a horizontal correlation scale of 12 m and a vertical correlation scale of 4 m are used. The left and right sides of the aquifer were constant head boundaries (with a prescribed hydraulic head of 80 m), while the top and the bottom sides were set to be no-flux boundaries.

The performance of each network design was evaluated using the average absolute error norm, L1 and the mean square error norm, L2, which are defined as follows:

$$L1 = \frac{1}{n} \sum_{i=1}^n |\hat{f}_i - f_i| \text{ and } L2 = \frac{1}{n} \sum_{i=1}^n (\hat{f}_i - f_i)^2 \quad (14)$$

where f_i and \hat{f}_i represent the true and estimated perturbation of the log transformed conductivity, respectively, i indicates the element number and n is the total number of elements. The smaller the L1 and L2 values are, the better the estimate is.

Conditional variance of estimated conductivity, $\varepsilon_f(x_o, x_o)$ (see equations 12 and 13), is also used to evaluate the performance of the network design. The smaller the variance is, the more accurate the estimate. If the value of conductivity at a location is known exactly, the conditional variance at that location is zero.

3.2. Optimal monitoring network:

One factor that must be considered during the design of a hydraulic tomography experiment is the separation distance of the two wells and the interval of packer placements within the well. To address this issue, the first well in the numerical experiments was fixed at one location in the aquifer ($x = 13.5$ m, x is the horizontal coordinate) and the second well was located at various distances to create different configurations. Subsequently, many monitoring network designs using different combinations of well separation distances and packer intervals were examined. For each monitoring network design, a steady state flow was established by pumping at the fixed point (13.5 m, 13.5 m) and at a constant rate of 20 m³/hr. The aquifer head values

collected at each monitoring network were then used with our inverse model to estimate the hydraulic conductivity field.

Effects of horizontal well spacing and vertical packer intervals are shown in Figures 1a and b, where the contour maps of L1 and L2 for different values of $\Delta x / \lambda_x$, and $\Delta z / \lambda_z$ are plotted. The correlation scales in the x direction and the z direction are denoted by λ_x and λ_z , Δx is the separation distance between the two wells, and Δz is the vertical distance between neighboring packers. The “optimal” horizontal and vertical intervals are defined as those that yield the minimum of L1 and L2 over the entire domain. According to the figures, the optimal distance between the two wells (horizontal interval) is approximately half of the horizontal correlation scale. This distance can not be too large or too small because the best estimate of conductivity values is near the vicinity of the wells where pressure changes are collected (see section 5). The optimal vertical distance between packers along the well (vertical interval) should be as small as possible (at least smaller than 0.5 times the vertical correlation scale). Also shown is that the separation distance between the two wells has more influence on the conductivity estimates than that between vertical monitoring points along the well.

3.3. Optimal pumping interval:

The main idea of hydraulic tomography is to collect a large number of aquifer responses using the same monitoring network by changing the pumping locations along the wells. It is important to know how the choice of pumping interval (the distance between two adjacent pumping locations) influences the effectiveness of hydraulic tomography.

To address this issue, numerical experiments were conducted. Based on the results of the previous analysis, the horizontal separation distance of the two wells in the experiments was chosen to be 6 m and the vertical monitoring interval to be 2 m. Consequently, two wells were set up at $x = 7.5$ m and $x = 13.5$ m, and 10 monitoring intervals along each well were employed. The well at $x = 7.5$ m was chosen as the well where various pumping intervals would be considered. By changing the distance between two adjacent pumping locations from 2 m, to 4 m, 6 m, 8 m, etc., the effect of the pumping interval was then evaluated. Figure 2 shows the number of elements of the aquifer with the conditional variance less than some given values for different designs of the pumping interval. Based on this figure, the size of the pumping interval has little effect on the conditional variance. However, a slightly better estimate is obtained if the pumping interval is greater than 2 m, which is half of the vertical correlation scale. The same result is also obtained by evaluating L1 and L2 for different pumping intervals. Consequently, we conclude that the pumping interval should be greater than the half of the vertical correlation scale.

3.4. Optimal number of pumping locations:

From the analysis of the optimal pumping interval, we found that once the pumping interval is greater than the half of the vertical correlation scale, a further increase of the interval does not significantly improve the f estimate. Nonetheless, for a given aquifer thickness, the larger the pumping interval we select, the fewer the pumping locations we have, and the less information we can obtain from the tomography.

Therefore, it is imperative to determine the optimal number of pumping locations so that hydraulic tomography can provide sufficient secondary information.

The influences of increasing numbers of pumping locations on the effectiveness of the tomography are shown in Figures 3a and b. Figure 3a plots the number of f estimates with conditional variance lower than the specified threshold value for different number of pumping locations. For a given threshold value of the conditional variance (for instance, 0.1), as the number of pumping locations increases from 2 to 4, the number of f estimates with conditional variance smaller than 0.1 increases from 47 to 147. As the number of pumping locations increases to 5, the number of good f estimates increases from 147 to 164, showing that the rate of improvement decreases. The same trend is also shown in Figure 3b, where the values of L1 and L2 decrease significantly when the number of pumping locations increases from 2 to 4. Then, the decrease becomes moderate and L1 and L2 gradually approach a constant value when 5 pumping locations are used. The results show that an increase in the number of pumping locations improves the final f estimate but the improvement diminishes as more pumping locations are used, indicating that certain data sets generated from hydraulic tomography may provide redundant information. Based on this example, the optimal number of pumping location is 5 (20 m/4 m, here 20 m is the aquifer depth and 4 m is the vertical correlation scale). For a generic aquifer, we may conclude that the optimal number of pumping location is the ratio of the aquifer depth to the vertical correlation scale.

3.5. Effect of pumping rate:

Our numerical experiments show that the pumping rate does not affect the final estimate of conductivity. Under steady-state flow conditions, an increase in the pumping rate leads to an increase in the hydraulic gradient, which subsequently affects the sensitivity of head with respect to saturated conductivity. Such an increase in hydraulic gradients also results in an increase in head variance but the cross-correlation between the head and the conductivity remains the same. Consequently, the increase in the pumping rate does not affect the cokriging weights and does not influence the estimate (Li and Yeh, 1998). In other words, different pumping rates will yield identical results. One must recognize, though, that in practice, pressure head data may be corrupted by noises. Thus, an increase in pumping rate may increase the signal-to-noise ratio such that the inversion of hydraulic tomography data can yield better results.

4. Uncertainty Analysis

Our inverse method for the hydraulic tomography requires the knowledge of mean, variance, and correlation structure of the conductivity field, head data sets and the associated pumping rates, and some conductivity values if they are available. While head data and pumping rates can be collected during the tomography, several means can be employed to obtain the mean, variance, and correlation structure of the conductivity. For example, one can estimate them based on core samples and well logs if they are available or one can employ the structure identification approach developed by Kitanidis and Vomvoris (1983). Geophysical survey is an alternative for determining correlation scales

(Rea and Knight, 1998) and the traditional aquifer test analysis assuming aquifer homogeneity is a good way to estimate the mean conductivity.

Nevertheless, these statistical parameters are estimates and not known precisely, and measurement errors in pressure heads are inevitable. Therefore, the influence of the uncertainty in the statistical parameters and the effects of measurement errors on the estimate by our sequential inverse method are discussed next.

4.1. Uncertainty in the mean and variance of hydraulic conductivity

Without collecting a large number of hydraulic conductivity data sets, the mean and variance estimates involve uncertainty. How the uncertainty affects the estimate of hydraulic conductivity by our inverse method needs to be addressed. Several numerical experiments were conducted and the results show that the uncertainty in the mean conductivity can cause the shift of the mean of our estimated conductivity field. The pattern of heterogeneity remains almost the same. On the other hand, the uncertainty associated with the variance of conductivity has no influence on the final estimate. This is attributed to the fact that our inverse approach relies on the correlation and cross-correlation, which do not involve the variance. Specifically, as the variance term appeared on both sides of the system of equations (6 and 8), it is factored out and canceled when solving the equations for weights.

4.2. Uncertainty in correlation scales

In order to study the effect of the uncertainty in correlation scales, we used the previous hypothetical aquifer with the optimal network design as our base case. Then, we conducted many test cases in which the correlation scales in horizontal and vertical

directions were either overestimated or underestimated up to 90%. For each test case, the percent changes in the values of the norm L1 and L2 from the base case were computed and the changes for all the cases were then contoured. Figures 4a and b show that our inverse solution is not very sensitive to the uncertainty in correlation scales unless the uncertainty is so large that it completely alters the direction of anisotropy (e.g., the upper left corner of the figures). This can be attributed to the fact that the correlation structure only provides a description of the average size of heterogeneity. Once more point measurements (such as head information from tomography) become available, the impact of the information about the average size of heterogeneity fades out rapidly. The same argument applies to the effect of uncertainty in the shape of the correlation structure (correlation functions).

4.3. Measurement errors in pressure heads

To investigate impacts of these errors, we generated random head measurement errors with a zero mean and a variance that is equal to a specified fraction of the head variance for each monitoring location. The head variance was calculated based on the first-order analysis for the given pumping rate. The pressure head measurements at the monitoring locations were then perturbed with these errors and then were used in the inversion. Results of the inversion show that the estimate by our sequential inverse model is very sensitive to the errors: small measurement errors can lead to erroneous estimates of the conductivity field.

To extract useful information from the head data corrupted with errors, the error variances were added to the diagonal terms of the head covariance matrix, corresponding

to the head measurement locations, when the weights for the SLE were sought. Because of the addition of the variance, the estimated conductivity field becomes smooth and head values at the sampling locations do not agree with the observed values.

The effects of errors on our estimates using the above approach are shown in Figure 5, where the L1 and L2 norms are plotted as a function of the error. As demonstrated in the figure, the norm L1 and L2 grow rapidly when the error increases, which indicates that the estimate of the conductivity field is sensitive to the errors. However, when the variance of the error approaches more than 50% of the head variance, the rate of increase in L1 and L2 declines. This implies that the larger error the data set has, the less useful information the data set contributes. Therefore, our inverse method results in a smooth conductivity field that is close to the unconditional mean value.

4.4. Effect of gravel pack

Wells are usually gravel-packed over the screen interval. Several numerical experiments were conducted to address the effects of omitting the gravel pack in the inverse modeling. In the experiments, gravel packs of different uniform conductivity value around the two wells were considered in the forward simulation to produce head measurements. The measured heads were then used in the inversion. Results of the inversion show that the influence of the gravel pack depends upon the contrast between the hydraulic conductivity of the back-filled gravel and the mean conductivity of the aquifer system. If the conductivity of the gravel pack is close to the geometric mean of the conductivity of the aquifer, then its effect is negligible. However, if the gravel pack has a conductivity value that is several orders of magnitude greater than the geometric

mean of the aquifer, then its impact is significant. Since the gravel pack changes the head distribution the effect can be minimized by treating it as the head measurement error.

5. Monte Carlo Simulations

As mentioned in section 2.2, the conditional covariance functions (ε_{hh}) and cross-covariance functions (ε_{hy}) are approximations. One way to evaluate the accuracy of the approximations is to compare them to those provided by the Monte Carlo simulations. Accordingly, we conducted Monte Carlo simulations using thirty realizations of f fields. For each realization, five steady-state pressure head data sets were produced based on the optimum design of hydraulic tomography (section 3). In addition, two f measurements, one from each well, were included as primary information. Then, our proposed sequential inverse approach was employed. The difference between our estimate and the true conductivity field for each realization at each element was then accumulated to determine the conditional variance at each element.

The spatial distribution of the resulting conditional variance is shown in Figure 6a. Compared to the conditional variance of f calculated using the linear approximation (Figure 6b), the conditional variances obtained from Monte Carlo simulations are larger. Nonetheless, these two conditional variance maps show a similar pattern. That is, lower variances of f occur at locations along the wells where either pressure head or conductivity was measured. Such a result indicates that significant improvements, due to primary or secondary information, are limited to the vicinity of the measurement locations.

6. 3-D Case Example

To demonstrate the robustness of the sequential iterative approach for real-world problems, it was applied to hydraulic tomography in a three-dimensional hypothetical aquifer that had dimensions of 10 m x 5 m x 20 m. The aquifer was discretized into 1000 elements with dimensions of 1m x 1m x 1m. Four sides of the aquifer were constant hydraulic head boundaries with a prescribed value of 80 m while the top and the bottom of the aquifer were no-flow boundaries (Figure 7). We assumed the heterogeneous hydraulic conductivity field had a horizontal correlation scale of 12 m and a vertical correlation scale of 4 m. We further assumed that the geometric mean of the hydraulic conductivity was 0.3452 m/hr with a variance of $\ln K$ equal to 0.625. With these assumed parameters, the conductivity value for each element was generated using the spectral method (Gutjahr, 1989) (Figure 8a). Based on the optimum-sampling scheme (section 3), a total of 20 pressure measurement locations were used. Two conductivity measurements were taken on each of the wells located in the synthetic flow domain (Figure 7). A three-dimensional steady-state flow field created by pumping at a selected interval, with a discharge of 20 m³/hr was then simulated and the head responses at other intervals were monitored. By sequentially pumping at five different vertical locations (figure 7), five pressure/discharge data sets were obtained.

For each set of data, the SLE was used to determine the conditional effective hydraulic conductivity field. The field obtained from this set of head measurements was used as prior information for the next estimation of the conductivity field, using the next set of pressure/discharge data. This procedure was performed sequentially.

Figure 8b shows the f estimates based on only the head data set created by pumping at location No.1. Figure 8c shows the f estimates when the head data set created by pumping at location No.2 was included. Accordingly, Figure 8f shows the final f estimates when the fifth data set was included. As illustrated in these figures, the major features of the heterogeneity are captured in the first sequence of the inversion. By incorporating the secondary information sequentially in the inversion, more details of heterogeneity are revealed and the estimate field increasingly resembles the true one. A scatter plot of the final estimated f versus the true f values along with the two statistical norms L1 and L2 is displayed in Figure 9.

7. Conclusion

The sequential inverse approach using data yielded from hydraulic tomography is a promising tool for characterizing aquifer heterogeneity. By using the secondary information sequentially, the size of the covariance matrix in our inverse approach remains small so that the matrix equations can be solved with ease. Thus, inversion of the large amount of secondary information collected during hydraulic tomography becomes feasible. Compared to the results yielded from the Monte Carlo simulations, the residual variance produced from our sequential approach reflects the pattern of the conditional variance.

Results of our numerical experiments show that the hydraulic tomography can be most effective if the horizontal separation distance between wells is set to be half of the horizontal correlation scale. The vertical interval between two pressure monitoring

locations should be no more than half of the vertical correlation scale. The optimal number of pumping locations is equal to the ratio of the aquifer depth to the vertical correlation scale. The pumping rate has no effect on the estimate.

Our analysis also leads to the conclusions that the uncertainty in the input variance for our inverse model has no influence on the estimates. Similarly, the uncertainty in correlation scales has no significant effect on the estimate unless the correlation scales are extremely under-estimated or over-estimated. Abundant secondary information (such as pressure head) in space can greatly reduce the effect caused by inaccurate knowledge of the correlation structure. If large measurement errors associated with pressure head exist, our inverse approach yields a smoother estimate than that obtained from the error-free data, reflecting the fact that less information is extracted from the measurements. Consequently, accurate measurements of the secondary information are needed to make hydraulic tomography successful.

Finally, hydraulic tomography appears to be a promising field technique for providing abundant secondary information for characterizing aquifer heterogeneity. Using our sequential inverse model, hydraulic tomography can reveal more detailed aquifer heterogeneity than classical aquifer tests.

Acknowledgments

This research is funded in part by a DOE EMSP96 grant through Sandia National Laboratories (contract AV-0655#1) and in part by an EPA grant R-827114-01-0.

References

- Butler, J.J., Jr. and W.Z. Liu, Pumping tests in nonuniform aquifers: the radially asymmetric case, *Water Resour. Res.*, 29(2), 259-269, 1993.
- Butler, J.J., Jr., C.D. McElwee and G.C. Bohling, Pumping tests in networks of multilevel sampling wells: methodology and implications for hydraulic tomography, *Water Resour. Res.*, To appear, 1999.
- Dettinger, M. D. and Wilson, J. L., First order analysis of uncertainty in numerical models of groundwater flow, Part 1, Mathematical development, *Water Resour. Res.*, 17(1), 149-161, 1981.
- Gottlieb, J., and P. Dietrich, Identification of the permeability distribution in soil by hydraulic tomography, *Inverse Problems*, 11, 353-360, 1995.
- Gutjahr, A., Fast Fourier transforms for random field generation, N. M. Tech Project Report, 106 pp., 1989.
- Hanna, S. and T.-C. J. Yeh, Estimation of co-conditional moments of transmissivity, hydraulic head, and velocity fields, *Adv. in Water Resour.*, 87-93, 22(1), 1998.
- Hoeksema, R. J., and P. K. Kitanidis, An application of the geostatistical approach to the inverse problem in two-dimensional groundwater modeling, *Water Resour. Res.*, 20(7), 1003-1020, 1984.
- Hughson, D. L., and A. Gutjahr, Effect of conditioning randomly heterogeneous transmissivity on temporal hydraulic head measurements in transient two-dimensional aquifer flow, *Stochastic Hydrol. Hydraul.* 12(3), 155-170, 1998.
- Hughson, D. L., and T.-C. J. Yeh, A geostatistically based inverse model for three-dimensional variably saturated flow, *Stochastic Hydrol. Hydraul.* 12(5), 285-298, 1998.
- Hughson, D. L., and T.-C. J. Yeh, An inverse model for three-dimensional flow in variably saturated porous media, *Water Resour. Res.*, 36(4), 829-839, 2000.
- Kitanidis, P. K., and E. G. Vomvoris, A geostatistical approach to the inverse problem in groundwater modeling and one-dimensional simulations, *Water Resour. Res.*, 19(3), 677-690, 1983.
- Kitanidis, P. K., Comment on "A reassessment of the groundwater inverse problem" by D. McLaughlin and L. R. Townley, *Water Resour. Res.*, 33(9), 2199-2202, 1997.

Rea, J. and R. Knight, Geostatistical analysis of ground-penetrating radar data: A means of describing spatial variation in the subsurface, *Water Resour. Res.*, 34(3), 329-339, 1998.

Li, B., and T.-C. J. Yeh, Sensitivity and moment analysis of head in variably saturated regimes, *Adv. in Water Resour.*, 21, 477-485, 1998.

Li, B., and T.-C. J. Yeh, Cokriging estimation of the conductivity field under variably saturated flow conditions, *Water Resour. Res.*, 35(12), 3663-3674, 1999.

Sun, N.-Z., and W. W.-G. Yeh, A stochastic inverse solution for transient groundwater flow: parameter identification and reliability analysis, *Water Resour. Res.*, 28(12), 3269-3280, 1992.

Sykes, J.-F., J. L. Wilson, and R. W. Andrews, Sensitivity analysis of steady state groundwater flow using adjoint operators, *Water Resour. Res.*, 21(3), 359-371, 1985.
van Genuchten, M. T., A closed-form equation for predicting the hydraulic conductivity of unsaturated soils. *Soil Sci. Soc. Am. J.* 44, 892-898, 1980.

Vargas-Guzman, A. J. and T.-C. J. Yeh, Sequential kriging and cokriging: two powerful geostatistical approaches, *Stochastic Environmental Research and Risk Assessment*, 13, 416-435, 1999.

Yeh, W. W.-G., Review of parameter identification procedures in groundwater hydrology: the inverse problem, *Water Resour. Res.*, 22(1), 95-108, 1986.

Yeh, T.-C. J., Stochastic modeling of groundwater flow and solute transport in aquifers, *J. of Hydrologic Processes*, Vol. 6, 369-395, 1992.

Yeh, T.-C. J., Scale issues of heterogeneity in vadose-zone hydrology, in *Scale Dependence and Scale Invariance in Hydrology*, edited by G. Sposito, Cambridge Press, 1998.

Yeh, T.-C. J., A.L. Gutjahr, and M. Jin, An iterative cokriging-like technique for groundwater flow modeling, *Ground Water*, 33(1), 33-41, 1995.

Yeh, T.-C. J., and J. Zhang, A geostatistical inverse method for variably saturated flow in the vadose zone, *Water Resour. Res.*, 32(9), 2757-2766, 1996.

Yeh, T.-C., M. Jin, and S. Hanna, An iterative stochastic inverse method: conditional effective transmissivity and hydraulic head fields, *Water Resour. Res.*, 32(1), 85-92, 1996.

Zhang, J., and T.-C. J. Yeh, An iterative geostatistical inverse method for steady flow in the vadose zone, *Water Resour. Res.*, 33(1), 63-71, 1997.

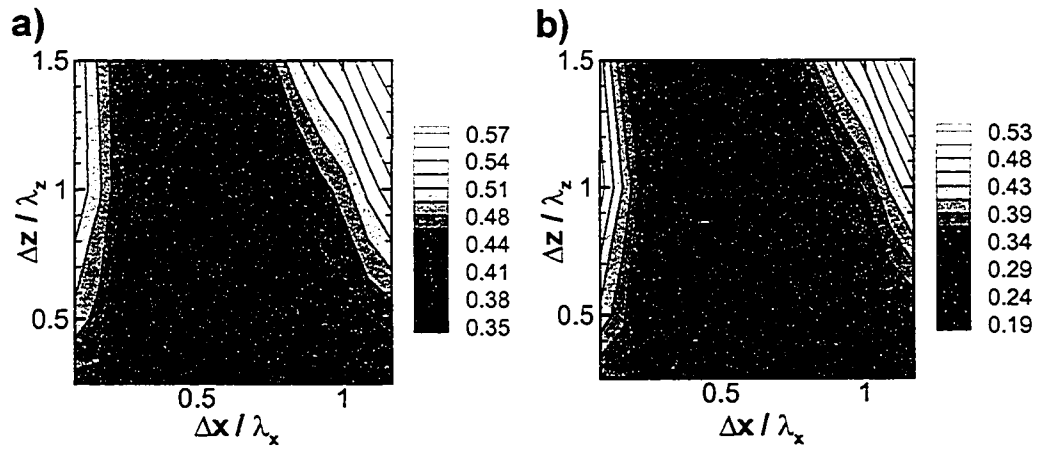


Figure 1. a) Contour map of norm L1 for different designs of hydraulic tomography. b) Contour map of norm L2 for different designs of hydraulic tomography. Here $\Delta x / \lambda_x$ represents the ratio of the well spacing to the horizontal correlation scale and $\Delta z / \lambda_z$ represents the ratio of the distance between packers to the vertical correlation scale.

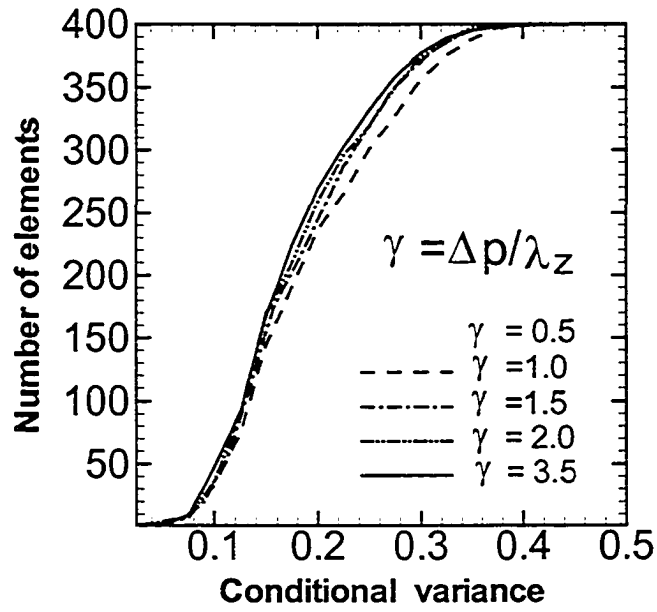


Figure 2. Comparison of the goodness of f estimate for various pumping intervals, represented by the number of elements whose conditional variance is less than a given threshold value. Here, γ is the ratio of the pumping interval Δp to the vertical correlation scale λ_z .

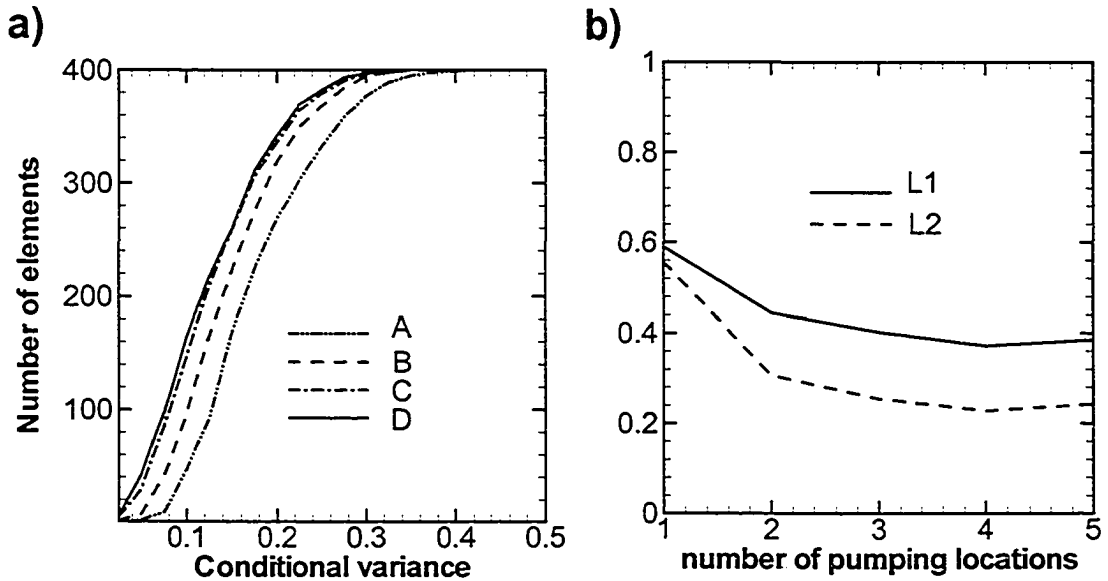


Figure 3. a) Comparison of the goodness of f estimate for various numbers of pumping locations, represented by the number of elements whose conditional variance is less than a given threshold value. A, two pumping locations; B, three pumping locations; C, four pumping locations; and D, five pumping locations. b) Norm L1 and L2 versus number of pumping locations.

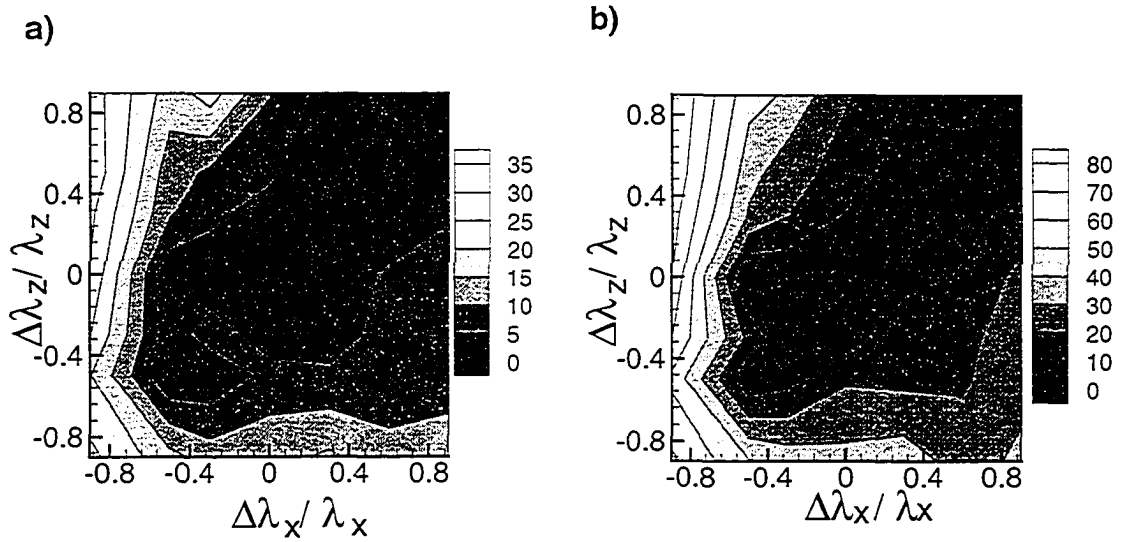


Figure 4. a) Contour map of the change of L1 in percentage for different values of $\Delta\lambda_x / \lambda_x$ (ratio of the change of horizontal correlation scale to the true correlation scale) and $\Delta\lambda_z / \lambda_z$ (ratio of the change of vertical correlation scale to the true correlation scale). b) Contour map of the change of L2 in percentage for different values of $\Delta\lambda_x / \lambda_x$ and $\Delta\lambda_z / \lambda_z$.

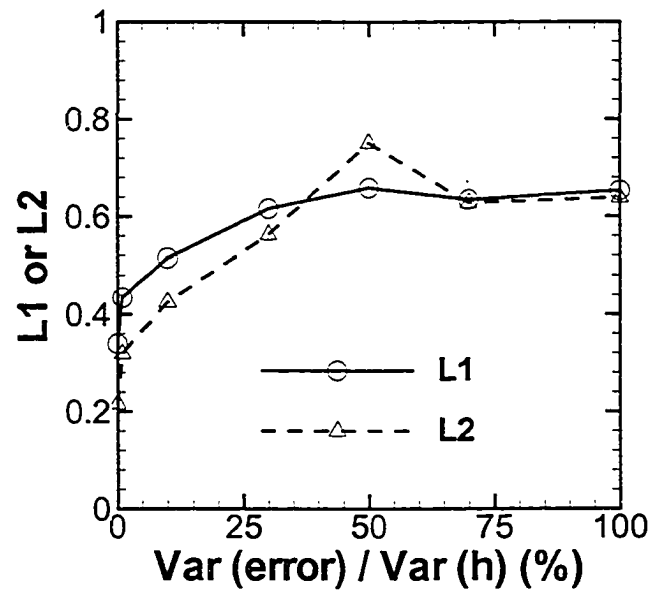


Figure 5. Norm L1 and L2 versus the percentage of the variance of measurement errors of head variance.

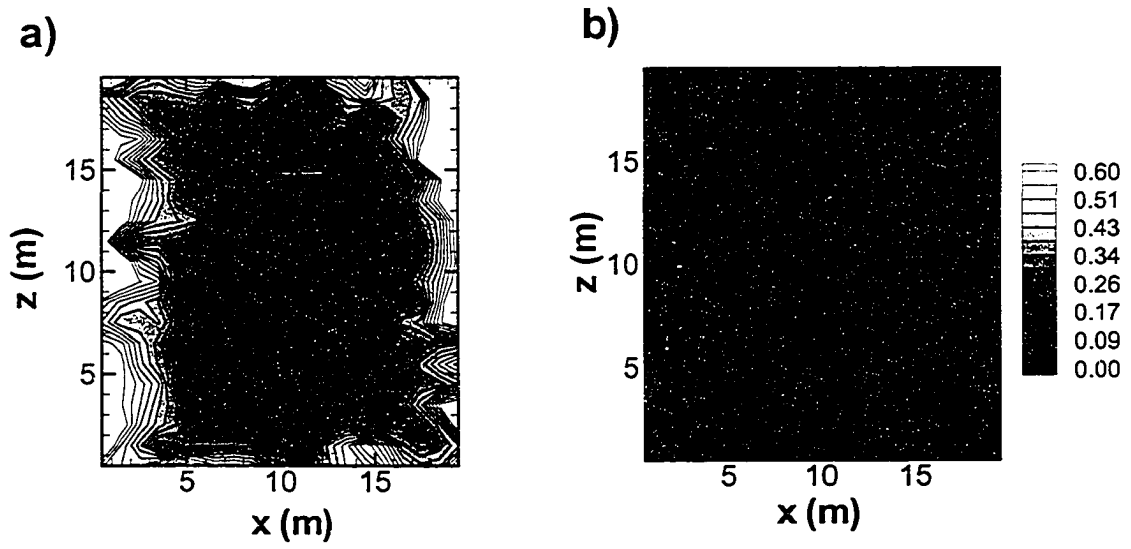


Figure 6. a) Contour map of the conditional variance of $\ln K$ (Monte Carlo simulations).
 b) Contour map of the conditional variance of $\ln K$ (our sequential inverse approach).

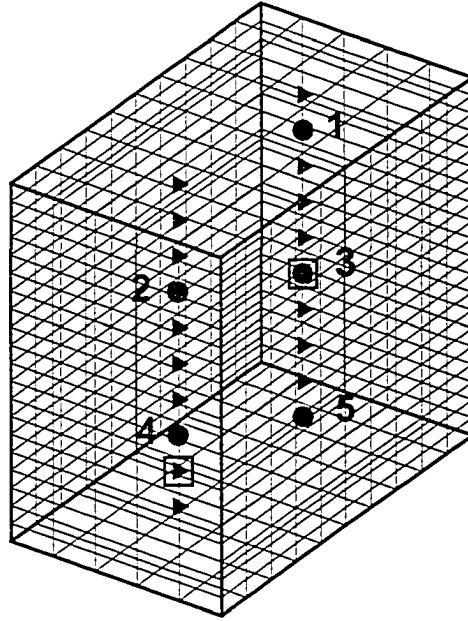


Figure 7. Schematic diagram of hydraulic tomography for a three dimensional aquifer. Right triangles indicate monitoring locations, circles represent pumping locations (the numbers next to them indicate the order of pumping), and squares represent f measurement locations.

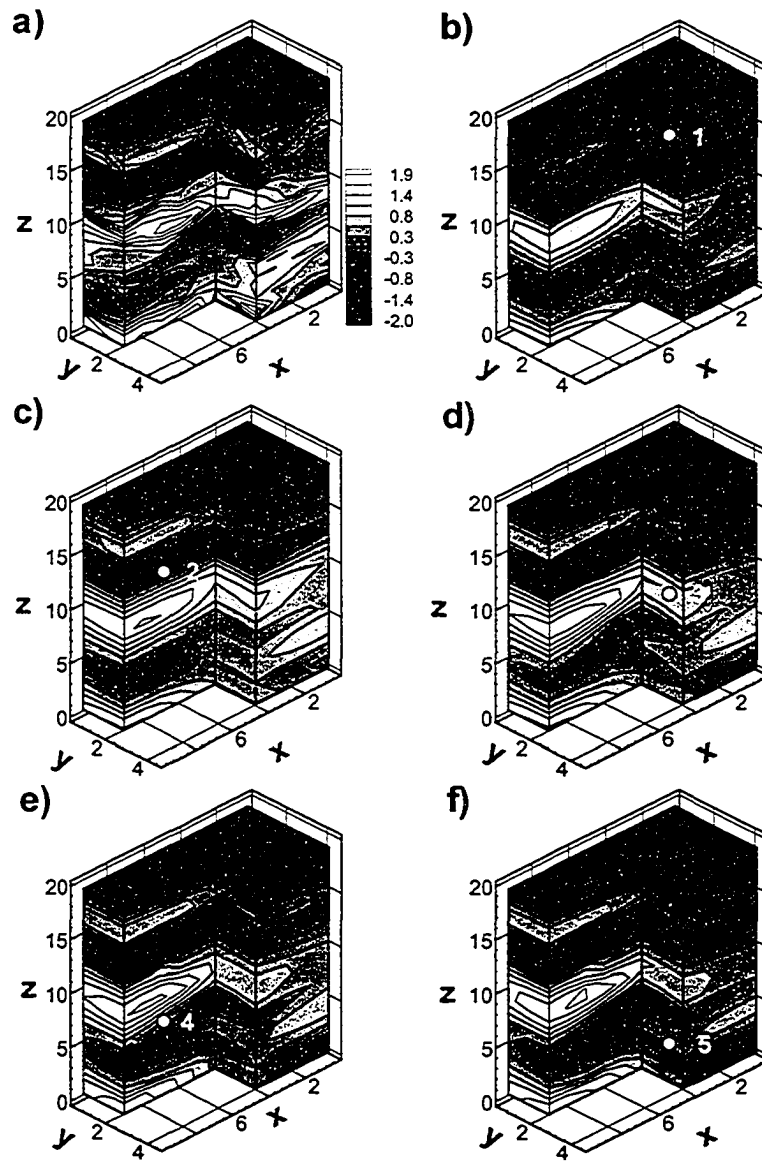


Figure 8. a) The synthetic true f field, b) estimated f field using data generated by pumping at location #1, c) estimated f field using data generated by pumping at location #1 and #2, sequentially, d) estimated f field using data generated by pumping at location #1, #2, and #3, sequentially, e) estimated f field using data generated by pumping at location #1, #2, #3 and #4, sequentially, f) estimated f field using data generated by pumping at location #1, #2, #3, #4, and #5, sequentially.

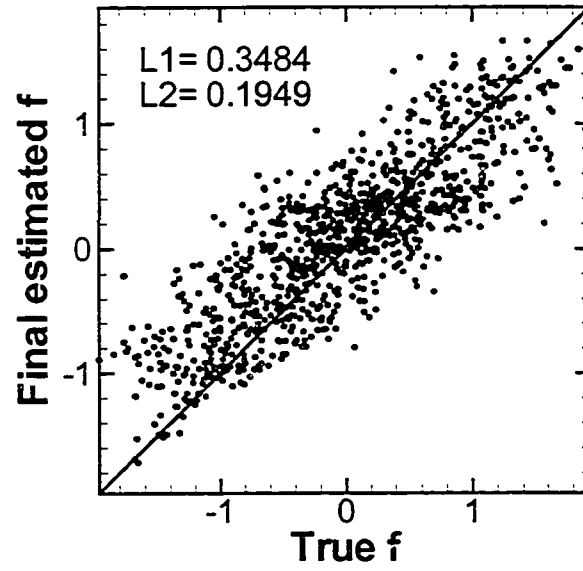


Figure 9. Scatter plot of estimated f field using five data sets sequentially versus true f field.

APPENDIX B

EFFECTIVENESS OF HYDRAULIC TOMOGRAPHY: SANDBOX EXPERIMENTS

Shuyun Liu, T. -C. Jim Yeh, Ryan Gardiner

Department of Hydrology and Water Resources

John W. Harshbarger Building

The University of Arizona,

Tucson, Arizona 85721.

accepted by
Water Resources Research

submitted : July, 2000

revised: January, 2001

Abstract

Two sandbox experiments were conducted to evaluate the performance of a sequential geostatistical inverse approach for hydraulic tomography in characterizing aquifer heterogeneity. One sandbox was packed with layered sands to represent a stratified aquifer while the other with discontinuous sand bodies of different shapes and sizes to represent a more complex and realistic heterogeneous aquifer. Parallel to the sandbox experiments, numerical experiments were conducted to assess the effects of measurement errors and uncertainties associated with laboratory data, and to diagnose the hydraulic conductivity estimates obtained from sandbox experiments.

Results of this study show that our sequential inverse approach works well under realistic conditions, in spite of measurement errors and uncertainties associated with pumping rates, boundary conditions, pressure head measurements, and other parameters required by our model. The tomography was found ineffective if abundant head measurements were collected at closely spaced intervals in a highly stratified aquifer. On the other hand, it was found beneficial when pressure head measurements were limited and the geological structure was discontinuous.

1. Introduction

Hydraulic tomography, a sequential aquifer test, has recently been proposed to characterize aquifer heterogeneity (Gottlieb and Dietrich, 1995; Butler and Liu, 1993; Butler et al., 1999; Yeh and Liu, 2000). Specifically, fully screened wells are divided into many vertical intervals using packers. Water is pumped from an aquifer at one of the intervals to create a steady state flow condition. Hydraulic head responses at other intervals are then monitored, yielding one set of head/discharge data. Then the pumping location is moved to another interval and the resulting steady state head responses at other locations are collected accordingly, resulting in a second data set. By performing this procedure sequentially, a large number of head/discharge data sets can be obtained. With a proper inverse methodology, these data sets can be used to produce a detailed image of heterogeneity in the aquifer.

Several researchers (Scarascia and Ponzini, 1972; Sagar et al., 1975; Giudici et al., 1995; and Snodgrass and Kitanidis, 1998) have investigated the use of data corresponding to different flow situations to improve the uniqueness of the inverse solution or to reduce uncertainties in the identification of flow model parameters. Until recently, very few researchers have investigated the idea of hydraulic tomography. Gottlieb and Dietrich (1995) proposed a hydraulic tomography method and employed a least-squares based inverse approach to illustrate its potential to identify the permeability distribution in a hypothetical two-dimensional saturated soil. Butler et al. (1999) applied the hydraulic tomography concept to networks of multi-level sampling wells. They developed new techniques for measuring drawdown at multi-level sampling ports that

had previously been unobtainable. They suggested that such sampling techniques could facilitate the implementation of hydraulic tomography in the field. Until recently, even fewer researchers have attempted to develop a realistic three-dimensional inverse model for hydraulic tomography because computational burdens hinder applications of classical inverse algorithms to 3-D hydraulic tomography. Yeh and Liu (2000) have developed a sequential geostatistical inverse approach that eases the burdens and allows one to efficiently interpret the abundant data sets produced by hydraulic tomography. In their study, not only did they demonstrate the robustness of their inverse approach, but they also investigated the network design issue for hydraulic tomography, and addressed uncertainty in the hydraulic conductivity estimate.

Hydraulic tomography has been tested using numerical experiments (Gottlieb and Dietrich, 1995; Yeh and Liu, 2000) but not laboratory or field experiments. In numerical experiments, effects of conceptual model errors are absent because synthetic tomography data are generated from the same model used in the inversion. Model inputs are also assumed error-free. Conversely, in field experiments, the effects of conceptual model errors are unknown. Model inputs, such as boundary conditions, pumping rates, the mean, variance, and correlation scales, are always subject to uncertainty. Further, the pressure head/discharge data inevitably contain unknown measurement errors. Field experiments are, thus, the most appropriate test for hydraulic tomography.

Nevertheless, field experiments are so costly that well-controlled sandbox experiments are a reasonable alternative. In this paper, we tested the effectiveness of our sequential inverse approach (Yeh and Liu, 2000) with two sandbox experiments. The

first experiment represented a stratified aquifer system, while the other represented a more complex and realistic heterogeneous aquifer. In addition, numerical experiments were conducted to diagnose anomalies in the inverse results from the sandbox experiments, and to explore conditions under which the hydraulic tomography can be effective.

2. Experimental Setup

2.1. Design of the Sandbox

The sandbox has outside dimensions of 92 cm in length, 4.5 cm in width, and 62 cm in height, and inside dimensions of 80 cm, 3.2 cm, and 50 cm, respectively. Two commercially sieved sands were used to pack the sandbox: a No. 30 and No. 60 silica sand. For No. 30 sand, greater than 60% of the sand is retained on sieve #30, whose mesh size is 0.6mm. For No. 60 sand, greater than 60% of the sand is retained on sieve #60, whose mesh size is 0.25mm. These two sands were selected because of the contrast in their grain sizes and the uniformity of their grain size distributions. The hydraulic conductivity of these two types of sand was determined using the constant head permeameter procedure (Klute and Dirksen, 1986). The resulting saturated hydraulic conductivity values were 0.165 cm/s for the medium sand (No. 30) and 0.038 cm/s for the fine sand (No. 60). These two sands were used to create two different structures of heterogeneity in the sandbox for flow experiments to be discussed in sections 2.2 and 2.3.

The sandbox was constructed with ¼ " acrylic, and supported by 1/8 " angle irons to brace the walls of the sandbox and to control bowing due to the mass of soil and water.

A network of 14 monitoring ports consisting of two columns of seven locations each was drilled into one face of the sandbox. A cylindrical filter with a diameter of 0.5 cm and a length of 2.5 cm was placed in each of the ports. These filters protruded into the soil, partially penetrated the sandbox, and were connected to the exterior of the sandbox through tubing. This allowed each location to be monitored by a pressure transducer or used as an extraction port. There are reservoirs on either side of the sandbox, and a constant head is maintained in these reservoirs through a mariotte device connected through inlets at the bottom of the reservoirs. This mariotte device consists of a sealed carboy with an atmospheric line set at the level of constant head in the sandbox. Water in the reservoirs enters the packed sand through perforated plates on either side of the box, which allow water to pass through, but prevent sand from leaking into the reservoirs (Figure 1).

During the tomography, some of the 14 monitoring ports were selected to be the pumping ports. Water was pumped using a vacuum pump and the flow field was allowed to reach steady state. The pumping rate was maintained constant throughout the experiment by use of a rotometer (Matheson Gas Products model #604). An increase in pumping rate causes a float to rise in relation to graduations on the rotometer, and a needle value of the rotometer allows one to adjust the pumping rate. The pumping rate was carefully selected during the two sandbox experiments. A pumping rate that is too low may cause changes in pressure smaller than the sensitivity of the instruments. A pumping rate that is too large could disrupt the upper boundary condition of the sandbox due to an insufficient communication between the reservoirs and the sand unit.

Pressure heads were monitored using gage pressure transducers during each pumping event. Data from the experiments were obtained using a Campbell Scientific Datalogger connected to two multiplexers, and were processed by the Campbell Scientific PC-208W software. The use of multiplexers allows for virtually simultaneous measurement of the transducers.

2.2. Description of Sandbox 1

Sandbox 1 was designed to represent a layered aquifer. A uniform and continuous horizontal layer of fine sand was packed in the middle of the sandbox with a thickness of 9.5cm and the remainder of the sandbox was packed with the medium sand. The configuration of sandbox 1 is shown in Figure 2.

During the data collection phase, the sandbox was pumped at one of the 14 ports, and the resultant steady-state pressure heads were recorded at the other 13 ports of the monitoring network. The flow in the sandbox reached steady state within approximately 10 seconds. Afterwards, the pump was moved to another port, and the corresponding pressure heads were collected, yielding the second data set. By performing this procedure sequentially, several data sets were obtained. For sandbox 1, three data sets were obtained by pumping at three different locations.

2.3. Description of Sandbox 2

Since the geological structure of an aquifer is typically more complex than that in sandbox 1, sandbox 2 was packed with the two types of sand but with a discontinuous and complex structure. Specifically, four lenses of fine sand were contained within a

medium sand matrix, with each lens of the fine sand exhibiting a different shape and size. The configuration of sandbox 2 is shown in Figure 3.

Our experience with sandbox 1 experiments (to be discussed in section 5.1) led to several modifications of the design of sandbox 2. Two more sampling ports on the upper part of the sandbox and two more at the lower part of the sandbox were added to each column of ports, for a total of 11 evenly spaced ports per column. These additional ports gave us more information of the pressure response of the system. The number of holes in the perforated plates connecting the reservoirs to the main portion of the sandbox was also doubled to ensure sufficient communication between these two regions. Finally, the diameter of the tubes connecting the mariotte device to the inlets in the reservoirs was increased to improve the reservoirs' response to changes in constant head level. Thus, the constant head boundary condition could be maintained at a stationary level with less uncertainty. Since there was some concern over the ability of the rotometer to accurately measure a low flow rate, in sandbox 2, the rotometer was replaced with a more accurate instrument of similar design (Key Instruments FR-4000 Model #4152).

During the implementation of hydraulic tomography in sandbox 2, data sets were again collected from the two columns of ports. Five data sets were created by pumping at five selected locations (see Figure 7), and each data set contained pressure head measurements for 21 locations.

3. Method of Analysis

A sequential geostatistical inverse approach was used to interpret the data yielded from hydraulic tomography in our sandbox experiments. Details of the approach can be found in Yeh and Liu (2000). Here only a brief description is provided.

Our approach is comprised of two steps. First, the successive linear estimator (SLE) is employed for each data set. This estimator starts with the classical cokriging technique using observed conductivity and head values collected in one pumping test during the tomography to create a cokriged, mean-removed log conductivity (f , i.e., perturbation of log conductivity) map. However, cokriging does not take full advantage of the observed head values because it assumes a linear relationship between heads and conductivity while the true relationship is nonlinear. To circumvent this problem, a linear estimator based on the difference between the simulated and observed head values is used successively to improve the estimate.

During the estimation, a simultaneous inclusion of all the head/discharge data collected during the tomography can lead to extremely large and ill-conditioned matrices that are difficult to solve (Hughson and Yeh, 2000). Thus, the second step of our approach is to use the head data sets sequentially. That is, once an estimated f field based on a set of head/discharge data is derived, it is employed along with the head data sets collected from the next pumping operation to obtain the next estimated f field. During this new estimation, the conditional effective parameters, the covariances and the cross-covariances derived from previous estimation are propagated to evaluate the weights of our new estimate (Li and Yeh, 1999). In essence, our sequential approach uses the estimated hydraulic conductivity field and covariances, conditioned on previous sets of

head measurements, as prior information for the next estimation based on a new set of pumping data. It continues until all the data sets are fully utilized. Such a sequential approach allows for the accumulation of high-density secondary information obtained from hydraulic tomography, while maintaining the covariance matrix at a manageable size that can be solved with minimal numerical difficulty. Vargas-Guzman and Yeh (1999) provided proof of the validity of such a sequential approach for linear systems.

4. Inputs to the Inverse Model

To solve the inversion problem, the sandbox was discretized into 1066 elements with dimensions of 1.95cm x 3.2cm x 1.95cm. Both sides and the top boundary were set to be constant head boundary conditions, while the bottom boundary of the sandbox was considered a no-flow boundary.

Inputs to our inverse model include the effective conductivity, the variance and correlation scales of hydraulic conductivity, pressure head/discharge data sets, and available point measurements of conductivity. The procedures we used to obtain the required input parameters are discussed below.

4.1. Effective hydraulic conductivity

Two approaches were used to obtain the effective hydraulic conductivity of the sandbox, K_{eff} . In the first approach, the geometric mean was computed to approximate K_{eff} . Since the conductivity of each sand used in the sandbox was measured and their spatial distributions were known, a simple calculation determines the geometric mean. That is,

$$\ln K_g = \frac{\sum_{i=1}^n \ln K_i}{n} \quad (1)$$

where K_g is the resulting geometric mean conductivity, n represents the total number of elements and K_i is the hydraulic conductivity of each element. However, this method does not consider the effect of packing and more importantly, the flow dynamics of the system. A more desirable approach to determine the effective hydraulic conductivity is by the use of model calibration. Specifically, the heterogeneous sandbox was considered as an equivalent homogeneous system. By adjusting the conductivity value of this fictitious medium to minimize the discrepancy between the simulated and the observed head values, the effective conductivity was obtained. Two criteria, L1 and L2, as described below, were used to evaluate the goodness-of-fit between the simulated head responses and the observed ones:

$$L1 = \frac{1}{n} \sum_{i=1}^n \left| \hat{H}_i - H_i \right| \quad (2)$$

$$L2 = \frac{1}{n} \sum_{i=1}^n \left(\hat{H}_i - H_i \right)^2 \quad (3)$$

where H_i and \hat{H}_i represent the observed and simulated pressure head, respectively.

The approach described above was applied to the simulated pressure responses at all 1066 elements based on the known f field subject to pumping at a given location. The contour map of the head distribution due to pumping at element #603 ($x=55.575\text{cm}$, $y=1.6\text{ cm}$, $z=28.275\text{ cm}$) of the heterogeneous field of sandbox 2, and that of the equivalent homogeneous field are plotted in Figure 4a. The corresponding scatter plot of

the pressure heads is shown in Figure 4b. Applications of this approach to the head distribution induced by pumping show that the effective conductivity value varies with the pumping location. This variation may be attributed to the non-ergodic flow condition due to the simple heterogeneous structure in the sandbox. Consequently, the final K_{eff} value was determined by taking the average of these values. Table 1 tabulates the K_{eff} values obtained from pumping at elements #341($x=24.375$ cm, $y=1.6$ cm, $z=16.575$ cm), #603($x=55.575$ cm, $y=1.6$ cm, $z=28.275$ cm), and #767($x=55.575$ cm, $y=1.6$ cm, $z=36.075$ cm). Averaging the three K_{eff} values yields the final K_{eff} of 0.1242 cm/s.

We also applied the same procedure to the pressure head data collected in the laboratory sandbox experiments. However, there are fewer points in the laboratory data (21 points) than in the synthetic data (1066 points). Estimated effective conductivity values for each pumping location are given in Table 2. The averaged K_{eff} value is 0.0783 cm/s. The estimated K_{eff} values using both simulated and observed heads were employed in our analysis for sandbox 2. The effect of this input parameter on our f final estimate is discussed in section 5.

4.2. Other inputs

The variance and the correlation scales of the conductivity field -- our inverse model assumes an exponential correlation structure -- are also required input to our inverse model. Table 3 lists values of these statistical parameters used in our inverse analysis for both sandbox 1 and sandbox 2.

Estimation of the variance always involves uncertainty. Our previous numerical study (Yeh and Liu, 2000), however, has demonstrated that the variance has negligible

effects on the estimated hydraulic conductivity using our inverse model. Therefore, an estimate of the variance was obtained based on the known conductivity distribution and measured conductivity of each sand.

Correlation scales represent the average size of heterogeneity that is critical for analyzing the average behavior of aquifers. Correlation scales of any geological formation are difficult to determine in general. The effects of uncertainty in correlation scales on the estimate based on the tomography are negligible because the tomography produces a large number of head measurements, reflecting detailed site-specific heterogeneity (Yeh and Liu, 2000). Therefore, the correlation scales were approximated based only on the average thickness and length of the heterogeneity.

5. Results

5.1. Sandbox 1

The “true” mean-removed natural log of the conductivity (the “true” f field) in sandbox 1 is depicted in Figure 5a, and the estimated f field based on the head data set produced by pumping at the first location is plotted in Figure 5b. Figure 5c shows the estimated f field using the head data set obtained by pumping at the second location, in addition to the data set used in Figure 5b. The final estimate, based on the head data sets from the pumping at the third location and those used in Figures 5b and 5c, is illustrated in Figure 5d. Note that the “true” f field depicted in Figure 5a is our conceptualization of the conductivity distribution based upon the geometry of the layered sands and conductivity measurements of the sand samples. This field may not correspond to the

actual conductivity field in the sandbox. According to the figures, the estimated f field upon the sequential inclusion of data sets, nevertheless, gradually resembles the “true” field at the region where we had pressure head measurements. At the upper and lower portions of the sandbox, where measurements were not available and the model boundaries were nearby, the estimate of f was poor. Several factors could be responsible for the poor estimates: a lack of pressure measurements at these regions; boundary effects; uncertainties in the input data.

To investigate possible causes of the poor estimate, numerical experiments were conducted. First, we assumed the “true” f field is identical to the one shown in Figure 5a. Forward simulations were then carried out using the same pumping rate, pumping locations, and boundary conditions. Afterwards, three error-free head data sets were collected from the simulations at the monitoring locations identical to those in the sandbox experiments. Our inverse model was then employed to estimate the f field using these synthetic data sets. The final estimate is displayed in Figure 6a. Compared to Figure 5d (the final estimated f field using the laboratory data), Figure 6a is a better estimate because the synthetic data sets do not involve any uncertainty inherent in our laboratory data sets. However, at the region where there are no pressure measurements, the f estimate is still poor. This indicates that some point measurements are lacking and may thus be necessary at this region. To substantiate this speculation, simulated head data were collected at two more measurement points of the top and the bottom of the two columns. Consequently, 21 pressure head measurements instead of 13 were sampled and were subsequently used in our inverse model. The resultant f estimate is shown in Figure

6b, which indicates that the increase of pressure measurements significantly improves the final f estimate.

Since the additional pressure measurements improved the f estimate, we then tested the inversion with the maximum number of pressure measurements along the two columns. In this case, the inversion employed 51 pressure head measurements instead of 21 for each pumping operation. As expected, the abundant point measurements significantly improved our estimate of the heterogeneity in the sandbox. More importantly, we observed that in this case, only one pumping test was necessary to closely reproduce the “true” f field, and the inclusion of additional data sets from pumping at the other locations did not improve the estimate. Figure 6c illustrates the estimated f field using 51 pressure head measurements corresponding to pumping at element #603 ($x=55.575\text{cm}$, $y=1.6\text{ cm}$, $z=28.275\text{ cm}$) only. This result suggests that in a layered aquifer, hydraulic tomography is not necessary if one can collect a large number of closely spaced pressure measurements during one pumping test.

Criteria similar to (2) and (3) were also employed to quantify the success of our estimated f fields. The values for L1 and L2 associated with these estimated fields for sandbox 1 are listed in Table 4. The smaller the values of L1 and L2, the better our estimates.

With the help of synthetic data sets, the causes of poor estimates based on the actual laboratory data appeared to be diagnosed. While a lack of pressure head measurements on the upper and lower portion of the sandbox was one reason for the poor estimates, the boundary effects during experiments could not be excluded. Specifically,

the design of sandbox 1 was not able to keep the upper boundary condition at the specified level during pumping tests. In order to reduce this boundary effect, several improvements were made in the design of sandbox 2. Details are discussed in section 2.3.

5.2. Sandbox 2

Because sandbox 2 has a more complex heterogeneous structure, data sets from five sequential pumping tests were used for the inversion. Figure 7 illustrates the comparison of the “true” f field and those produced from the successive inclusion of the five data sets. The conductivity of 0.0783cm/s determined from laboratory data was used as the effective conductivity in this inversion. As shown in Figure 7, the estimated f field progressively resembles the true one and successively reveals more details of heterogeneity.

To investigate the effects of the uncertainty associated with effective conductivity, another inversion was conducted using 0.1242cm/s as the effective conductivity while keeping other inputs the same. The result is shown in Figure 8. Comparing Figure 7f with Figure 8--two final f estimates corresponding to the use of two different effective values--we find that the resulting conductivity is different in magnitude but the major heterogeneous patterns are similar.

An inversion was also conducted using synthetic data sets. Again, the synthetic data sets were sampled from the pressure head fields derived from flow simulations based on the conceptualized “true” f field under the same conditions as those in the lab. Figure 9 displays the final inversion result. Comparing Figure 7f and Figure 8 to Figure 9, we

find that all three figures adequately captured the major features of the heterogeneity of sandbox 2 (the four lenses of fine sand contained in the medium sand matrix). However, Figure 9 appears to have a slightly better result over the entire domain for the reason that synthetic data sets do not contain any measurement errors and other uncertainties. Again, please note that the exact true f field in sandbox 2 is unknown except for the general pattern. Considering the fact that measurement errors and some uncertainties in boundary conditions and input parameters are inevitable, the result (Figure 7f) of our inverse modeling is promising.

To evaluate the efficiency of hydraulic tomography under the conditions of sandbox 2, numerical experiments were conducted. These experiments considered measurements taken at five columns with 26 locations each, instead of the previous laboratory configuration of two columns with 11 locations each, and kept other conditions the same. Therefore, for each pumping operation, head responses at 129 locations were collected. This large amount of secondary information dramatically improved the final estimated f field (Figure 10). The values for L1 and L2 associated with these estimated fields for sandbox 2 are listed in Table 5. It is interesting to observe that the 129 head responses generated by a single pumping event in sandbox 2 did not reproduce the true f field as effectively as the 51 pressure head measurements in sandbox 1. The discontinuous and non-uniform nature of the sand structures in sandbox 2 explains the difference. Consequently, multiple head/discharge sets obtained by hydraulic tomography are necessary to produce a more detailed hydraulic conductivity distribution in this case.

6. Conclusion

The performance of our sequential inverse approach for hydraulic tomography was evaluated using two sandbox experiments. One sandbox was packed with layered sands to represent a stratified aquifer. The other was packed with discontinuous sand bodies of different shapes and sizes to represent a more complex and realistic heterogeneous aquifer. For both sandbox experiments, our inverse model was able to reproduce the major heterogeneous patterns. The results show that our approach works well under realistic conditions, in spite of measurement errors and uncertainties associated with the pressure head/discharge data sets and other input parameters required by our model.

Results of our analysis indicate that in the cases we investigated, hydraulic tomography does not improve the conductivity estimate significantly if abundant head measurements are available. This is especially true for a stratified aquifer system represented in sandbox 1. Hydraulic tomography can be useful and effective when pressure head measurements are not available at a large number of sample locations, and when aquifer heterogeneity exhibits highly discontinuous and non-uniform nature as presented in sandbox 2.

Paralleled numerical experiments were useful in this study. Not only did they assess the effects of measurement errors and uncertainties associated with laboratory data, but also helped to diagnose the causes of those poor estimates. This diagnosis improved our design of sandbox 2.

Our well-controlled sandbox experiments tested the effectiveness of our inverse method for realistic problems where measurements are inherently imperfect. Our successful laboratory verifications of the inverse approach is a step towards application of our inverse model to field-scale problems.

Acknowledgements

The authors are grateful for useful comments by Mauro Giudici and Michael H. Young. This research is funded in part by a DOE EMSP96 grant through Sandia National Laboratories (contract AV-0655#1) and a DOE EMSP99 grant through University of Wisconsin, A019493, and in part by an EPA grant R-827114-01-0. This work does not necessarily reflect the views of DOE and EPA, and no official endorsement should be inferred.

References

- Butler, J.J., Jr. and W.Z. Liu, Pumping tests in non-uniform aquifers: the radially asymmetric case, *Water Resour. Res.*, 29(2), 259-269, 1993.
- Butler, J.J., Jr., C.D. McElwee and G.C. Bohling, Pumping tests in networks of multilevel sampling wells: methodology and implications for hydraulic tomography, *Water Resour. Res.*, 35(11), 3553-3560, 1999.
- Giudici M., Morossi G., Parravicini G., and Ponzini G., A new method for the identification of distributed transmissivities, *Water Resour. Res.*, 31, 1969-1988, 1995.
- Gottlieb, J., and P. Dietrich, Identification of the permeability distribution in soil by hydraulic tomography, *Inverse Problems*, 11, 353-360, 1995.
- Hughson, D. L., and T.-C. J. Yeh, An inverse model for three-dimensional flow in variably saturated porous media, *Water Resour. Res.*, 36(4), 829-839, 2000.
- Klute A. and C. Dirksen, Hydraulic conductivity and diffusivity: laboratory methods, in A. Klute (ed.) *Methods of Soil Analysis, Part I*, Chapter 9: Agronomy, 687-734, Am. Soc. Agron., Madison, Wisc., 1986.
- Li, B., and T.-C. J. Yeh, Cokriging estimation of the conductivity field under variably saturated flow conditions, *Water Resour. Res.*, 35(12), 3663-3647, 1999.
- Sagar B., Yakowitz S., and Duckstein L., A direct method for the identification of the parameters of dynamic nonhomogeneous aquifers, *Water Resour. Res.*, 11, 563-570, 1975.
- Scarascia S., and Ponzini G., An approximate solution for the inverse problem in hydraulics, *UEnergia Elettrica*, 49, 518-531, 1972.
- Snodgrass M. F., and Kitanidis P.K., Transmissivity identification through multi-directional aquifer stimulation, *Stochastic Hydrol. Hydraul.*, 12, 299-316, 1998.
- Vargas-Guzman and T. -C. J. Yeh, Sequential kriging and cokriging: two powerful geostatistical approaches, *Stochastic Environmental Research and Risk Assessment*, 13, 416-435, 1999.
- Yeh, T. -C. J., and S. Liu, Hydraulic tomography: development of a new aquifer test method, *Water Resour. Res.*, 36(8), 2095-2105, 2000.

Table 1. Summary of K_{eff} values computed using synthetic data for sandbox 2

Pumping location	K_{eff} (cm/s)	L1	L2
Element # 341	0.1040	0.14032	0.03604
Element # 603	0.1335	0.08361	0.03108
Element # 767	0.1350	0.06552	0.00777
Average	0.1242		

Table 2. Summary of K_{eff} values computed using laboratory data for sandbox 2

Pumping location	K_{eff} (cm/s)	L1	L2
Element # 341	0.080	0.3362	0.1920
Element # 603	0.080	0.2748	0.1123
Element # 767	0.075	0.3219	0.1724
Average	0.0783		

Table 3. Inputs specification for sandbox 1 and sandbox 2

	K_{eff} (cm/s)	σ_f^2	λ_x (cm)	λ_z (cm)	covariance model for f	pumping rate (cm ³ /s)
Sandbox 1	0.1142 (from laboratory data)	0.34	400	20	exponential	2.94
Sandbox 2	0.1242 (from synthetic data) 0.0783 (from laboratory data)	0.46	300	20	exponential	3.33

Table 4. L1 and L2 values for estimates of sandbox 1

	Fig. 5b	Fig. 5c	Fig. 5d	Fig. 6a	Fig. 6b	Fig. 6c
L1	0.8984	0.8031	0.8542	0.1474	0.1339	0.0518
L2	1.4450	1.1852	1.2868	0.0476	0.0474	0.0095

Table 5. L1 and L2 values for estimates of sandbox 2

	Fig. 7b	Fig. 7c	Fig. 7d	Fig. 7e	Fig. 7f	Fig. 8	Fig. 9	Fig. 10
L1	0.7475	0.6027	0.5251	0.5229	0.5178	0.4563	0.3137	0.1459
L2	0.8573	0.5844	0.3897	0.4245	0.4160	0.3195	0.1677	0.0470

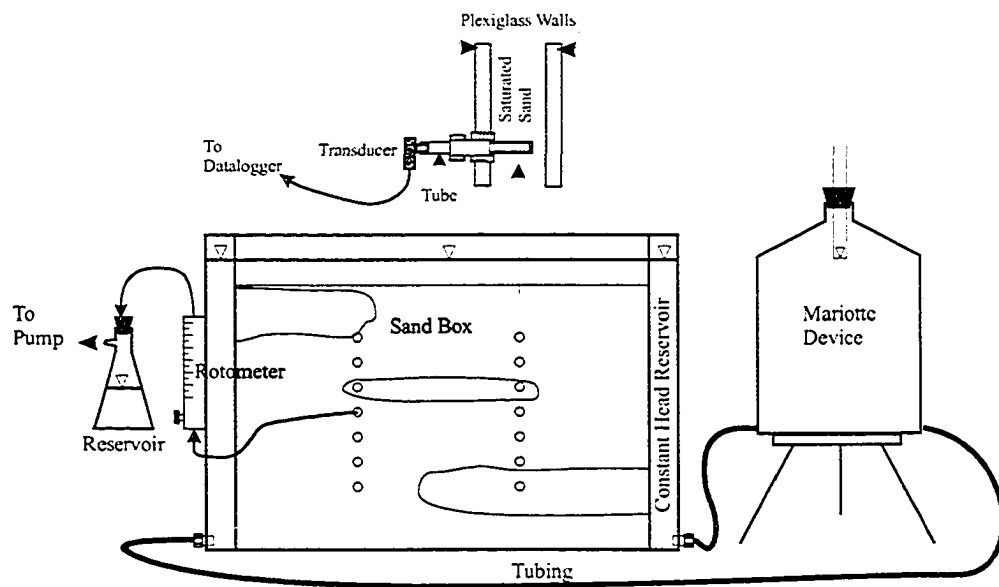


Figure 1. Sandbox design and experimental apparatus.

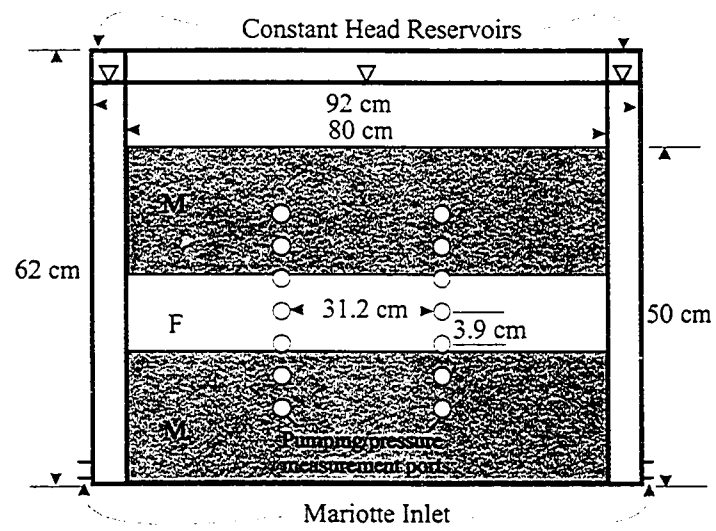


Figure 2. Sandbox 1 configuration. F = fine sand, and M = medium sand.

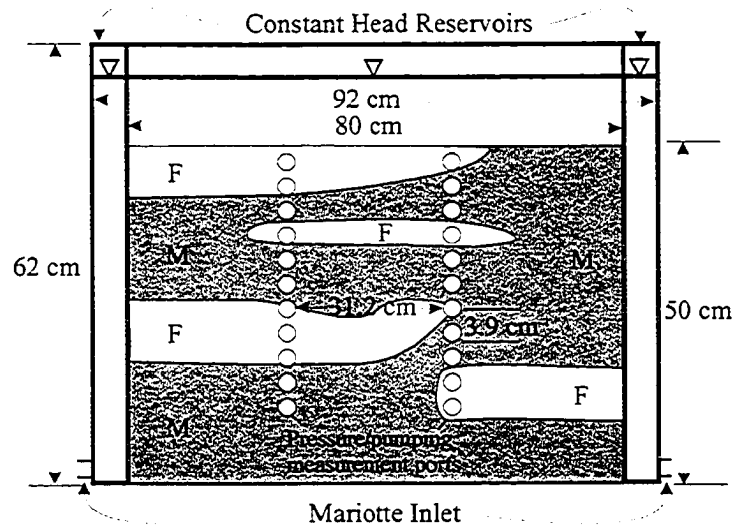


Figure 3. Sandbox 2 configuration. F = fine sand, and M = medium sand.

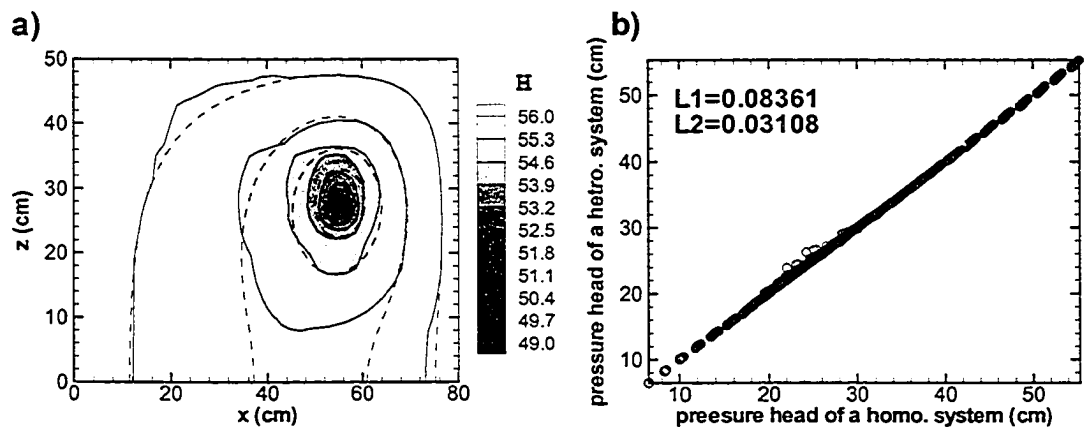


Figure 4. a). Comparison of the total head field for a single pumping event at element # 603 of heterogeneous and equivalent homogeneous systems. Shaded contours are the head field for the heterogeneous system and the dashed line for the equivalent homogeneous system. b). The scatter plot corresponding to (a).

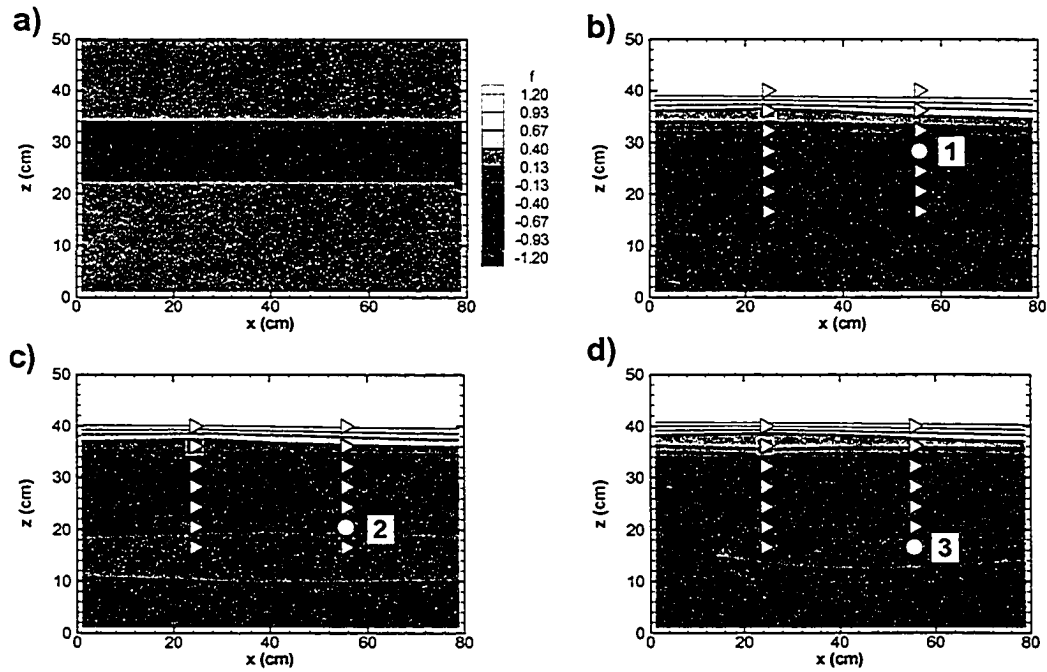


Figure 5. a) The "true" f field for sandbox 1; b) estimated f field using laboratory head data for pumping at location #1 (the circle); c) estimated f field based on data from pumping at the location #1 and 2); d) estimated f field using data produced by pumping at locations #1, 2, and 3. The triangles indicate the monitoring locations, and the square show the conductivity measurement locations.

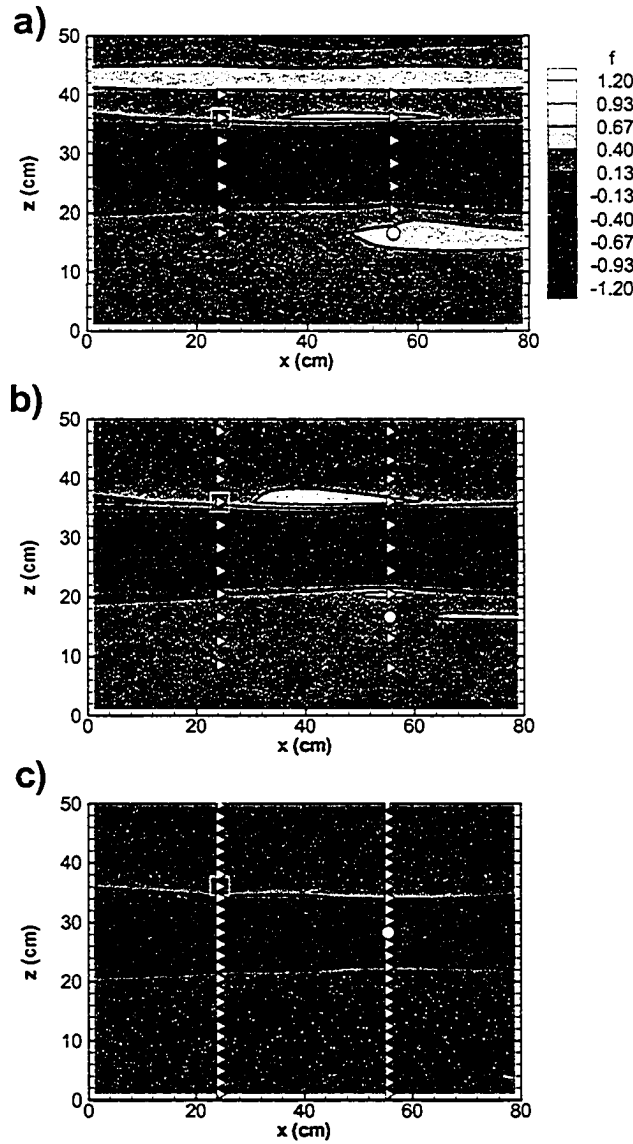


Figure 6. a) Estimated f field using three synthetic head data sets generated by the same pumping operations and locations as in Figure 5; b) estimated f field using the three synthetic data sets but with 8 more monitoring locations for each pumping; c) estimated f field using only one synthetic data set generated by pumping at the location of circle and monitoring at the locations indicated by triangles. The square shows the conductivity measurement location.

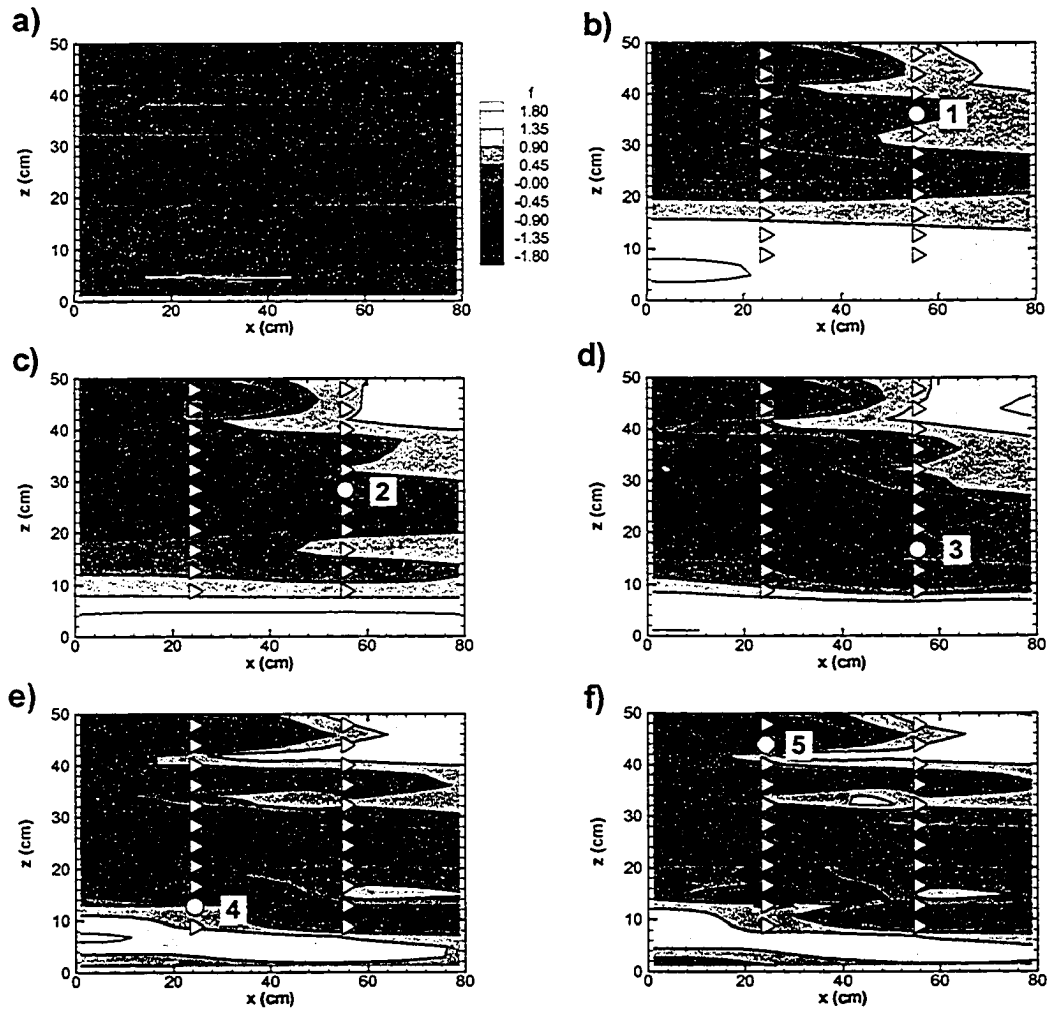


Figure 7. a) The "true" f field for sandbox 2; b) estimated f field using laboratory head data corresponding to pumping at location #1 (the circle) and the effective conductivity of 0.0783 cm/s; c) estimated f field after including head data corresponding to pumping at location #2 (the circle) in addition to the data from pumping at location #1; d) f estimate using head data sets from pumping at locations #1, 2, and 3 indicated by the circles; e) estimated f field using data sets from pumping at the locations #1, 2, 3, and 4; f) estimated f field using head data sets from pumping at location #1, 2, 3, 4, and 5. The triangles indicate the monitoring locations. The square shows the conductivity measurement location.

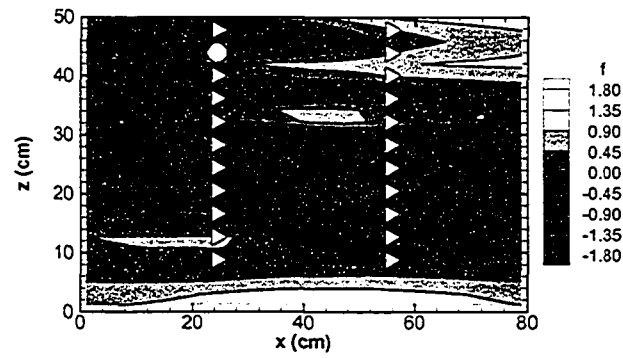


Figure 8. The final estimated f field using the same five laboratory data sets as those in Figure 7, but a different effective conductivity of 0.1242 cm/s.

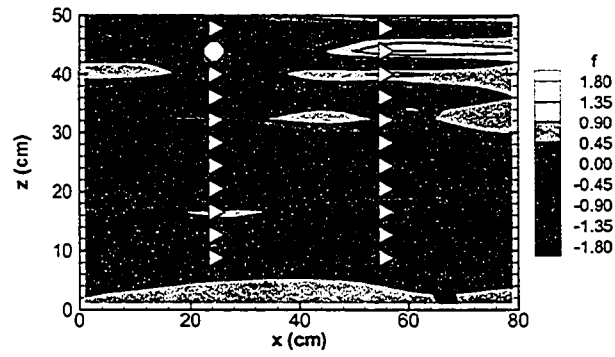


Figure 9. The final estimated f field using five synthetic data sets generated by using the same configuration as that in Figure 7.

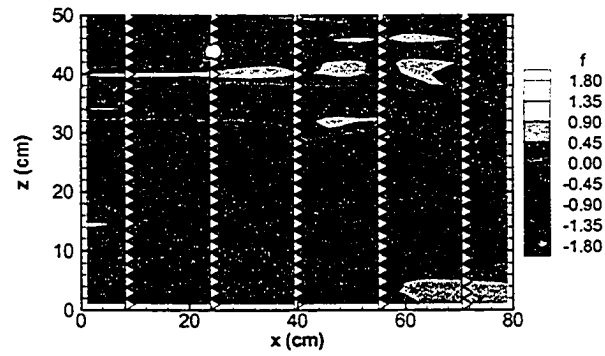


Figure 10. The final estimated f field using five synthetic data sets, generated by pumping at the same locations as those in Figure 7, and monitored at the locations indicated by triangles. The square shows the conductivity measurement location.

APPENDIX C

UNCERTAINTIES IN INTERPRETATION OF ELECTRICAL RESISTIVITY SURVEYS IN SUBSURFACE HYDROLOGICAL APPLICATIONS

Yeh, T.-C. J, Shuyun Liu,

Department of Hydrology and Water Resources
The University of Arizona

K. Baker

Idaho Environmental and Engineering Laboratory

R. Glass, J. R. Brainard

Sandia National Laboratory

D. Alumbaugh

University of Wisconsin

D. LaBrecque

Multiphase Flow

Submitted to
Water Resources Research

January 22, 2001

Abstract

A sequential, geostatistical inverse approach is developed for electrical resistivity tomography. The sequential approach mimics the sequential ERT data collection scheme commonly employed in the field survey to reduce equipment costs. The approach also allows one to include point measurements of resistivity, in addition to potential measurements from the ERT survey, and information on geological structures through statistical covariances to constrain the estimate of the resistivity field. The approach is computationally efficient, allows fine-grid discretization of the solution domain, and permits sequential inclusion of different data sets. Furthermore, the conditional variance in the inverse model quantifies the uncertainty of the estimate.

Numerical experiments were conducted to demonstrate the robustness of the inverse approach for delineating the resistivity distribution in the subsurface and to investigate effectiveness of different sampling arrays of the ERT: surface, down-hole, and a combination of surface and down-hole arrays. The orientation of bedding was found to dictate the effectiveness of the ERT layout.

A statistical analysis was undertaken to explore effects of spatial variability of the resistivity-moisture relationship on uncertainty in relating the change in resistivity to the change in water content in the vadose zone. Samples were collected to quantify spatial variability of the resistivity-moisture relationship in the field. Numerical experiments then illustrated how the spatially varying relationship exacerbated the level of uncertainty in the interpretation of change of moisture content based on the estimated change in resistivity.

1. Introduction

The dc resistivity survey is an inexpensive and widely used technique for investigation of near surface resistivity anomalies and it recently has become popular for the investigation of subsurface pollution problems (NRC, 2000). In principle, it measures the voltage generated by transmission of current between electrodes implanted at the ground surface. Apparent (bulk or effective) resistivity is then calculated and used to interpret subsurface structures.

The conventional resistivity survey includes vertical sounding and profiling (Sharma, 1997). Vertical sounding intends to provide a resistivity map as a function of depth. In a sounding, voltage probes are fixed at a center location in between two source electrodes and voltages are measured at a variety of source electrode separation distances (i.e., the Schlumberger array). The depth of investigation increases with separation distance. In the classical interpretation of the sounding survey, the apparent resistivity for a given source electrode separation distance is determined using the voltage measurement and an analytical model that assumes resistivity homogeneity of the subsurface. Because of the homogeneity assumption, the calculated resistivity represents a spatially averaged resistivity value over a volume of geological media that varies with the distance between the source electrodes. The greater the distance between the source electrodes, the greater volume the apparent resistivity represents. As a result, sounding is most suitable for the cases where the geological formation is made of only a few layers with significant resistivity contrast or where a relatively uniform formation embeds some simple objects of resistivity distinctly different from the surrounding media. For more complex heterogeneity patterns, deciphering

signals from the survey becomes more difficult, subjective, non-unique and highly uncertain due to the averaging nature of the apparent resistivity.

Profiling is used to detect lateral changes in resistivity. In profiling, the spacing between current electrodes and between the two voltage probes is fixed, and the relative position of the electrodes and probes array is also fixed in space, but the entire array is moved laterally (i.e., the Wenner array). At a given array position, measurements of current and voltage are used to determine the apparent resistivity, by using an analytical formula that assumes subsurface homogeneity. Again, the estimated apparent resistivity is a volume-averaged property. As a consequence, the estimated resistivity field is generally very smooth unless there is a distinct resistivity anomaly in the subsurface.

Because the homogeneity assumption is implicit in the formulas for calculating apparent resistivity, and the potential field is smooth due to its highly diffusive nature, conventional interpretations of resistivity survey data have been virtually ineffective in environmental hydrology or pollution applications, where resistivity anomalies are subtle, complex, and multi-scale. To overcome these difficulties, a contemporary resistivity survey collects extensive current and electrical potential data sets in multi-dimensions. Without assuming subsurface homogeneity, a mathematical computer model is employed to invert the data sets to estimate the resistivity field, using the minimum output error (MOE) criterion (e.g., Ellis and Oldenburg, 1994; Li and Oldenburg, 1994; Zhang et al., 1995; and Daily et al., 1992). However, the general uniqueness and resolution of the three-dimensional resistivity inversion have not been sufficiently investigated thus far (NRC, 2000).

While the physical process is different, the governing equation for electrical currents

and potential fields created in the resistivity survey is analogous to that for steady flow in saturated porous media. The mathematical solution to the inversion of a resistivity survey is, thus, similar to that of a groundwater hydrological survey. Groundwater hydrologists and reservoir engineers have attempted to solve the inverse problem of flow through multidimensional, heterogeneous porous media for the last three decades (Galvalas, 1976). Yeh (1986) and McLaughlin and Townley (1996) provided extensive reviews on the inverse problem of subsurface hydrology and various solution techniques. They concluded that, in general, prior information on the geological structure, and some point measurements of parameters to be estimated, such as hydraulic conductivity, are necessary to better constrain the solution of the inverse problem when a MOE approach is used.

Groundwater hydrologists also have employed a multi-component linear estimator (cokriging) to estimate the hydraulic conductivity field from scattered measurements of pressure head and hydraulic conductivity in saturated flow problems (Kitanidis and Vomvoris, 1983; Hoeksema and Kitanidis, 1984). Its popularity is attributed to its ability to incorporate spatial statistics and point measurements of conductivity and head into the estimation and to yield conditional mean estimates. Moreover, it is capable of quantifying the uncertainty associated with the estimate. Cokriging is, however, a linear estimator and is limited to mildly nonlinear systems, such as groundwater flow in geological formations of mild heterogeneity (variance of the natural log of conductivity, $\sigma^2_{\log K}=0.1$). When the degree of aquifer heterogeneity is large ($\sigma^2_{\log K}>1$) and the linear assumption is inappropriate, cokriging does not provide a good estimate of the conditional mean conductivity field (Yeh et al., 1996). In other words, it does not take full advantage of the head information to obtain

an optimal estimate of the hydraulic properties.

To overcome this shortcoming, Yeh et al. (1995 and 1996), and Zhang and Yeh (1997) developed an iterative geostatistical technique in which a linear estimator was used successively to incorporate the nonlinear relationship between hydraulic properties and pressure head. This method is referred to as a successive linear estimator (SLE). They demonstrated that with the same amount of information, the SLE revealed a more detailed conductivity field than cokriging. Hughson and Yeh (1998 and 2000) showed that the SLE is computationally efficient compared to the classical inverse method. They extended it to the inverse problem in three-dimensional, variably saturated, heterogeneous porous media. Based on the SLE, Yeh and Liu (2000) recently developed a sequential inverse technique for hydraulic tomography (similar to electrical resistivity tomography) to process the large amount of data created by tomography to characterize aquifer heterogeneity. While demonstrating the robustness of the inverse method, they also investigated the effect of monitoring intervals, pumping intervals, and the number of pumping locations on the final estimate of hydraulic conductivity. Guidelines for optimal design of a hydraulic tomography test are subsequently established.

In this paper, we extend the inverse methodology developed by Yeh and Liu (2000) to the three-dimensional, electrical resistivity tomography (ERT) problem. This method allows prior information of the resistivity fabric, and point measurements of voltage and resistivity, if any, to be included in the interpretation of the results of the ERT. We used numerical simulations to illustrate the robustness of the approach and discussed pros and cons of surface and down-hole resistivity surveys. We sampled twenty-seven cores in a field,

conducted laboratory measurements to determine the relationship between resistivity and moisture content of the core samples, and analyzed its spatial variability. Subsequently, impacts of the spatial variability on the estimated changes in moisture content in the vadose zone, based on ERT, were explored and discussed.

2. Stochastic Conceptualization of Resistivity Field and a Geostatistically-Based Inversion Technique

Assume that in the geological formation, the current flow induced by electrical resistivity survey can be described by

$$\nabla \cdot (\sigma(x) \nabla \phi) + I(x) = 0 \quad (1)$$

subject to boundary conditions

$$\phi|_{\Gamma_1} = \phi^* \quad \text{and} \quad \sigma(x) \nabla \phi \cdot n|_{\Gamma_2} = i \quad (2)$$

where ϕ is electrical potential [V], I represents the electrical current source [A/m^3], i denotes the electrical current density per unit area, and σ is the electrical conductivity [S/m], a reciprocal of resistivity, ρ [Ωm], which is assumed to be locally isotropic. Electrical conductivity or resistivity of geological media varies spatially due to inherent heterogeneous geological processes (Sharma, 1997). One way to describe the spatial variability of the electrical conductivity is the stochastic representation approach, similar to that used by geohydrologists for the variability of hydraulic properties of aquifers and vadose zones (see

Gelhar, 1993; Yeh, 1998). Specifically, the natural log of electrical conductivity, $\log \sigma(x)$, of a geological formation is to be considered as a stochastic process with a mean, $\langle \log \sigma \rangle = F$ ($\langle \rangle$ denotes the expected value) and perturbation, f , which has an infinite number of possible realizations, characterized by a joint probability distribution. Note that the use of natural logarithm transformation is merely a mathematic convenience. Similarly, the electrical potential field induced during an ERT survey is considered as a stochastic process and presented by $\phi(x) = H(x) + h(x)$, where $H = \langle \phi(x) \rangle$ and h is the unconditional perturbation of electrical potential.

Suppose that we have electrical conductivity measurement (referred to as primary information), $f_i^* = (\log \sigma^* - F)$ where $i=1, 2, \dots, n_f$, of core samples at n_f locations. Additionally, we have estimated the mean and correlation structure of the electrical conductivity field from these core samples. It is further assumed that during an ERT survey, we have collected m sets of n_h observed electrical potential values, h_j^* , where $j = n_f+1, n_f+2, \dots, n_f+m \times n_h$ during m ERT surveys. These electrical potential data sets are hereafter referred to as secondary information. We then seek an inverse model that can produce electrical potential and electrical conductivity fields that preserve the observed electrical potential and electrical conductivity values at sample locations, and satisfy their underlying statistical properties (i.e., mean and covariance, etc.) and the governing electrical potential equation. In the conditional probability concept, such an electrical potential field or electrical conductivity field is a conditional realization of ϕ or $\log \sigma$ field, respectively, among many possible realizations of the ensemble. A conditional electrical conductivity

field, then, can be expressed as the sum of conditional mean electrical conductivity and its conditional perturbation, $\log \sigma_c(x) = F_c(x) + f_c(x)$. Similarly, the conditional potential field can be written as $\phi_c = H_c(x) + h_c(x)$ (the subscript c denotes conditional). While many possible realizations of such conditional $\log \sigma$ and ϕ fields exist, the conditional mean fields (i.e., $F_c(x)$ and $H_c(x)$) are unique although not necessarily the true fields.

One way to derive these conditional mean fields is to solve the inverse problem to derive all possible realizations of resistivity fields that preserve measured resistivity and potential values at sampled locations and satisfy the underlining spatial statistics of the resistivity field and the governing equations. Then, an average of all the possible realizations produces the conditional mean resistivity field (see Hanna and Yeh, 1998, for hydrological inverse problems). Another way to derive the conditional mean field is to solve the inverse problem in terms of the conditional mean flow equation. The conditional mean equation can be formulated by substituting the conditional stochastic variables into the governing electrical current flow equation (1) and taking the expected value. The conditional mean equation takes the form:

$$\nabla \cdot [F_c(x) \nabla H_c(x)] + \left\langle \nabla \cdot [f_c(x) \nabla h_c(x)] \right\rangle + I(x) = 0 \quad (3)$$

where the current source $I(x)$ is deterministic. Notice that the true conditional mean $F_c(x)$ and $H_c(x)$ fields do not satisfy the continuity equation (3) unless the second term involving the product of perturbations, $\left\langle \nabla \cdot [f_c(x) \nabla h_c(x)] \right\rangle$, in (3) is zero. This term represents the uncertainty due to lack of information of the two variables at nonsampled locations. It

becomes zero only under two conditions: 1) all the electrical conductivity values in the domain are specified (i.e., $f_c(x)=0$); or 2) all the electrical potential values in the domain are known (i.e., measured) so that $h_c(x)$ is zero everywhere. In practice, these two conditions will never be met and evaluation of this term is intractable. Consequently, we will assume that this term is proportional to the conditional mean potential gradient such that we can rewrite the mean equation as

$$\nabla \cdot [F_{ceff}(x) \nabla H_c(x)] + I(x) = 0 \quad (4)$$

Notice this conditional mean equation has the same form as (1) but the variables are expressed as the conditional effective electrical conductivity, $F_{ceff}(x)$, and conditional mean electrical potential field, $H_c(x)$. The conditional effective electrical conductivity is a parameter field that combines the conditional mean electrical conductivity $F_c(x)$ and the ratio of the second term to the conditional mean potential gradient. Based on the concept of the conditional mean equation (4), the optimal inverse methodology is the one that can derive the conditional effective electrical conductivity that will produce a conditional mean electrical potential field in (4), a smooth field that preserves values of potential measurements. The successive linear estimator (SLE) approach, developed by Yeh and his coworkers, is most appropriate. The SLE starts with the classical cokriging technique using observed f_i^* and h_j^* collected in one ERT survey to construct a cokriged, mean-removed log electrical conductivity map. That is,

$$f_k(x_o) = \sum_{i=1}^{n_f} \lambda_{io} f_i^*(x_i) + \sum_{j=n_f+1}^{n_f+n_h} \mu_{jo} h_j^*(x_j) \quad (5)$$

where $f_k(x_o)$ is the cokriged f value at location x_o . Then, electrical conductivity $\sigma_k(x_o)$ is obtained by $\exp [F+f_k(x_o)]$. λ_{io} and μ_{jo} are the cokriging weights associated with x_o , which can be evaluated as follows:

$$\begin{aligned} \sum_{i=1}^{n_f} \lambda_{io} R_{ff}(x_\ell, x_i) + \sum_{j=n_f+1}^{n_f+n_h} \mu_{jo} R_{fh}(x_\ell, x_j) &= R_{ff}(x_o, x_\ell) \quad \ell = 1, 2, \dots, n_f \\ \sum_{i=1}^{n_f} \lambda_{io} R_{hf}(x_\ell, x_i) + \sum_{j=n_f+1}^{n_f+n_h} \mu_{jo} R_{hh}(x_\ell, x_j) &= R_{hf}(x_o, x_\ell) \quad \ell = n_f + 1, n_f + 2, \dots, n_f + n_h \end{aligned} \quad (6)$$

where R_{ff} , R_{hh} , and R_{fh} , are covariances of f and h , and the cross-covariance of f and h , respectively. The covariance R_{hh} , and the cross-covariance R_{fh} in (6) are derived from the first-order numerical approximation (similar to equations (9) - (11)).

As mentioned in the introduction, the information on electrical potential may not be fully utilized by cokriging because of the nonlinear relationship between f and h and the linear assumption embedded in cokriging. To circumvent this problem, a successive linear estimator is used. That is,

$$\hat{Y}_c^{(r+1)}(x_o) = \hat{Y}_c^{(r)}(x_o) + \sum_{j=n_f+1}^{n_f+n_h} \omega_{jo}^{(r)} [\phi_j^*(x_j) - \phi_j^{(r)}(x_j)] \quad (7)$$

where ω_{jo} is the weighting coefficient for the estimate at location x_o with respect to the potential measurement at location x_j , and r is the iteration index. $\hat{Y}_c^{(0)}$ is an estimate of the conditional mean of $\log \sigma$, which is equal to the cokriged log electrical conductivity field, f_k

+ F , at $r=0$. The residual about the mean estimate at an iteration r is y^r (i.e., $y^r = \log \sigma - \hat{Y}_c^{(r)}$). In (7), $\phi_j^{(r)}$ is the potential at the j^{th} location of the solution to (4) at iteration r and ϕ_j^* is the observed potential at location j (i.e., $\phi_j^* = H_j + h_j^*$). The values of ω are determined by solving the following system of equations:

$$\sum_{j=n_f+1}^{n_f+n_h} \omega_{jo}^{(r)} \varepsilon_{hh}^{(r)}(x_\ell, x_j) + \kappa \delta_{\ell\ell} = \varepsilon_{hy}^{(r)}(x_o, x_\ell) \quad \ell = n_f + 1, \dots, n_f + n_h \quad (8)$$

where ε_{hh} and ε_{hy} are the error covariance (or conditional covariance function) and error cross-covariance (or conditional cross-covariance), respectively, at each iteration. κ is a stabilizing term and $\delta_{\ell\ell}$ is an identity matrix. During the iteration, the stabilizing term is added to the diagonal terms of the left-hand side matrix of equation (8) to numerically condition the matrix, and thus to assure a stable solution. A larger term can result in a slower convergence rate, and a smaller value may lead to numerical instability. In our approach, this stabilizing term is determined dynamically as the product of a constant weighting factor and the maximum value of the diagonal terms of ε_{hh} at each iteration.

The solution to (8) requires knowledge of ε_{hy} and ε_{hh} , which are approximated at each iteration. Based on the first-order analysis, electrical potential at the r^{th} iteration can be written as a first-order Taylor series:

$$\phi = \hat{\phi}_c^{(r)} + h^{(r)} = G(\hat{Y}_c^{(r)} + y_c^{(r)}) \approx G(\hat{Y}_c^{(r)}) + \left. \frac{\partial G}{\partial \ln \sigma} \right|_{\hat{Y}_c^{(r)}} y_c^{(r)} \quad (9)$$

where $G(\hat{Y}_c^{(r)})$ represents the resulting potential of the conditional mean equation (4)

evaluated with parameters, $\hat{Y}_c^{(r)}$, which was previously estimated. In other words, the first-order approximation of the residual $h^{(r)}$ is written as

$$h^{(r)} \approx \left. \frac{\partial G}{\partial \ln \sigma} \right|_{\hat{Y}_c^{(r)}} y_c^{(r)} = J|_{\hat{Y}_c^{(r)}} y_c^{(r)} \quad (10)$$

where J can be evaluated using an adjoint state sensitivity method (Sykes et al., 1985; Sun and Yeh, 1992; Li and Yeh, 1998) subject to boundary conditions. Using (10), we then derive the approximate covariance of $h^{(r)}$ and cross-covariances between $y^{(r)}$ and $h^{(r)}$.

$$\begin{aligned} \varepsilon_{hh}^{(r)}(x_i, x_j) &= J^{(r)} \varepsilon_{yy}^{(r)}(x_\ell, x_m) J^{(r)T} \\ \varepsilon_{hy}^{(r)}(x_i, x_j) &= J^{(r)} \varepsilon_{yy}^{(r)}(x_\ell, x_m) \end{aligned} \quad (11)$$

where J is the sensitivity matrix of n_h XN , and superscript T represents the transpose. ε_{yy} is the covariance of y , which is given by

$$\varepsilon_{yy}^{(1)}(x_o, x_k) = R_{ff}(x_o, x_k) - \sum_{i=1}^{n_f} \lambda_{io} R_{ff}(x_i, x_k) - \sum_{j=n_f}^{n_f+n_h} \mu_{jo} R_{fh}(x_j, x_k) \quad (12)$$

at iteration $r=0$, where $k=1, 2, \dots, N$, and λ and μ are cokriging coefficients. Equation (12) is the cokriging variance if $x_o=x_k$. For $r \geq 1$, the covariances are evaluated according to

$$\varepsilon_{yy}^{(r+1)}(x_o, x_k) = \varepsilon_{yy}^{(r)}(x_o, x_k) - \sum_{i=n_f+1}^{n_f+n_h} \omega_{io}^{(r)} \varepsilon_{yh}^{(r)}(x_i, x_k) \quad (13)$$

These covariances are approximate conditional covariances. Hanna and Yeh (1998)

investigated the accuracy of this approximation.

After updating $\hat{Y}_c(x)$, the mean flow equation (4) is solved again with the newly updated $\hat{Y}_c(x)$ for a new potential field, ϕ . Then, both the change of the variance of the estimated electrical conductivity field and the change of the largest potential misfit, among all the monitoring locations between two successive iterations are evaluated. If both changes are smaller than prescribed tolerances, the iteration stops. If not, a new ε_{hy} and ε_{hh} are evaluated using (11). Equation (8) is then solved to obtain a new set of weights which are used in (7) with $(\phi_j^* - \phi_j^{(n)})$ to obtain a new estimate of $\hat{Y}_c(x)$.

The above discussion describes the SLE for only one set of primary and secondary information during an ERT experiment. This algorithm can simultaneously include all of the potential data collected during all the ERT operations in the sequence. Nevertheless, the system of equations in (6) and (8) can become extremely large and ill conditioned, and stable solutions to the equations can become difficult to obtain (Hughson and Yeh, 2000).

To avoid this problem, the potential data sets are used sequentially. Specifically, our method starts the iterative process with the available electrical conductivity measurements and the potential data set collected from one of the ERT surveys. Once the estimated field converges to the given criteria, the newly estimated electrical conductivity field, $\hat{Y}_c(x)$, is the effective electrical conductivity conditioned on potential data, due to emission of the current source at the first location, and the residual electrical conductivity covariance is the corresponding conditional electrical conductivity covariance. This conditional effective

electrical conductivity is, then, used to evaluate the conditional mean potential and sensitivity matrix, associated with the current source at the next location. Based on (11), the sensitivity matrix in conjunction with the conditional electrical conductivity covariance then yields the potential covariance and cross-covariance of potential and electrical conductivity that reflect the current source at the next location, which are subsequently employed in (8) to derive the new weights. With the conditional mean potential, new weights, and the observed potential, equation (7) yields the electrical conductivity estimate, representing the first estimate based on the information from the current source at the new location. The iterative process is then employed to include the nonlinear relationship between electrical potential and electrical conductivity. The same procedure is used for the next current source location. In essence, our sequential approach uses the estimated electrical conductivity field and covariances, conditioned on previous sets of potential measurements, as prior information for the next estimation based on a new set of current source data. It continues until all the data sets are fully utilized. Such a sequential approach allows accumulation of high-density, secondary information obtained from ERT, while maintaining the covariance matrix at a manageable size that can be solved with the least numerical difficulties. More importantly, this sequential approach allows one to collect potential data sets over a large area sequentially and thus, avoids complex and expensive cables, probes, and data loggers. The algorithm is similar to the one developed for subsurface hydrology, which has been tested numerous times with numerical examples and even sandbox laboratory examples (Yeh et al., 1996; Yeh and Zhang, 1996; Hughson and Yeh, 2000; Yeh and Liu, 2000). Vargas-Guzman and Yeh (1999) provided a theoretical proof to show that such a sequential approach is identical to

the simultaneous approach for linear systems.

3. Numerical Examples

To demonstrate our inverse method, the vertical profile of a hypothetical geological formation (200 cm x 200 cm) was created and discretized into 400 elements of 100 cm². A stochastic random field generator developed by Gutjahr (1989) was employed to assign an electrical conductivity value to each element, assuming that the electrical conductivity field had a mean of 0.01261 S/m and an exponential correlation structure with a variance of 0.5 for $\log\sigma$. The correlation structure was anisotropic with a horizontal correlation of 240 cm and a vertical correlation scale of 20 cm. This anisotropic structure yielded heterogeneous and stratified electrical conductivity distribution shown in Figure 1a.

On the basis of this hypothetical field, three ERT survey layouts were investigated: 1) the surface ERT survey--deployment of the electrode array on the surface (Figure 1b); 2) the down-hole ERT survey-- the electrode array deployed along two vertical bore holes (Figure 1c); and 3) the combination of surface and down-hole ERT survey (Figure 1d). During each ERT survey in all the three layouts, a pole-pole array was used. That is, one current electrode was placed at a great distance from the field so that only one source electrode was considered. Similarly, for measuring the voltage potential, one electrode was placed at a fixed location as a reference and the potential was obtained from the other at different locations. By moving the current electrode from one position to different locations, a large number of voltage/current data sets were obtained for the ERT survey.

Once the voltage/current data were obtained, our sequential inverse approach was

employed to interpret the data. Figures 1b, c, and d show the estimated f fields for layouts 1, 2, and 3, respectively. According to these figures, the surface ERT provides detailed information of electrical resistivity distribution only close to the land surface (Figure 1b), while the down-hole electrode array resulted in a better estimate of electrical resistivity field throughout the entire domain (Figure 1c). A combination of the surface and the down-hole electrode array yields an image of the resistivity field with the best resolution overall (Figure 1d). This conclusion is also manifested in Figures 1e, f, and g, where the corresponding conditional variance distribution for each scenario is shown.

The conditional variance at a location (Equation 13 with $x_o = x_k$) reflects the uncertainty of an estimate at the location. For example, if the resistivity at a location is known exactly, the conditional variance at the location is zero. Otherwise, the conditional variance is equal to the variance of the resistivity field. Therefore, the smaller the conditional variance at a given location, the better the estimate. Figure 1e shows that surface ERT yields small conditional variances only near the land surface where voltage measurements were taken. The variance increases rapidly with depth, indicating that the effectiveness of the survey decreases due to the stratification of the resistivity field of the medium. Notice that the stratification is denoted statistically by the long correlation scale in the horizontal direction and short correlation scale in the vertical direction during the generation of the resistivity field.

In the case of down-hole ERT, the conditional variance distribution shows that high-resolution estimates again were obtained at the locations where voltage measurements were collected (Figure 1f). However, the long correlation scale of resistivity(stratification) in the

horizontal direction enhances the propagation of the effect of voltage measurements over a greater distance. As a consequence, the down-hole electrode array covers a greater area than the surface array and is more effective for depicting the resistivity distribution in horizontally-stratified geological formations.

While the conditional variance provides uncertainty of the estimate, it is an ensemble statistics, which may not be appropriate for a single realization as in these examples. A better means to compare the estimated resistivity field with the true field is to use the average absolute error norm, L1 and the mean square error norm, L2, which are defined as:

$$L1 = \frac{1}{n} \sum_{i=1}^n |\hat{f}_i - f_i| \quad \text{and} \quad L2 = \frac{1}{n} \sum_{i=1}^n (\hat{f}_i - f_i)^2 \quad (14)$$

where f_i and \hat{f}_i represent the true and estimated perturbation of the log-transformed electrical conductivity, respectively, i indicates the element number and n is the total number of elements. The smaller the L1 and L2 values, the better the estimate. Figures 2a, b, and c show plots of the true field vs. the estimated and the L1 and L2 values associated with the three layouts. The results are consistent with those based on the conditional variance criterion. Also illustrated in the figures is the discrepancy between the true and the estimate (scattering around the 45-degree line) due to the limited measurements of the potential field.

In the above inversion examples, the voltage/current measurements were assumed to be error-free and statistical parameters such as mean, variance, and correlation scales required for the inversion were assumed to be known or estimated beforehand. Effects of error in measurements and uncertainty of the statistical parameters on the estimate were

reported by Yeh and Liu (2000) for hydraulic tomography. In short, they found that uncertainty of the statistical parameters does not influence the estimate significantly if sufficient and accurate secondary information is available. However, errors in point measurement of electrical conductivity or voltage can have significant impacts on the estimate. They reported that the benefit vanishes rapidly when increasing the number of data sets by varying the source location during the tomography. In addition, they investigated network design issues, such as the sample interval for head measurements and the location of pumping in terms of the correlation scale of the heterogeneity. We believe these results also hold for the ERT.

4. Relating Water Content to Resistivity Distribution

During an infiltration event, water content of geological media is generally the only element that undergoes dramatic changes. Therefore, tracking the change in resistivity has often been regarded as a useful means to delineate the change of the water content in the vadose zone. Specifically, an ERT survey is conducted on a site before an infiltration event in order to obtain the background distribution of electrical resistivity. Following an infiltration event, the ERT survey is undertaken again to obtain the resistivity distribution after the infiltration. Next, the change in resistivity is used to interpret the movement of the water plume from infiltration, assuming a relationship between resistivity and water content.

In order to relate the water content to resistivity, a power law has often been used

$$\rho = \rho_o \theta^{-m} \quad (15)$$

(e.g., Knight, 1991):

where ρ is bulk resistivity, ρ_o is a fitting parameter that is related to the resistivity of pore water, m is a fitting parameter, and θ denotes water content. Using (15), the difference between the log resistivity before and after infiltration then becomes:

$$\Delta \log(\rho) = -m \Delta \log(\theta) \quad (16)$$

This equation shows that if m is constant and is known precisely, then the change of log resistivity is linearly proportional to the change of log water content. However, the change in log resistivity may not directly correspond to the change of log moisture content if m exhibits significant spatial variability or is a random variable. This implies that the same amount of change in moisture content may lead to different amounts of change in resistivity in different media. Notice the variability of ρ_o does not play any role in (16). A statistical analysis based on (16), assuming independence between m and θ , leads to an expression for the variability in change in log resistivity:

$$\text{var}[\Delta \log(\rho)] = M^2 \text{var}[\Delta \log(\theta)] + \Theta^2 \text{var}[m] \quad (17)$$

where $\text{var}[\Delta \log(\theta)]$, $\text{var}[\Delta \log(\rho)]$, and $\text{var}(m)$ are variances of $\Delta \log(\theta)$, $\Delta \log(\rho)$ and m , respectively. The change in mean $\log(\theta)$ is denoted by Θ and M is the mean value of m . As suggested by (17), the variability of $\Delta \log(\rho)$ depends on not only the variance of $\Delta \log(\theta)$ but also the variance (spatial variability) of m and the mean of Θ . It is, then, logical to ask what the magnitude of variability of these parameters might be in the field.

5. Variability of Resistivity-Moisture Content Relationship

To investigate the spatial variability of ρ_o and m in the field, sediment hydraulic properties, including electrical resistivity as a function of moisture content, were measured for samples collected from the Sandia-Tech Vadose Zone (STVZ) infiltration field site located in Socorro, NM. The field site sediments are mapped as part of the Sierra Ladrones Formation, Upper Santa Fe Group consisting of fine-coarse grained, poorly consolidated, ancestral Rio Grande axial-river deposits with intermittent layers of debris flow sediments and sedimentary layers of eolian sands (see Brainard et al., 2001 for a complete site description). Twenty-seven samples were collected from eight 5-ft lengths of a continuous core from a borehole at the field site. Because the samples were highly unconsolidated and easily disintegrated, they had to be repacked into sample rings to bulk density values based on preliminary *in situ* measurements and tabulated values for deposits of similar texture (van Genuchten et al., 1991). The desired bulk density was estimated to be 1.53 g/cc for fine-medium sand, 1.61 g/cc for medium-coarse sand, and 1.34 g/cc for clays. The samples were then placed in the hanging column apparatus and were allowed to reach moisture equilibrium at tensions from 100 cm down to 0 cm to obtain the main wetting curve (MWC). Also, we reversed the process measuring moisture retention for the main drainage curve (MDC) starting at the satiated moisture content. Pressure chambers were used to drain the samples at high pressures greater than 100 cm. Moisture equilibrium was determined during imbibition by weighing the samples daily and observing changes in moisture content. Equilibrium was determined during drainage by monitoring the water level in the burette.

Electrical resistivity was determined at each moisture equilibrium point for both the MWC and MDC by placing the sample in the impedance analyzer sample holder, and applying a logarithmic sweep of frequencies across the sample. A Hewlett Packard model 4129A LF (Knight, 1991) impedance analyzer was connected to a personal computer for automated data acquisition of impedance measurements during application of a logarithmic sweep of frequencies of current to the sample. The impedance value corresponding to the frequency not affected by polarization at the sample/electrode interface was used to calculate electrical resistivity by multiplying the sample impedance by the ratio of the sample cross-sectional area to the sample length (Knight, 1991). A plot of resultant resistivity at each moisture content for the twenty-seven cores is shown in Figure 3. Significant variability of the relationship between resistivity and moisture content exists.

Equation (15) was fit to the measured resistivity and moisture data to determine the values for ρ_o and m . Assuming both ρ_o and m follow log normal distributions, the statistics for these two parameters of the core samples are shown in Table 1. A spatial statistical analysis was also conducted and results are shown in Table 2. In general, the two parameters exhibit significant spatial variability, especially, the parameter m , but they are correlated over space, and the variation appears to correspond to the lithology of the field site. Further, we found that the relationship between electrical resistivity did not appear to be hysteretic [Baker, 2001].

6. Uncertainty in Hydrological Interpretation

To illustrate the effect of spatial variation of m on the interpretation of change in

water content based on change in resistivity, we investigated two possible scenarios in a hypothetical vadose zone of 200 cm x 200 cm: 1) the resistivity field before infiltration and the resistivity field after infiltration were known precisely; and 2) the resistivity fields were estimated with some uncertainty from a down-hole ERT survey.

The hypothetical vadose zone was discretized into 200 elements, and each element has a dimension of 20 cm in the horizontal direction and 10 cm in the vertical. The unsaturated hydraulic properties of each element were assumed to be described by the Mualem-van Genuchten model [van Genuchten, 1980]:

$$K(\psi) = K_s (1 - (\alpha\psi)^{n-1} [1 + (\alpha\psi)^n]^{-m})^2 / [1 + (\alpha\psi)^n]^{m/2}$$

$$\theta(\psi) = (\theta_s - \theta_r) [1 + (\alpha\psi)^n]^{-m} + \theta_r$$
(18)

The variability of saturated moisture content, θ_s , and residual moisture content, θ_r , is generally negligible; both were treated as deterministic constants with a value of 0.366 and 0.029, respectively. However, the parameters, K_s , α and n were considered as random fields with the geometric mean of 0.0063 cm/sec, 0.028 1/cm and 2.0, respectively. The variances of $\log K_s$, $\log \alpha$ and $\log n$ were 0.1, 0.1, and 0.01, respectively. Also assumed was that all three parameters possessed the same exponential correlation structure with a horizontal correlation scale of 240 cm and a vertical correlation scale of 20 cm. Following the generation of random hydraulic parameter fields, a hydrostatic pressure distribution with zero pressure at the bottom was assigned to the vadose zone as the initial condition and the corresponding water content distribution was considered as the background water content distribution (Figure 4a). Next, a steady infiltration event was simulated using a finite

element model for flow and solute transport in variably saturated media: MMOC2, developed by Yeh et al. (1993). The top center of the vadose zone (from $x=80$ cm to 120 cm at $z = 200$ cm) was treated as a constant head boundary with pressure head of -80 cm, the remainder of the surface and the two sides of the zone as no-flux boundaries, and the bottom as the water table. Once the simulation of the steady flow field was completed, the resulting water content distribution was denoted as the water content after infiltration (Figure 4b). The change of the log-transformed water content distribution before and after the infiltration was then computed (Figure 4c).

In order to convert the simulated moisture content distribution to a resistivity field, each element of the vadose zone was assigned a pair of ρ_θ and m values using the random field generator. For the two aforementioned scenarios, three m fields were generated with a mean of 1.35 and $\log m$ variances, 0.0, 0.033, and 0.1 for cases 1, 2, and 3, respectively. While the three cases have different m fields, they have an identical ρ_θ field with a geometric mean of 8.5 and variance of $\log \rho_\theta$ of 0.1. Again, similar to the hydraulic parameter field, these fields have an exponential correlation structure with a horizontal correlation scale of 240 cm and the vertical correlation scale of 20 cm. While hydraulic parameter fields, ρ_θ , and m fields are spatially correlated, they are statistically uncorrelated among themselves.

For scenario 1, where the resistivity field is assumed to be known precisely, equation (15) was used in conjunction with the generated ρ_θ , m , and the background water content distribution to construct the background resistivity map for this hypothetical site. Similarly, a resistivity distribution was obtained, corresponding to the water content distribution after infiltration. Then, the change in log transformed resistivity was derived by subtracting the

log resistivity infiltration from the background log resistivity. The change in $\log \rho$ for cases 1, 2, and 3 are shown in Figures 5a, 5b, and 5c, respectively and are plotted against $m\Delta\log(\theta)$ of case 1 (Figures 6a, 6b, and 6c) with the values of L1 and L2.

According to Figures 4c, 5a, 5b, and 5c, the change in log resistivity reflects the change in log water content only if the information of resistivity is known exactly and m is a constant (i.e., $\text{var}(m)=0$ in (17), see Figure 6a). However, the discrepancy between the change in log resistivity and the change in log of water content grows as the variance of m increases (Figures 6b and 6c). In other words, due to variability of the parameter, m , different parts of a geological medium can exhibit different amounts of change in resistivity even if they undergo the same amount of change in water content.

In scenario 2, the background resistivity distribution and the distribution after infiltration are no longer known exactly. Instead, both resistivity distributions were estimated using our sequential inverse approach to interpret the ERT data collected from the down-hole survey, illustrated in Figures 5d, e, and f. Specifically, forward simulations of ERT surveys of the resistivity fields, created from the random ρ_0 and m fields and water content distributions before and after infiltration in scenario 1, were conducted to yield potential measurements at specified monitoring locations. Afterwards, these measurements were used in the inverse model to derive estimated resistivity fields. The change in $\log \rho$ for cases 1, 2, and 3 were then calculated and shown in Figures 5d, 5e, and 5f, respectively. They also are plotted against $m\Delta\log(\theta)$ of case 1 and shown in Figures 6d, 6e, and 6f) with the values of L1 and L2. Again, the measurements were considered error free and other inputs to the model were assumed to be known exactly.

In this case, our estimated resistivity fields involve uncertainty due to limited information. A comparison of Figure 4c and Figure 5d (or Figure 6d) shows that even with this uncertainty, the change in log resistivity still resembles the change in log water content when m is constant. The resemblance deteriorates though as the variance of m increases (Figures 6e and 6f). Anomalous change in resistivity was estimated near the locations (Figure 5f) where potential measurements were taken, indicating that the greater variation in m can exacerbate the effect of the limited data set on the interpretation of ERT results as indicated by (17). As a consequence, interpretation of the change in moisture content based on the change in resistivity can be misleading, depending on the accuracy of ERT data inversion, the mean value of m , the amount of change in mean log moisture content, and the variability of m .

We note that our illustrations consider only variation of parameters of the simple power law for the resistivity-moisture relationship in the synthesized vadose zone. Under field conditions, many other factors can further complicate the interpretation of an ERT survey, and the validity of the power law deserves further explorations regarding the resistivity-moisture relationship. For instance, while the power law fits our field data quite well, it may not be suitable for other geological media. It is also well known to be sensitive to salt concentration, clay content, ion exchange, temperature (Keller, 1987) or other site-specific attributes.

While the resistivity in this study is assumed to be locally isotropic, in the field it can be anisotropic and measurement-scale dependent. The resistivity anisotropy of a medium at a given measurement scale, similar to hydraulic conductivity anisotropy, is an artifact due

to averaging distinct resistivity values of layers of material at scales smaller than the measurement scale. The anisotropy, therefore, depends on the average length and thickness of the layers, and the variance of layer resistivity, which may vary with the scale of measurement (or the size of discretization of the domain used in ERT inversion). In general, the resistivity is greatest in the direction perpendicular to layering and least in the direction parallel to layering. Moreover, because the resistivity of each layer can vary with moisture content and thus its variability among the layers, anisotropy of the averaged bulk resistivity is expected to vary with moisture content. Specifically, we expect that the ratio of the bulk resistivity, in the direction perpendicular to layering, to the bulk resistivity, in the direction parallel to layering, increases as the medium becomes less saturated, in a manner similar to moisture-dependent anisotropy in unsaturated hydraulic conductivity described by Yeh et al., (1985 a and b). These possible complications necessitate further theoretical and experimental investigations of the fundamental resistivity-moisture relationship. Their effects on the inversion of ERT and its hydrological interpretation deserve further investigations.

7. Conclusions

A sequential, geostatistical inverse approach for hydraulic tomography was adapted for electrical resistivity tomography. The sequential inverse approach mimics the sequential ERT data collection scheme commonly employed in the field survey to reduce equipment costs. The inverse method also allows one to include point measurement of resistivity, in addition to potential measurements from the ERT survey, and information of geological

structures through statistic covariances to constrain the estimate of the resistivity field. The sequential approach is computationally efficient, allows fine-grid discretization of the solution domain, and permits sequential inclusion of different data sets. Furthermore, the conditional variance in the inverse model quantifies uncertainty in the estimate.

Through numerical experiments based on our inverse approach, we showed that geological bedding dictates effectiveness of the sampling array of ERT: sampling perpendicular to bedding (down-hole array) increases resolution of the resistivity estimate due to the long correlation in the direction parallel the bedding. On the other hand, the long correlation scale along bedding and the short correlation scale perpendicular to bedding restricts the effectiveness of the surface array (sampling parallel to bedding) to a shallow depth.

Great variability of the resistivity-moisture relationship was found to exist in our field samples. Both the theoretical analysis and numerical experiments suggested that such a spatially varying relationship exacerbates the level of uncertainty in the interpretation of change of moisture content based on the estimated change in resistivity. These results call for additional studies of the underlying physics of the resistivity-moisture relationship and its spatial variation, and for development of better methodologies for incorporating this variability in the interpretation of the ERT survey, such that ERT can be better applied for hydrologic purposes.

Acknowledgments

This research is funded in part by a DOE EMSP96 grant through Sandia National Laboratories (contract AV-0655#1) and a DOE EMSP99 grant through University of Wisconsin, A019493.

References

- Baker, K., Analysis of hydrological and electrical properties at the Sandia-Tech Vadose Zone Facility, Master Thesis, New Mexico Tech., Socorro, NM, 2001.
- Brainard, J. R., R. J. Glass, D. L. Alumbaugh, L. Paprocki, D. Labrecque, X. Yang, T.-C. J. Yeh, K. E. Baker, and C. A. Rautman, The Sandia-Tech Vadose Zone Facility: Experimental design and data report of a constant flux Infiltration experiment, Sandia National Laboratories Internal report, 2001.
- Daily, W., A. Ramirez, D. LaBrecque and J. Nitao, Electrical resistivity tomography of vadose water movement, *Water Resour. Res.*, 28(5), 1429-1442, 1992.
- Ellis, R. G., and S. W. Oldenburg, The pole-pole 3-d dc resistivity inverse problem: a conjugate gradient approach, *Geophysical journal international* 119,187-194, 1994.
- Gavalas, G. R., P. C. Shan, and J. H. Seinfeld, Reservoir history matching by Bayesian estimation, *Society of Petroleum Engineers Journal*, 337-350, December 1976.
- Gelhar, L. W., *Stochastic subsurface hydrology*, Prentice Hall, Englewood Cliffs, New Jersey. 1993.
- Gutjahr, A., Fast Fourier transforms for random field generation, N. M. Tech Project Report, 106 pp., 1989.
- Hanna, S., and T.-C. J. Yeh, Estimation of co-conditional moments of transmissivity, hydraulic head, and velocity fields, *Adv. in Water Resour.*, 87-93, 22(1), 1998.
- Hoeksema, R. J., and P. K. Kitanidis, An application of the geostatistical approach to the inverse problem in two-dimensional groundwater modeling, *Water Resour. Res.*, 20(7), 1003-1020, 1984.
- Hughson, D. L., and T.-C. J. Yeh, A geostatistically based inverse model for three-dimensional variably saturated flow, *Stochastic Hydrol. Hydraul.* 12(5), 285-298, 1998.
- Hughson, D. L., and T.-C. J. Yeh, An inverse model for three-dimensional flow in variably saturated porous media, *Water Resour. Res.*, 36(4), 829-839, 2000.
- Keller, G. V., Rock and mineral properties. Electromagnetic methods in applied geophysics, investigations in geophysics No.3, Volume 2, theory, 13-51, 1987.
- Kitanidis, P. K., and E. G. Vomvoris, A geostatistical approach to the inverse problem in groundwater modeling and one-dimensional simulations, *Water Resour. Res.*, 19(3), 677-690, 1983.

Knight, R., Hysteresis in the electrical resistivity of partially saturated sandstones, *Geophysics*, Vol. 56, No. 12: 2139-2147, 1991.

Li, B., and T.-C. J. Yeh, Sensitivity and moment analysis of head in variably saturated regimes, *Adv. in Water Resour.*, 21, 477-485, 1998.

Li, Y., and D. W. Oldenburg, Inversion of 3D dc-resistivity data using an approximate inverse mapping, *Geophysical journal international* 116, 527-537, 1994.

McLaughlin, D. and L. R. Townley, A reassessment of the groundwater inverse problem, *Water Resour. Res.*, 32(5), 1131-1161, 1996.

NRC, *Seeing into the earth: noninvasive characterization of the shallow subsurface for environmental and engineering application*, Board on earth sciences and resources, water science and technology board, Commission on Geoscience, Environment, and Resources National Research council, National academy press, Washington D.C, 2000.

Sharma, P. V., *Environmental and engineering geophysics*, Cambridge University Press, Cambridge, UK, 1997

Sun, N.-Z., and W. W.-G. Yeh, A stochastic inverse solution for transient groundwater flow: parameter identification and reliability analysis, *Water Resour. Res.*, 28(12), 3269-3280, 1992.

Sykes, J.-F., J. L. Wilson, and R. W. Andrews, Sensitivity analysis of steady state groundwater flow using adjoint operators, *Water Resour. Res.*, 21(3), 359-371, 1985.

van Genuchten, M. T., A closed-form equation for predicting the hydraulic conductivity of unsaturated soils. *Soil Sci. Soc. Am. J.* 44, 892-898, 1980.

van Genuchten, M. Th., F. J. Leij, and S. R. Yates, The RETC code for quantifying the hydraulic functions of unsaturated soils. United States Environmental Protection Agency, Office of Research and Development, Washington, DC. EPA/600/2-91/061, December, 1991.

Vargas-Guzman, A. J. and T.-C. J. Yeh, Sequential kriging and cokriging: two powerful geostatistical approaches, *Stochastic Environmental Research and Risk Assessment*, 13, 416-435, 1999.

Yeh, T.-C. J., Stochastic modeling of groundwater flow and solute transport in aquifers, *J. of Hydrologic Processes*, Vol. 6, 369-395, 1992.

Yeh, T.-C. J., Scale issues of heterogeneity in vadose-zone hydrology, in *Scale Dependence and Scale Invariance in Hydrology*, edited by G. Sposito, Cambridge Press, 1998.

Yeh, T.-C. J., L. W. Gelhar, and A. L. Gutjahr, Stochastic analysis of unsaturated flow in

heterogenous soils: 2, statistically anisotropic media, *Water Resour. Res.*, 21(4), 457-464, 1985a.

Yeh, T.-C. J., L.W. Gelhar, and A.L. Gutjahr, Stochastic analysis of unsaturated flow in heterogenous soils: 3, observation and applications, *Water Resour. Res.*, 21(4), 465-471, 1985b.

Yeh, T.-C. J., A. L. Gutjahr, and M. Jin, An iterative cokriging-like technique for groundwater flow modeling, *Groundwater*, 33(1), 33-41, 1995.

Yeh, T.-C., M. Jin, and S. Hanna, An iterative stochastic inverse method: conditional effective transmissivity and hydraulic head fields, *Water Resour. Res.*, 32(1), 85-92, 1996.

Yeh, T.-C., and S. Y. Liu, Hydraulic tomography: development of a new aquifer test method, *Water Resour. Res.*, 36(8), 2095-2105, 2000.

Yeh, T.-C. J., R. Srivastava, A. Guzman, and T. Harter, A numerical model for two dimensional flow and chemical transport, *Groundwater*, 31(4), 634-644, 1993.

Yeh, T.-C. J., and J. Zhang, A geostatistical inverse method for variably saturated flow in the vadose zone, *Water Resour. Res.*, 32(9), 2757-2766, 1996.

Yeh, W. W-G., Review of parameter identification procedures in groundwater hydrology: the inverse problem, *Water Resour. Res.*, 22(1), 95-108, 1986.

Zhang, J., and T.-C. J. Yeh, An iterative geostatistical inverse method for steady flow in the vadose zone, *Water Resour. Res.*, 33(1), 63-71, 1997.

Zhang, J., R. I. Mackie, and T. Madden, 3-D resistivity forward modeling and inversion using conjugate gradients. *Geophysics* 60, 1313-1325, 1995.

Table. 1. Statistics of fitting parameters ρ_o and m

parameter	Mean(Ωm)	Variance(Ωm) ²	Std. Dev.(Ωm)	% C.V.
ρ_o	7.036	0.633	0.796	40.8
m	1.336	0.034	0.185	63.72

Table 2. Parameters of fitted sample variogram models for ρ_o and m.

Parameter	Model	Sill (Ωm) ²	range (m)	Nugget (Ωm) ²
ρ_o	exponential	20	4.6	2.8
m	exponential	0.05	3	0.035

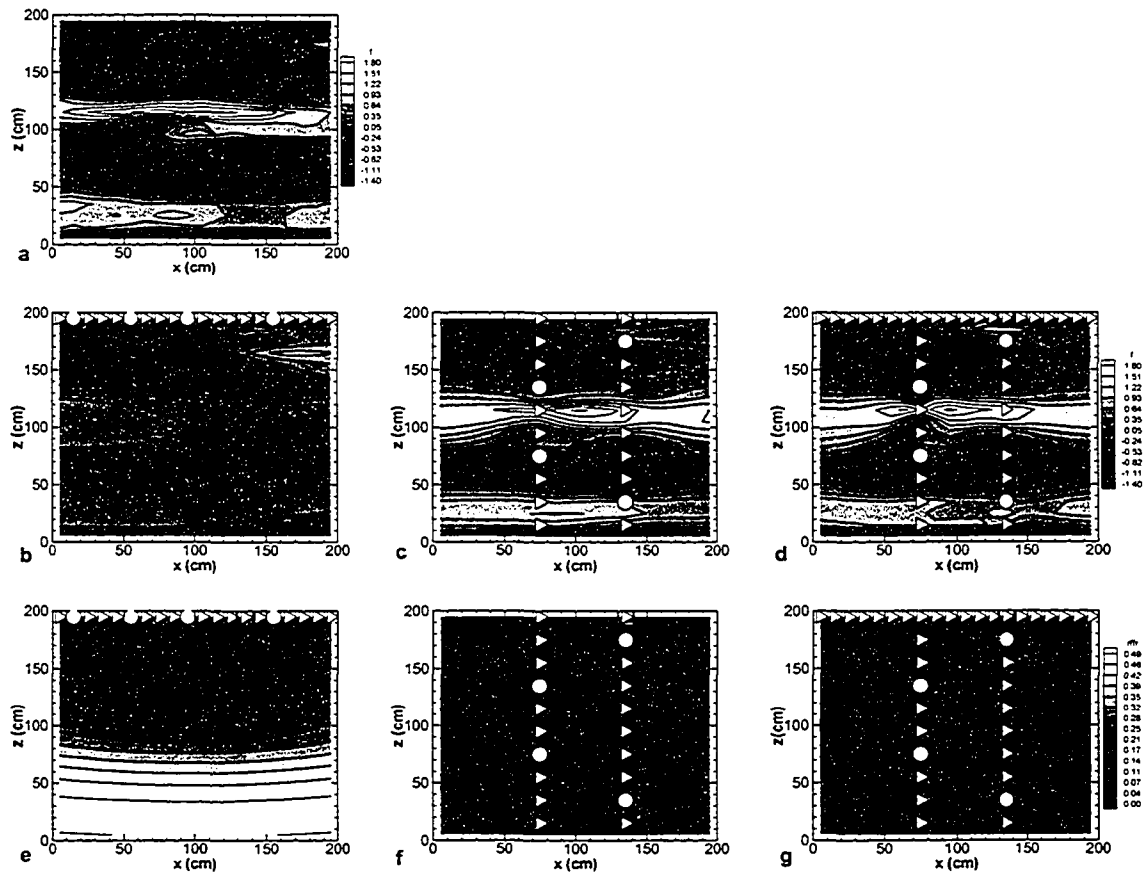


Figure 1.

Illustrations of effectiveness of the electrical resistivity survey: a) the synthesized “true” resistivity field, b) the estimated resistivity field from the surface array, c) the field from the down-hole array, d) the field from the combination of the surface and down-hole array; figures e, f. and g are the conditional variance distributions correspond to figures b, c, and d. The square presents the resistivity sample location, circles indicate current source locations and triangles indicate voltage measurement locations.

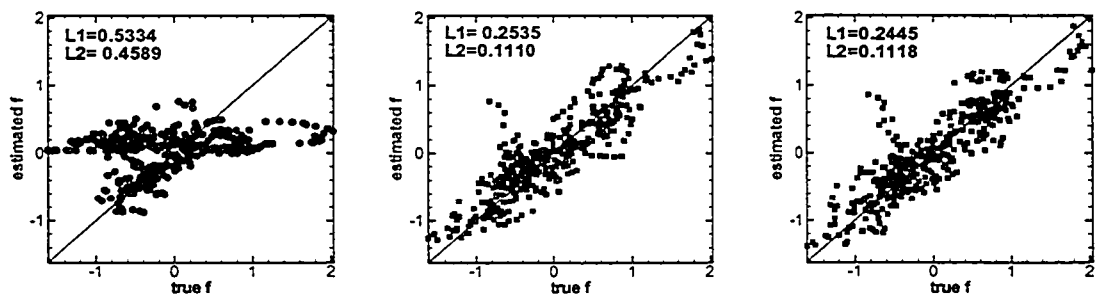


Figure 2. The scatter plots and values of L1 and L2 for the surface array, down-hole array and the combination of surface and down-hole array in Figure 1.

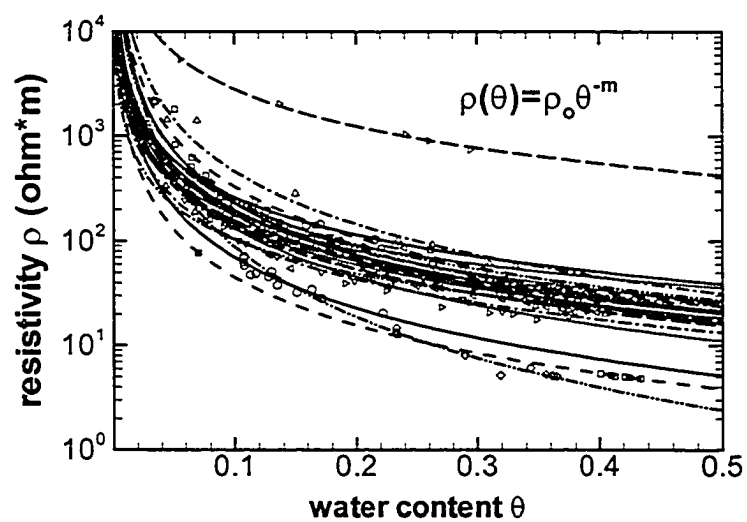


Figure 3. Resistivity-moisture relationships of the field.

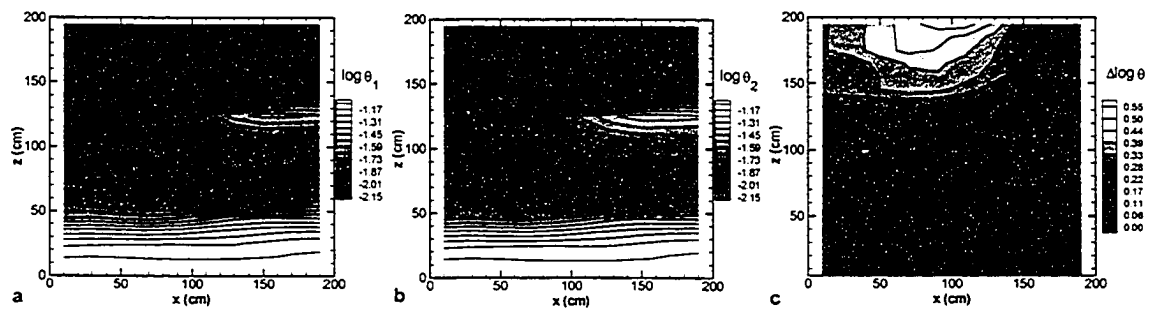


Figure 4. Simulated moisture content distributions: a) before infiltration, 2) after infiltration, 3) the difference.

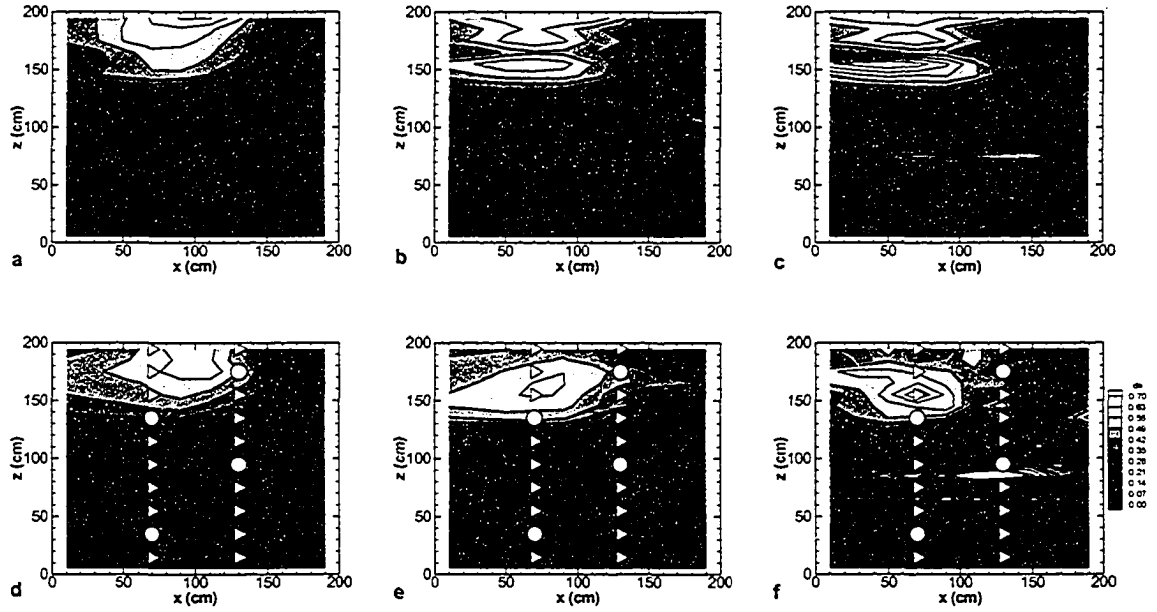


Figure 5. a, b, and c show the change in log resistivity for scenario #1 with three different values for the variance of m : 0.0, 0.033, and 0.1, respectively. The changes in log resistivity for scenario #2 with the same variances are shown in d, e, and f. The square presents the resistivity sample location, circles indicate current source locations and triangles indicate voltage measurement locations.

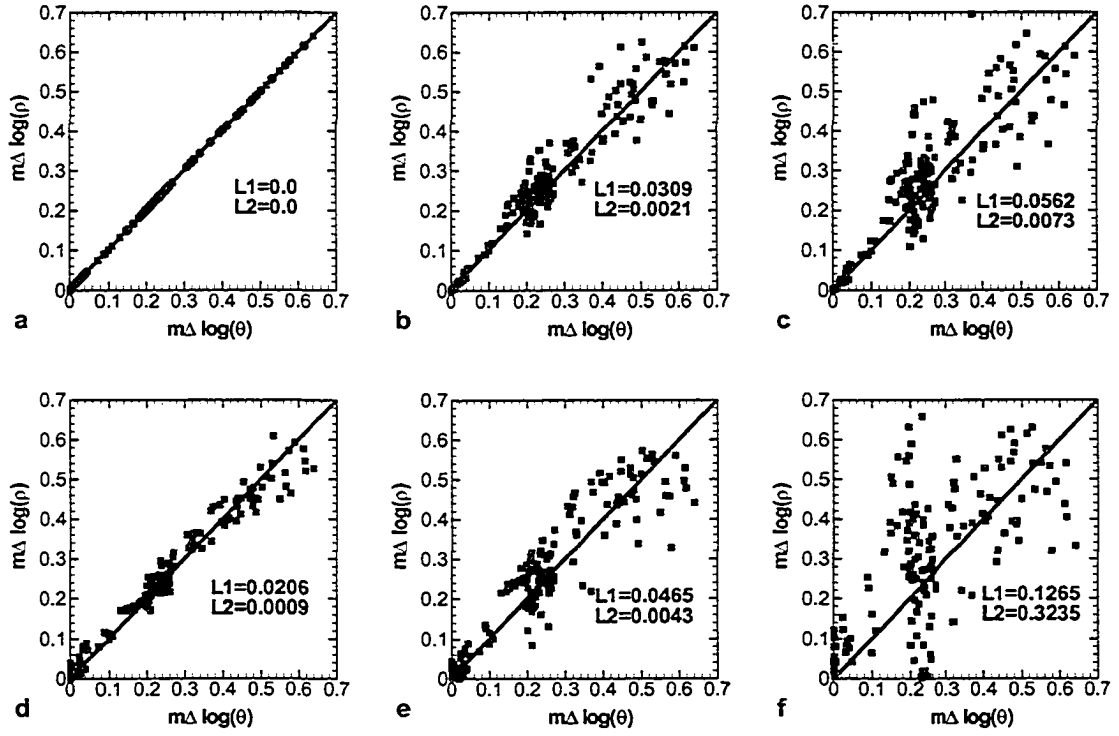


Figure 6. The scatter plots and values of $L1$ and $L2$ for the cases in Figure 5.

APPDENDIX D

A HYDRO-GEOPHYSICAL INVERSE APPROACH FOR ELECTRICAL
RESISTIVITY TOMOGRAPHY: AN EFFECTIVE TOOL FOR MONITORING
WATER MOVEMENT IN VADOSE ZONE

Shuyun Liu, T. -C. Jim Yeh

Department of Hydrology and Water Resources

John W. Harshbarger Building

The University of Arizona,

Tucson, Arizona 85721.

to be submitted to

Water Resources Research

April 9, 2001

Abstract

The electrical resistivity tomography (ERT) technique, which utilizes a limited number of bore holes has been a natural tool for detecting moisture content in the vadose zone without intensive and destructive sampling. However, a reliable and accurate image of water content distribution requires a sound inversion algorithm to interpret the ERT data sets. In this paper, a hydro-geophysical inverse approach, which conditions on available point measurements of resistivity, water content and voltage, was proposed to better interpret ERT data sets with less uncertainty. While the classical conversion of the resultant resistivity field to water content distribution often assumes a constant empirical relationship between resistivity and water content, our approach attempted to reflect the true image of water content distribution by taking into account the strong spatial variability of this relationship exhibited by field data. To process the ERT data sets more efficiently with less numerical difficulty, our conditioning approach was performed sequentially.

In this study, 2-D numerical experiments were first conducted to investigate the effect of uncertainties associated with model input such as mean and covariance function of water content. Then the usefulness of our approach was demonstrated by directly estimating the moisture distribution at a certain time after an infiltration event for a hypothetical 3-D vadose zone. Results show that our estimate reveals the general pattern of the true water content distribution, and that the incorporation of moisture measurements significantly constrains our estimate. Results also illustrate how the

spatially varying resistivity-moisture relationship may result in uncertainty in the interpretation of change of moisture content based on estimated resistivity change.

1. Introduction

Detailed and accurate knowledge of electrical properties can provide valuable information for characterizing waste sites and monitoring contaminant movement in the vadose zone. Consequently, electrical resistivity tomography (ERT) survey has been widely employed to collect extensive current and electrical potential data sets in multi-dimensions to image the subsurface electrical resistivity distribution (Ellis and Oldenburg, 1994; Li and Oldenburg, 1994; Zhang et al., 1995; Daily et al., 1992). Recently, the ERT survey has found its way into subsurface hydrological applications. This is attributed to the fact that resistivity can be related to water content with some empirical relationships, i.e. the power law (Knight, 1991). During an infiltration event, water content of geological media is generally the only element that undergoes dramatic changes. Therefore, tracking the resistivity difference at different time has often been regarded as a useful mean to demonstrate the temporal changes of water content in the vadose zone (Daily et al., 1992). To do so, current/voltage data sets are collected using ERT survey before and after infiltration. With the help of inverse models, the images of resistivity distribution before and after infiltration are obtained and then the change in resistivity is computed accordingly. By assuming a constant deterministic relationship between resistivity and water content, the change in resistivity is converted to the change in water content.

However, Yeh et al. (2001) showed that uncertainties in the interpretation of ERT surveys in subsurface hydrological applications can be significant. Several factors could be responsible for these uncertainties. One factor is the inverse model currently used for ERT inversion. Though ERT surveys can produce abundant current/voltage data sets that are essential in characterizing subsurface resistivity distribution, a proper inverse model is more critical. Currently employed inverse approaches for ERT inversion are the minimum-output-error (MOE) based approach, and there are some inherent numerical difficulties associated with it, such as the non-uniqueness. These difficulties can result in great uncertainty in the estimated resistivity distributions. On the other hand, the computational burden of MOE often hinders its application to a three-dimensional ERT inversion.

Another factor is the spatial variability of the relationship between resistivity and water content. The conversion of change of estimated resistivity to change of water content often assumes a constant relationship between them in current practice. While our preliminary field study indicates that the resistivity-moisture content relationship exhibits strong spatial variability in the field (Yeh, et al., 2001). Therefore, neglecting the great spatial variability while using the simplified assumption exacerbates the level of uncertainty in the interpretation of change of moisture content based on the estimated change in resistivity.

Regardless of the uncertainties in the interpretation of the change of moisture content, this change of moisture content only provides qualitative information of water movement in vadose zone due to the infiltration. The exact water content distribution

remains unknown. Since unsaturated hydraulic conductivity is a function of water content instead of water content change, the converted change of moisture content cannot be directly used by hydrological inversions. Therefore, a novel methodology that can produce detailed water content distribution with less uncertainty, consider the spatial variability of the resistivity-moisture relationship and efficiently process the large number of ERT data sets is desired for a better characterization of the vadose zone.

While the physical process is different, the governing equation for electrical current and potential fields created in the ERT survey is analogous to that for steady flow in saturated porous medium. The mathematical solution to the inversion of an ERT survey is, thus, similar to that of a hydraulic tomography. In this paper, the sequential inverse approach for hydraulic tomography (Yeh and Liu, 2000) is extended for the ERT survey. By sequentially including the ERT data sets, this inverse model makes it numerically feasible and computationally efficient to process the large number of current/voltage data yielded by ERT survey. In addition, this inverse approach incorporates point measurements of moisture content and geological information, and estimates the actual water content distribution. More importantly, this model considers the spatial variability of the resistivity-water content relationship. Two-dimensional numerical experiments were first conducted to evaluate the effect of the uncertainties associated with our inverse model input such as the mean, variance and correlation structure of water content. Then, three-dimensional numerical experiments were carried out to illustrate the robustness of our sequential inverse approach in delineating water content distribution at time of 50,000 minutes after an infiltration event. Meanwhile,

change in resistivity due to infiltration is also obtained to track the change of moisture content, and this converted change of water content is then compared with true change of water content. By doing so, the effect of the spatial variability of the resistivity-water content relationship on the interpretation of water movement in vadose zone is investigated.

2. Methodology

2.1 Three-dimensional electrical potential equation

Assume that in the geological formation, the current flow induced by electrical resistivity survey can be described by

$$\nabla \cdot (\sigma(x) \nabla \phi) + I(x) = 0 \quad (1)$$

subject to boundary conditions

$$\phi|_{\Gamma_1} = \phi^* \quad (2)$$

$$\sigma(x) \nabla \phi \cdot \underline{n}|_{\Gamma_2} = i \quad (3)$$

where ϕ is electrical potential [v], I represents the electrical current source density per volume [A/m^3], i denotes the electrical current density per unit area [A/m^2], and σ is the

electrical conductivity [S/m], $\sigma = \frac{I}{\rho}$, and ρ [Ωm] is electrical resistivity, which is

assumed to be locally isotropic.

2.2. Relating water content to resistivity distribution

A power law has often been used to relate the water content to resistivity (e.g. Knight, 1991):

$$\rho = \rho_0 \theta^{-m} \quad (4)$$

where ρ is bulk resistivity, ρ_0 is a fitting parameter that is related to the pore water resistivity, m is a fitting parameter, θ denotes moisture content. Assuming ρ_0 doesn't change during the infiltration event, using equation (4), the difference of the log resistivity before and after an infiltration then becomes:

$$\Delta \log(\rho) = -m \Delta \log(\theta) \quad (5)$$

This equation shows that if m is constant and is known precisely, then the change of log resistivity is linearly proportional to the change of the log water content. However, the change in log resistivity may not directly correspond to the change of log moisture content if m exhibits significant spatial variability or is a random variable. This implies that the same amount of change in moisture content may lead to different amounts of change in resistivity in different media.

According to Sharma (1997), the resistivity of porous medium is highly variable, depending on the degree of saturation and the nature of the pore electrolytes. Considering the equation (4), the spatial variability of ρ_0 and m may represent that of the pore electrolytes in the porous medium. Since most mineral grains (except metallic ores and clay materials) are insulators, electrical conduction is mainly being through interstitial water in pores. Groundwater filling the pore space is a natural electrolyte with a considerable amount of ions present contributing to conductivity. When clay materials are present, a relatively large number of ions may be released from such minerals by ion

exchange process, increasing the electrical conductivity significantly. In addition, during an infiltration event, many chemical reactions/or processes may become possible due to different water chemistry carried in the infiltrated water, altering the composition of ions present in pores and changing the nature of the pore electrolytes, and hence make resistivity vary even more spatially.

To investigate the spatial variability of ρ_0 and m in the field, sediment hydraulic properties, including electrical resistivity as a function of moisture content, were measured for samples collected from the Sandia-Tech Vadose Zone (STVZ) infiltration field site located in Socorro, NM (Baker, 2001). Twenty-seven samples were collected from eight 5-ft lengths of a continuous core from a bore hole at the field site. Electrical resistivity was determined at each moisture equilibrium by placing the sample in the impedance analyzer sample holder and applied a logarithmic sweep of frequencies across the sample. A plot of resultant resistivity at each moisture content for the twenty-seven cores is shown in Figure 1. This figure illustrates that significant variability of the relationship between resistivity and moisture content exists in the field. Equation (4) was fitted to the measured resistivity and moisture data to determine the values for ρ_0 and m . Figure 2 displays fitted values of ρ_0 and m along the vertical distance. Assuming both ρ_0 and m follow log normal distributions, the statistics for these two parameters for the core samples are shown in Table 1. A spatial statistical analysis was also conducted and results are shown in Table 2. Based on these tables, we conclude that, in general, the two parameters exhibit significant spatial variability, especially the parameter m whose coefficient of variation exceeds 50%.

2.3. Sequential inverse algorithm

Since field data demonstrates that parameters ρ_0 , θ , and m vary significantly in space, delineating the spatial distribution of these parameters at high resolution is not generally possible. These parameters may best be represented as random fields (Yeh, 1992 and 1998). We assume that these random fields are characterized by exponential covariance functions with assumed known parameters of mean, variance, and correlation scales. Accordingly, the electrical potential ϕ can be characterized by its statistical moments. In the following analysis, we assume $\log(\rho_0) = F + f$, $\log(\theta) = A + a$, $\log(m) = N + n$, $\phi = H + h$, where F , A , N and H are the mean values, f , a , n and h are the perturbations.

Using first-order second moment analysis, state variable ϕ can be expanded in a Taylor series about the mean values of parameters. Neglecting the second and higher order terms of Taylor series leads to a linear relationship between electrical potential and these parameters

$$\phi = \langle \phi \rangle + \sum_i \chi_i \left. \frac{\partial \phi}{\partial \chi_i} \right|_{\langle \chi_i \rangle \langle \phi \rangle} \quad (6)$$

where ϕ is the state variable, $\chi_i = X_i - \langle X_i \rangle$ represents the zero mean perturbation in a log transformed parameter, for instance, $f = \log(\rho_0) - F$, $a = \log \theta - A$, $n = \log m - N$, perturbation in the state variable is $h = \phi - \langle \phi \rangle = \phi - H$, and it has a zero mean $\frac{\partial \phi}{\partial \chi_i}$

represents the sensitivity derivatives of electrical potential with respect to the parameters, and is computed using the adjoint state method. Details of the derivation of these

sensitivities can be found in Sun and Yeh (1992), Li and Yeh(1998) and Hughson and Yeh (2000). The sensitivity of electrical potential at location i to a perturbation in a parameter at location k can be obtained by

$$\frac{\partial \phi_i}{\partial \chi_k} = \int_{\Omega_k} \frac{\partial \sigma}{\partial \chi} \nabla \langle \phi \rangle \cdot \nabla \Phi d\Omega \quad (7)$$

specifically,

$$\frac{\partial \phi_i}{\partial f_k} = \int_{\Omega_k} \sigma \nabla \langle \phi \rangle \cdot \nabla \Phi d\Omega \quad (8)$$

$$\frac{\partial \phi_i}{\partial a_k} = \int_{\Omega_k} -m \sigma \nabla \langle \phi \rangle \cdot \nabla \Phi d\Omega \quad (9)$$

$$\frac{\partial \phi_i}{\partial n_k} = \int_{\Omega_k} -m \text{Log}(\theta) \sigma \nabla \langle \phi \rangle \cdot \nabla \Phi d\Omega \quad (10)$$

Ω_k is the domain of the element containing the node k . Φ represents the adjoint state variable and can be solved by the adjoint state equation described below:

$$\nabla \cdot (\sigma(x) \nabla \Phi) = \delta(x - x_k) \quad (11)$$

where δ is Dirac delta function and x_k is the measurement location of electrical potential. Notice that sensitivities are evaluated using mean electrical potential $\langle \phi \rangle$. To do so, the mean electrical governing equation is solved by assuming that the mean equation is in the same form of the original electrical governing equation (1), and that the relationship between electrical resistivity and water content is described by (4) with parameters set to their mean values.

Once the mean electrical potential field is obtained, the above sensitivity equations can be used to calculate covariances and cross-covariances which are required by our inverse approach. Rewriting equation (6) in a matrix form yields

$$\{h\} = \sum_x J_{hx} \Big|_{H, \{X\}} \{x\} \quad (12)$$

where $\{ \}$ indicates the vector of the discretized variable; J_{hx} is a jacobian matrix representing the derivatives of potential with respect to the parameters, i.e. $\frac{\partial \phi}{\partial x_i}$, which can be obtained using equation (8) through (10) and has dimensions of $n_h \times nelem$. n_h is the number of voltage measurement locations and $nelem$ is the total number of elements in the domain. Multiplying (12) by the transpose of $\{x\}$ (i.e. $\{f\}$, $\{a\}$, $\{n\}$) and $\{h\}$, then taking the expectations on both sides, we obtain

$$\begin{aligned} R_{hx} &= J_{hx} R_{xx} \\ R_{hh} &= \sum_x J_{hx} R_{xx} J_{hx}^T \end{aligned} \quad (13)$$

where T indicates transpose, R_{hx} represents the cross-covariance functions between h and f , or h and a , or h and n with dimensions of $n_h \times nelem$. R_{xx} denotes the covariance functions of f , a and n with dimensions of $nelem \times nelem$, and it can be represented as exponential models (*De Marsily, 1986*) and assumed known. R_{hh} is the covariance function of h with dimensions of $n_h \times n_h$. It is assumed that f , a , and n are independent parameters, this assumption represents the worst scenario which means that the least information is available for the analysis.

Using these cross-covariance functions and covariance functions, we can obtain a first-order estimate of the perturbations in the log transformed parameters, conditioning on observed primary information χ^* and secondary information h^* collected in one ERT test in the tomography, that is

$$\hat{\chi} = \lambda_{\chi}^T \chi^* + \lambda_h^T h^* \quad (14)$$

where $\hat{\chi}$ is a $nelem \times 1$ vector of the estimated perturbation for parameters ρ_0, m and θ , χ^* and h^* are data of perturbation in the parameters and electrical potential. λ_{χ} and λ_h are the cokriging weights applied to data of the primary variable and the secondary information of electrical potential, which can be evaluated as follows:

$$\begin{bmatrix} C_{\chi\chi} & C_{\chi h} \\ C_{h\chi} & R_{hh} \end{bmatrix} \begin{bmatrix} \lambda_{\chi} \\ \lambda_h \end{bmatrix} = \begin{bmatrix} R_{\chi\chi} \\ R_{h\chi} \end{bmatrix} \quad (15)$$

where χ indicates the primary variable being estimated, and $C_{\chi\chi}$, $C_{h\chi}$ represents covariances and cross-covariances of the data locations which are subsets of covariance and cross covariance matrices obtained from (13). The right-hand of (15) are the covariances and cross-covariances of the data locations with the primary variable to be estimated.

2.3.1 Successive linear estimator

As mentioned in introduction, the information of electrical potential may not be fully utilized because of the nonlinear relationship between electrical potential and those parameters, and the linear assumption embedded in cokriging. To circumvent this

problem, we employed a successive linear estimator similar to Yeh et al. (1996), Zhang and Yeh (1997) and Hughson and Yeh (2000). That is,

$$\hat{\chi}^{(r+1)} = \hat{\chi}^{(r)} + \lambda_h^{(r)T} (\phi^* - \phi^{(r)}) \quad (16)$$

where $\hat{\chi}^{(r+1)}$ and $\hat{\chi}^{(r)}$ represent the parameter estimated at iteration $r+1$ and r , $\phi^{(r)}$ is the electrical potential at the the measurement locations calculated from the the forward simulation using parameters estimated at iteration r . $\lambda_h^{(r)}$ is weights at iteration r and it can be computed through the following:

$$\varepsilon_{hh}^r \lambda_h^r = \varepsilon_{xh}^{(r)T} \quad (17)$$

The solution to (17) requires knowledge of $\varepsilon_{hh}^{(r)}$ and $\varepsilon_{hx}^{(r)}$ which can be approximated at each iteration using the following:

$$\begin{aligned} \varepsilon_{hh}^{(r)} &= \sum_x J_{hx}^{(r)} \varepsilon_{xx}^{(r)} J_{hx}^{(r)T} \\ \varepsilon_{hx}^{(r)} &= J_{hx}^{(r)} \varepsilon_{xx}^{(r)} \end{aligned} \quad (18)$$

where J_{hx} is the sensitivity matrix of $n_h \times n_{elem}$, and superscript T stands for the transpose. At iteration $r = 0$, ε_{xx} is given by

$$\varepsilon_{xx}^I = R_{xx} - \tilde{R}_{xx} \lambda_x - \tilde{R}_{xh} \lambda_h \quad (19)$$

where \tilde{R}_{xx} is a subset of R_{xx} . For $r \geq 1$, the residual covariances are evaluated according to

$$\varepsilon_{xx}^{(r+1)} = \varepsilon_{xx}^{(r)} - \varepsilon_{xh}^{(r)} \lambda_h^{(r)} \quad (20)$$

These covariances are approximated conditional covariances.

Once we update all the three parameters by fully utilizing the potential data and thus updating the electrical conductivity through equation (4). Then mean potential equation is solved again with the newly updated conductivity for a new potential field, ϕ . Then, the maximum change of σ_x^2 (the variance of the estimated parameters of f , a , and n) and the change of the biggest potential misfit among all the monitoring locations between two successive iterations are evaluated. If both changes are smaller than prescribed tolerances, the iteration stops. If not, new ε_{hx} and ε_{hh} , are evaluated using (18). Equation (17) is then solved to obtain a new set of weights that are used in (16) with $(\phi^* - \phi^{(r)})$ to obtain a new estimate of parameters

2.3.2 Sequential approach

The above discussion described inverse approach for only one set of primary and secondary information obtained in one ERT operation. This algorithm can simultaneously include all of the data sets collected during all the ERT operations in the sequence. However, the system of equations in (15) and (17) can become extremely large and ill conditioned, and stable solutions to the equations can become difficult to obtain (Hughson and Yeh, 2000).

To avoid the numerical difficulty in solving the system of equations, the voltage data sets are included sequentially. The sequential algorithm is similar to the one developed for hydraulic tomography (Yeh and Liu, 2000). In essence, our sequential approach uses the estimated electrical conductivity field derived from the estimated ρ_e , m and θ fields, and covariances, conditioned on previous sets of voltage measurements, as prior information for the next estimation based on a new set of current/voltage data. It

continues until all the data sets are fully utilized. Consequently, information carried by all the data sets are fully processed by propagating the conditional first and second moments from one data set to another. Such a sequential approach allows accumulation of high-density secondary information obtained from ERT surveys, while maintaining the covariance matrix at a manageable size that can be solved with the least numerical difficulties. More importantly, this sequential approach demonstrates a significant advantage in terms of cost. Specifically, this sequential approach allows one to collect voltage data sets over a large area sequentially and thus, avoids complex and expensive cables, probes and data loggers.

3. Two-dimensional numerical experiments

The advantage of numerical experiments is that synthetic data sets allow the results of the inverse model to be compared to the parameter fields that are generated and fully characterized. To start our inverse model, we need to provide model inputs that may contain uncertainty under realistic situations. In the following numerical experiments, we focus on the effect of uncertainty of the mean and covariance functions of water content θ on the estimation of θ distribution, the main objective of our research. Therefore, we assume the parameters of ρ_o and m are random variables but we have complete information about them.

3.1. Generation of true water content distribution

The hypothetical site has dimensions of 200 cm x 200 cm and is discretized into 10 horizontal x 20 vertical elements of 200 cm². The unsaturated hydraulic properties of

each element were assumed to be described by the Mualem-van Genuchten model (van Genuchten, 1980):

$$K(\psi) = K_s \frac{\left(1 - (\alpha\psi)^{(n-1)} [1 + (\alpha\psi)^n]^{-m}\right)^2}{[1 + (\alpha\psi)^n]^{m/2}} \quad (21)$$

$$\theta(\psi) = (\theta_s - \theta_r) [1 + (\alpha\psi)^n]^{-m} + \theta_r$$

The variability of saturated water content, θ_s , and residual moisture content, θ_r , is generally negligible; both were treated as deterministic constants with a value of 0.366 and 0.029, respectively. However, the parameters, K_s , α , and n were considered as random fields and were generated using the method by Gutjahr (1989). The mean values, variances, and correlation structures used for generating hydraulic parameters of K_s , α , and n are listed in Table 3. These generated random fields are treated as our true hydraulic parameter fields.

The initial condition of this site is assumed to be hydrostatic. Specifically, no-flux boundary conditions are on the two sides, the bottom of the site is water table, and a constant pressure head of -200 cm boundary is on the top. Then the infiltration to this hypothetical site is started by changing the pressure head from -200 cm to -80 cm at the center of the top boundary, where $z = 200$ cm, x ranges from 80 cm to 120 cm. This hypothetical site is then allowed to reach steady state.

The water content distribution due to the infiltration is simulated by solving the Richards equation subject to the boundary conditions mentioned above. This resulting water content distribution is used as our true water content field in our ERT experiments. Similarly, the mean water content distribution is obtained by conducting a simulation for

infiltration under identical boundary conditions, but using mean hydraulic parameters instead of true heterogeneous parameters. The mean water content distribution and the true one are shown in Figure 3a and b.

3.2. Generation of true fields for ρ_o and m

Since electrical resistivity ρ is a function of ρ_o , m and θ , in addition to the generated true field of θ , the other two parameters, ρ_o and m were considered as random fields with the geometric mean of 8.5 Ωm and 1.35, respectively. The variances of $\log\rho_o$ and $\log m$ were 0.1 and 0.01, respectively. Also assumed was that both of the two parameters possessed the same exponential correlation structure with a horizontal correlation scale of 240 cm and vertical correlation scale of 20 cm. Figure 4a and b show the generated true fields for these two parameters.

3.3. ERT experiments

Based on these generated ρ_o , m and θ fields, the true resistivity field can be formulated using equation (4). ERT experiments were then conducted. First, two bore holes were drilled, 10 electrodes were placed in each hole, and one electrode was placed far away from the domain that is used as a reference electrode. Then one electrode in the bore hole and the reference electrode were driven a known source current, and the voltage difference between the reference electrode and the rest electrodes in the bore holes were measured, yielding one voltage/current data set. By moving the source location along the bore hole, and repeating the same procedure, many data sets can be obtained. In our analysis, four voltage data sets were collected and these data sets are referred to as secondary information. In addition, we assume that one θ was measured

from core samples and it is referred to as primary information. The current sources, voltage and θ measurement locations are displayed on Figure 5.

3.4. Estimating water content using ERT data

In addition to the collected primary and secondary information, our inverse model requires input parameters such as mean, variance and correlation structure for the parameter to be estimated. For water content θ , these properties cannot be estimated easily since the true water content distribution is controlled by many factors such as heterogeneous hydraulic properties and boundary conditions. In our analysis, three different methods were used to approximate the required input for water content estimation, and the effect of the uncertainty associated with these approximations is investigated.

3.4. 1. Using geometric mean and exponential covariance function

As we discussed in the analysis of hydraulic tomography (Yeh and Liu, 2000), variance of parameters appears on both sides of the system of equations and can be canceled out. Therefore, it has no effect on the estimate of parameters. This conclusion holds for ERT, and we will skip it from now on in our analysis. For the mean value of water content, it is first approximated by a geometric mean method. Specifically, the mean of water content distribution is assumed to be a constant geometric mean that can be computed based on the water content distribution. The covariance structure is approximated based on those of hydraulic parameters, which is assumed to be an exponential model with horizontal and vertical correlation scale of 240 cm and 20 cm, respectively. Employing our sequential inverse model and using these approximated

input parameters and other necessary inputs, we obtained the estimated perturbation of water content. The resulting estimated water content distribution was then obtained by adding the constant geometric mean to the estimated perturbations. The estimated water content using the geometric mean and exponential covariance function is shown on Figure 5b. The corresponding scatter plot is displayed on Figure 6a.

3.4. 2. Using true mean and exponential covariance function

In this case, the approximation of the covariance function is kept the same as in the above case. While the mean of water content becomes more meaningful, which is a mean plume instead of a geometric mean, indicating the mean direction of water movement due to the infiltration. This mean distribution of water content was simulated using mean hydraulic parameters (shown on Figure 3a). Substituting the geometric mean with the true mean into our inverse model, we obtained the estimated water content perturbation. The estimated perturbation distribution was then added to the mean water content distribution, resulting in the estimated water content distribution. The results are shown on Figure 5c and Figure 6b.

3.4. 3. Using true mean and computed covariance function

In this case, the mean of water content is also simulated using the mean hydraulic parameters. However, the covariance function is no longer assumed to be an exponential model, instead, we computed the covariance function using numerical first order method and then imported it into our inverse model. The covariance function was computed according to the following formula:

$$R_{\theta\theta} = \sum_{\zeta} J_{\theta\zeta} R_{\zeta\zeta} J_{\theta\zeta}^T \quad (22)$$

where, $R_{\theta\theta}$ is covariance function of water content, $R_{\zeta\zeta}$ denotes the covariance functions of the log transformed perturbations of the hydraulic properties of Ks , α and n which are assumed known. $J_{\theta\zeta}$ is the Jacobian matrices, details of computing $J_{\theta\zeta}$ can be found in Hughson and Yeh (2000). The final estimate of water content using the true mean and computed covariance function is shown on Figure 5d and Figure 6c.

3.5. Results and discussion

Comparing Figures 5b, c and d to Figure 5a, we find that the estimated water content distribution captured major patterns of the true water content distribution regardless of the statistical parameters we used in our model, i. e., the mean, variance and covariance function. The same conclusion can be drawn from the scatter plots shown on Figure 6. On this plot, our estimated water content values scatter around the 45 degree line indicating good agreements with those of true ones. The goodness of fit can also be evaluated using L1 and L2 norms described in the following:

$$L1 = \frac{1}{n} \sum_{i=1}^n |\hat{\theta}_i - \theta_i| \quad (23)$$

$$L2 = \frac{1}{n} \sum_{i=1}^n (\hat{\theta}_i - \theta_i)^2 \quad (24)$$

where θ_i and $\hat{\theta}_i$ represent the true and estimated water content, respectively. The L1 and L2 norms are close to each other for the three cases, however, the norms of using true mean tend to be smaller than those of using geometric mean. Based on Figure 5 and Figure 6, we can conclude that choices of mean and covariance function of water content have small effect on our estimate if sufficient information is available. Under realistic

situations, estimation of these input parameters always involves uncertainty. Therefore, to obtain better and more reliable estimation of water content requires collecting abundant primary or secondary information. These site-specific data can greatly outweigh the coarse descriptive information such as mean, variance, and correlation structure, and the uncertainty associated with these parameters will thus be minimized.

4. Three-dimensional numerical examples

Typically, flow through heterogeneous porous media is three-dimensional, and water movement due to infiltration can hardly reach steady state conditions. In this numerical example, water movement at time of 1,000 minutes and 50,000 minutes is simulated on a three-dimensional hypothetical site. Water content distributions at these two times, $\theta_{1,000}$ and $\theta_{50,000}$, are used as our true water content fields, and their difference is denoted as the true water content change in the following analysis. Following the generation of random fields of ρ_o and m , the true resistivity fields at 1,000 minutes and 50,000 minutes are formulated using equation (4) with the generated ρ_o , m , $\theta_{1,000}$ and $\theta_{50,000}$ fields. Next, electrical resistivity tomography (ERT) experiments are performed on these two resistivity fields. Following collecting voltage/current data sets, two different inverse approaches were attempted to interpret the water movement due to the infiltration event. The first one is to directly estimate moisture distribution at the time of our interest using our new approach. The second one is first to estimate the resistivity fields at the time of 1,000 minutes and 50,000 minutes using the inverse model developed by Yeh et al., (2001). Then change in resistivity from 1,000 minutes to 50,000 minutes is computed.

Finally, the estimated change in resistivity is used to interpret the change in water content.

4.1. Case description

4.1.1. 3-D flow simulation

This hypothetical site is a cube of 200 cm on each side and consists of 2000 elements of 20 cm x 20 cm x 10cm. On this site, random fields of heterogeneous hydraulic parameters, K_s , α and n (van Genuchten, 1980), are generated using the spectral method (Gutjahr, 1989) with required parameters shown in Table 4. Figures 7a, b and c show the generated $\log K_s$, $\log \alpha$ and $\log n$ fields.

The initial condition is assumed to be hydrostatic, that is: the bottom is set to be a prescribed pressure head of -50 cm, and the top is set to be a pressure head of -250 cm. Then an infiltration is introduced to the site by assigning an area of 1600 cm^2 on the top center of the cube to a pressure head of -50 cm, and setting the remainder of the top and the four sides to be no-flux boundaries. This represents a non-uniform vertical infiltration from a constant source on the top center of the study domain. This infiltration is then simulated using MMOC3 (Srivastava and Yeh, 1992) at time of 1,000 minutes and 50,000 minutes. Figure 7d shows the water content distribution at time of 1,000 minutes. Similarly, mean water content distributions at time of 1,000 minutes and 50,000 minutes are obtained using MMOC3 with effective mean fields of hydraulic parameters. True log water content change was computed as the difference between the true water content distributions at time of 1000 minutes and 50,000 minutes (Figure 11a).

4.1.2. Generation of random ρ_o and m fields

Once the true water content fields for the two times are simulated, the other two parameters, ρ_o and m were considered as random fields with the geometric mean of 7.036 Ωm and 1.336. The variances of $\log \rho_o$ and $\log m$ were 0.633 and 0.034. Also assumed was that both of the two parameters possessed the same exponential correlation structure with a horizontal correlation scale of 80 cm and vertical correlation scale of 20 cm. Figures 8a and b show the generated true fields for these two parameters.

4.1.3. Formulation of true random ρ fields and conducting ERT experiments

Based on these synthetic fields of ρ_o , m , $\theta_{1,000}$ and $\theta_{50,000}$, the true resistivity fields at time of 1,000 minutes and 50,000 minutes, $\rho_{1,000}$ and $\rho_{50,000}$, are formulated using the power law described in equation (4). On these two resistivity fields, ERT experiments are conducted. The potential distribution induced by each ERT survey is then simulated using equation (1), and voltage data are collected at given sampling locations. Figure 9d displays the schematic diagram of our ERT survey. According to the diagram, the network of ERT consists of four boreholes penetrating the entire depth of the domain. The XY coordinates of the four boles are $x = 50$ cm, $y = 50$ cm; $x = 150$ cm, $y = 50$ cm; $x = 50$ cm, $y = 150$ cm; and $x = 150$ cm, $y = 150$ cm, respectively. Twenty electrodes were placed along each bore hole. Electrodes are aslo placed along the four lines with the above XY coordinates on the surface. Five sequential current sources were driven along the upper right bore hole, and their XYZ coordinates are (150 cm, 150 cm, 25 cm), (150 cm, 150 cm, 55 cm), (150 cm, 150 cm, 95 cm), (150 cm, 150 cm, 135 cm), and (150 cm, 150 cm, 175 cm), respectively. Using the same voltage data collecting procedure which is desribed in the 2-D numerical examples, five voltage data sets were collected with 111

voltage measurements on each ERT survey. In addition, $20\rho_o$ and $20m$ along each of the four bore holes, with a total of 80, were assumed to be available in our analysis, and 20θ were sampled at locations indicated by squares shown on Figure 9d. To investigate the usefulness of θ measurements on conditioning our estimate of water content, zero θ and 20θ measurements were used to estimate water content distribution for time of 50,000 minutes.

4.2. Directly estimating water content distribution

The above mentioned five voltage data sets were used in our proposed sequential conditioning approach. Figure 9a shows the true water content distribution at time of 50,000 minutes; Figure 9b shows our estimated water content using 111×5 voltage, $80\rho_o$ and m , and no θ measurements; Figure 9c shows our estimate using the same number of voltage, ρ_o and m measurements, but 20θ measurements. Compare the three figures, we find that our inverse approach capture the general pattern of the water content distribution, and that θ measurements help greatly delineate the θ distribution. A scatter plot provides a visual evaluation of the estimate. Figures 9e and f illustrate the scatter plots corresponding to Figures 9b and c. A 45° line indicates the perfect estimation. The goodness of fit were also evaluated using L1 and L2 norms. The smaller the L1 and L2 norms are, the better our estimates. The decrease of the L1 and L2 norms from Figures 9e to f reveals that additional moisture measurements (from 0 to 20θ) dramatically help reduce the uncertainty in our estimate. Another criteria for evaluating our estimate is to check the conditional variance of our estimate, smaller conditional variance indicates less uncertainty in our estimate. The conditional variances corresponding to our estimate by

using $\text{no}\theta$ and 20θ are shown on Figures 10a and b. According to these figures, we find that relative small conditional variance tend to locate closely to the four bore holes where secondary information is available. At locations where we have moisture measurements (primary information) the conditional variance becomes zero, which means that these measurements are preserved in our model and there are no uncertainties associated with them at all.

Our estimation results show that our proposed sequential conditioning approach is a useful tool to efficiently process the ERT data sets and yield water content distribution with less uncertainty. These results also prove that the incorporation of moisture measurements can significantly help constrain our estimate, and that better estimates are obtained in between the four bore holes. The estimated water content distribution provides valuable information on water movement in the vadose zone, especially at places where moisture measurement devices are hard or impractical to install. Since unsaturated hydraulic properties are functions of water content, the estimated water content distribution at high resolution from ERT provides large amount of secondary information required by the hydraulic inversion. These sufficient information which can not be obtained easily with other monitoring tools can be directly used by the hydraulic inversion to better constrain the estimates of hydraulic parameters, thus to better characterize vadose zone.

4.3. Using resistivity change to interpret water movement

For comparison purpose, resistivity change was also computed to reflect water movement in vadose zone. ERT experiments were performed at 1,000 minutes and

50,000 minutes after the beginning of the infiltration. Using the ERT network shown on Figure 9d, the same five voltage data sets were collected and then used in the sequential inverse approach developed by Yeh et al. (2001) to estimate the resistivity fields at these two times. Then, the resistivity change between 1,000 minutes and 50,000 minutes which was caused by the infiltration was computed using these two estimated resistivity fields. Figure 11a displays the true water content change, the estimated resistivity change was shown on Figure 11b. Comparing these two figures, we see that our interpretation of water movement based on the estimated resistivity change greatly distorts the true water movement. From 1,000 minutes to 50,000 minutes, the true main water plume moves toward the south west direction, while according to the estimated resistivity change, we mispredict that the major water flow direction is to the south east. Several factors could contribute to the uncertainties in our interpretation. One factor is the uncertainty in our estimated resistivity fields introduced by using the limited knowledge of voltage to do the inverse modeling. Another crucial factor is the strong spatial variability of the resistivity-moisture relationship, especially the spatial variability of parameter m . In our study, the variance of $\log m$ is only 0.034. According to equation (5), the change in resistivity is linearly proportional to change in water content only under the condition that m is constant and can be known precisely. While field data demonstrates that m does exhibit spatial variability and can not be known precisely. We believe that the larger the variance of $\log m$ in the field, the more uncertain our interpretation will be (Yeh et al. 2001). Consequently, the interpretation of water movement in vadose zone simply relying on

resistivity change and neglecting the spatial variability of the resistivity-moisture relationship may yield misleading interpretations.

5. Conclusion

In this paper, we presented a sequential inverse approach to effectively and directly estimate water content distribution for a three-dimensional synthetic field using voltage information yielded by electrical resistivity tomography and available point measurements of moisture content. By applying our inverse approach to the ERT surveys conducted at different times, the 3-D development of water plume in the vadose zone with time can be monitored with less uncertainty, and this information is significantly beneficial to the quantitative characterization of the vadose zone since unsaturated hydraulic properties are functions of water content.

Our analysis investigates the effect of uncertainty associated with our model inputs such as mean, variance, covariance function of parameters to be estimated. Since all these input parameters can not be known precisely in reality, any approximation might yield some uncertainties to our inverse model. Our investigation shows that these uncertainties have no significant effect on our final estimate, and this effect can be greatly minimized once sufficient primary and secondary information are available for conditioning.

This study indicates that interpretation of water movement in the vadose zone based on the estimated resistivity change may be misleading. This is primarily attributed to the fact that the resistivity-moisture relationship exhibits strong spatial variability.

Our analysis also shows that good estimate are at the locations where primary and secondary information is available (i.e. the locations in between the four bore holes). Primary information, the moisture measurements, contributes more significantly than the secondary information, the voltage, to the estimated water content distribution in our model. In other words, a large number of voltage measurements did not dramatically improve our estimated water content distribution as we would expect. This may be explained that the voltage measurements can be used to identify the resistivity at a high resolution, but the resistivity is a function of three parameters, ρ_o , θ and m , and the knowledge of resistivity obtained from voltage can not be easily differentiated among the three parameters. This fact implies that the voltage information alone may not be adequate to characterize the water movement in vadose zone in greater detail, and other types of information will be necessary to combine with ERT data to yield better results.

Acknowledgements

This research was funded in part by a DOE EMSP96 grant through Sandia National Laboratories (Contract AV- 0655#1) and a DOE EMSP99 grant through University of Wisconsin, A019493.

References

- Baker, K., Analysis of hydrological and electrical properties at the Sandia-Tech Vadose Zone Facility, Master Thesis, New Mexico Tech., Socorro, NM, 2001.
- Daily, W, A. Ramirez, D. LaBrecque and J. Nitao, Electrical Resistivity Tomography of Vadose Water Movement, *Water Resour. Res.*, 28(5), 1429-1442, 1992.
- de Marsily, G., *Quantitative Hydro Geology*, Academic Press, 1986.
- Ellis, R.G., and S.W. Oldenburg, The Pole-Pole 3D DC Resistivity Inverse Problem: A Conjugate Gradient Approach, *Geophysical journal international* 119,187-194, 1994.
- Gutjahr, A., Fast Fourier transforms for random field generation, N. M. Tech Project Report, 106 pp., 1989.
- Hughson, D. L., and T.-C. J. Yeh, An inverse model for three-dimensional flow in variably saturated porous media, *Water Resour. Res.*, 36(4), 829-839, 2000.
- Knight, R., Hysteresis in the electrical resistivity of partially saturated sandstones, *Geophysics*, Vol. 56, No. 12: 2139-2147, 1991.
- Li, B., and T.-C. J. Yeh, Sensitivity and moment analysis of head in variably saturated regimes, *Adv. Water Resour.*, 21, 477-485, 1998.
- Li, Y., and D.W. Oldenburg, Inversion of 3D dc-resistivity data using an approximate inverse mapping, *Geophysical journal international* 116, 527-537, 1994.
- Sharma, Perm V., Environmental and engineering geophysics, Cambridge University Press, 1997.
- Srivastava, R., and T.-C. J. Yeh, A three-dimensional numerical model for water flow and transport of chemically reactive solute through porous media under variably saturated conditions. *Adv. Water Resour.*, 15(5), 275-287, 1992.
- Sun, N.-Z., and W. W.-G. Yeh, A stochastic inverse solution for transient groundwater flow: parameter identification and reliability analysis, *Water Resour. Res.*, 28(12), 3269-3280, 1992.
- van Genuchten, M. T., A closed-form equation for predicting the hydraulic conductivity of unsaturated soils. *Soil Sci. Soc. Am. J.* 44, 892-898, 1980.
- Yeh, T.-C. J., Stochastic modeling of groundwater flow and solute transport in aquifers, *J. of Hydrologic Processes*, Vol. 6, 369-395, 1992.

Yeh, T.-C. J., A.L. Gutjahr, and M. Jin, An iterative cokriging-like technique for groundwater flow modeling, *Ground Water*, 33(1), 33-41, 1995.

Yeh, T.-C. J., and J. Zhang, A geostatistical inverse method for variably saturated flow in the vadose zone, *Water Resour. Res.*, 32(9), 2757-2766, 1996.

Yeh, T.-C., M. Jin, and S. Hanna, An iterative stochastic inverse method: conditional effective transmissivity and hydraulic head fields, *Water Resour. Res.*, 32(1), 85-92, 1996.

Yeh, T.-C. J., Scale issues of heterogeneity in vadose-zone hydrology, in *Scale Dependence and Scale Invariance in Hydrology*, edited by G. Sposito, Cambridge Press, 1998.

Yeh, T.-C., Liu, S.Y., Hydraulic tomography: Development of a new aquifer test method, *Water Resour. Res.*, 36(8), 2095-2105, 2000.

Yeh, T. -C. J., and S. Liu, K. Baker, R. Glass, J. R. Brainard, D. Alumbaugh, D. LaBrecque, Uncertainties in interpretation of electrical resistivity surveys in subsurface hydrological applications, submitted to *Water Resour. Res.*, 2001.

Zhang, J., and T.-C. J. Yeh, An iterative geostatistical inverse method for steady flow in the vadose zone, *Water Resour. Res.*, 33(1), 63-71, 1997.

Zhang, J., R.I. Mackie, and T. Madden, 3-D resistivity forward modeling and inversion using conjugate gradients. *Geophysics* 60, 1313-1325, 1995.

Table 1. Statistic properties of fitting parameters and m

parameter	Mean (Ωm)	Variance (Ωm) ²	Std. Dev. (Ωm)	% C.V.
ρ_o	7.036	0.633	0.796	40.8
m	1.336	0.034	0.185	63.72

Table 2. Fitted variogram model parameters for ρ_o and m

parameter	Model	Sill (Ωm) ²	Range (m)	Nugget (Ωm) ²
ρ_o	exponential	20	4.6	2.8
m	exponential	0.05	3	0.035

Table 3. Hydrological and statistical parameters used in 2-D analysis

parameter	mean	variance	λ_x (cm)	λ_z (cm)	Covariance model
K_s (cm/s)	0.0063	0.1	240	20	Exponential
α (1/cm)	0.028	0.1	240	20	Exponential
n	2.0	0.01	240	20	Exponential

Table 4. Hydrological and statistical parameters used in 3-D analysis

parameter	mean	variance	λ_x (cm)	λ_y (cm)	λ_z (cm)	Covariance model
K_s (cm/min)	0.043	0.893	80	80	20	Exponential
α (1/cm)	0.067	0.631	80	80	20	Exponential
n	1.811	0.015	80	80	20	Exponential

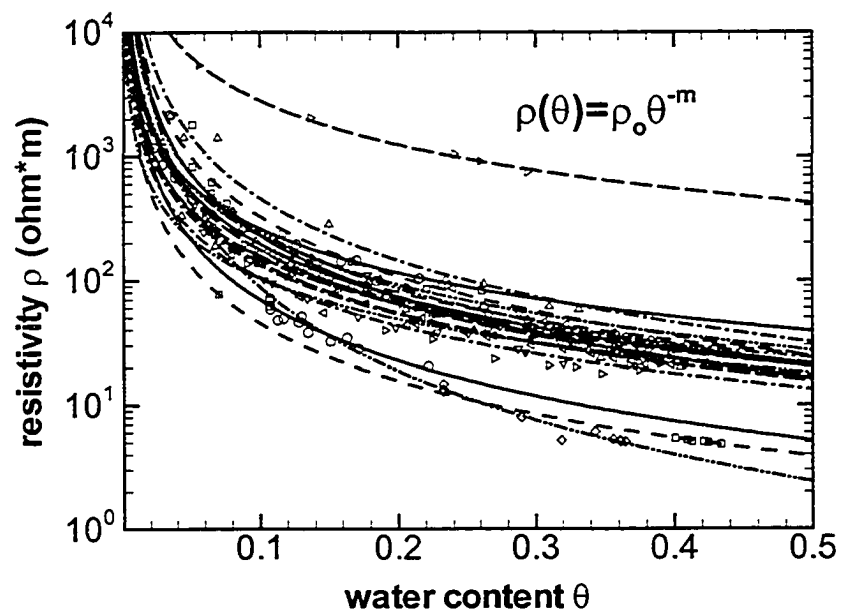


Figure 1. Resistivity vs. water content for the NW bore hole in STVZ field site from 1 ft to 36 ft depth.

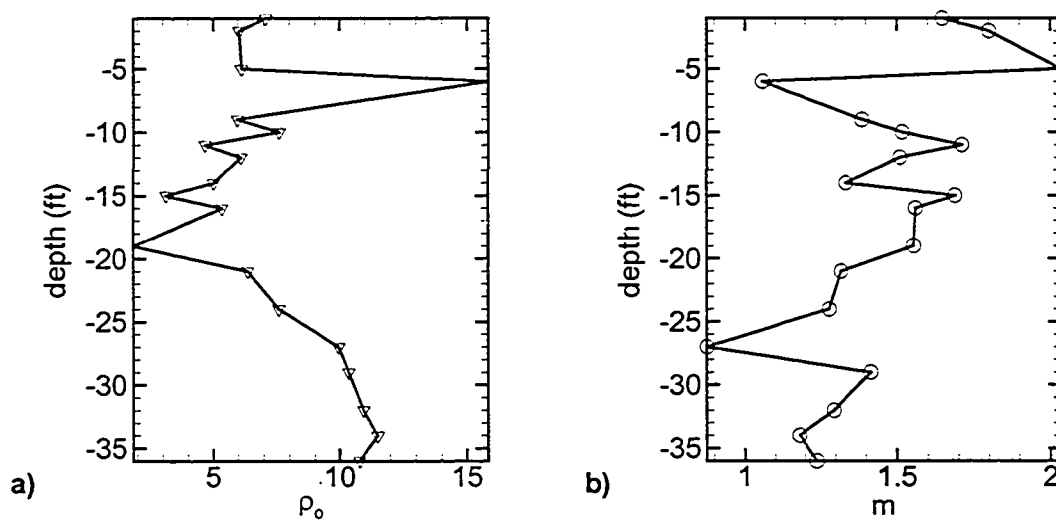


Figure 2. a) Fitted ρ_0 values vs. the depth of the NW bore hole; b) Fitted m values vs. the depth of the NW bore hole.

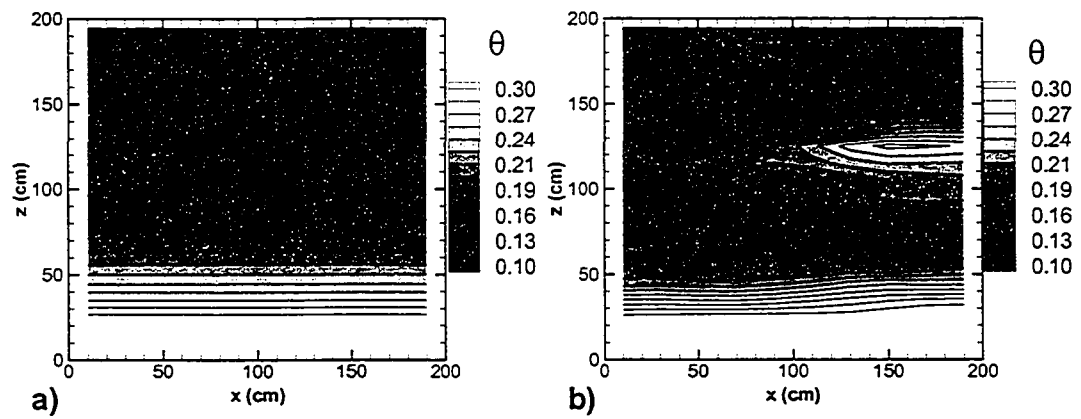


Figure 3. a) The mean water content distribution simulated using homogeneous hydraulic parameters; b) The true water content distribution simulated using heterogeneous hydraulic parameters.

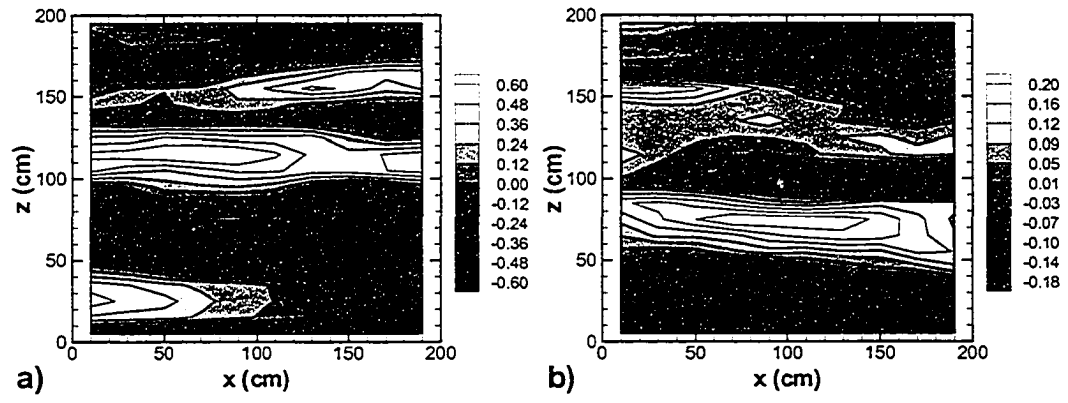


Figure 4. a) Generated random field for $\log \rho_0$; b) Generated random field for $\log m$.

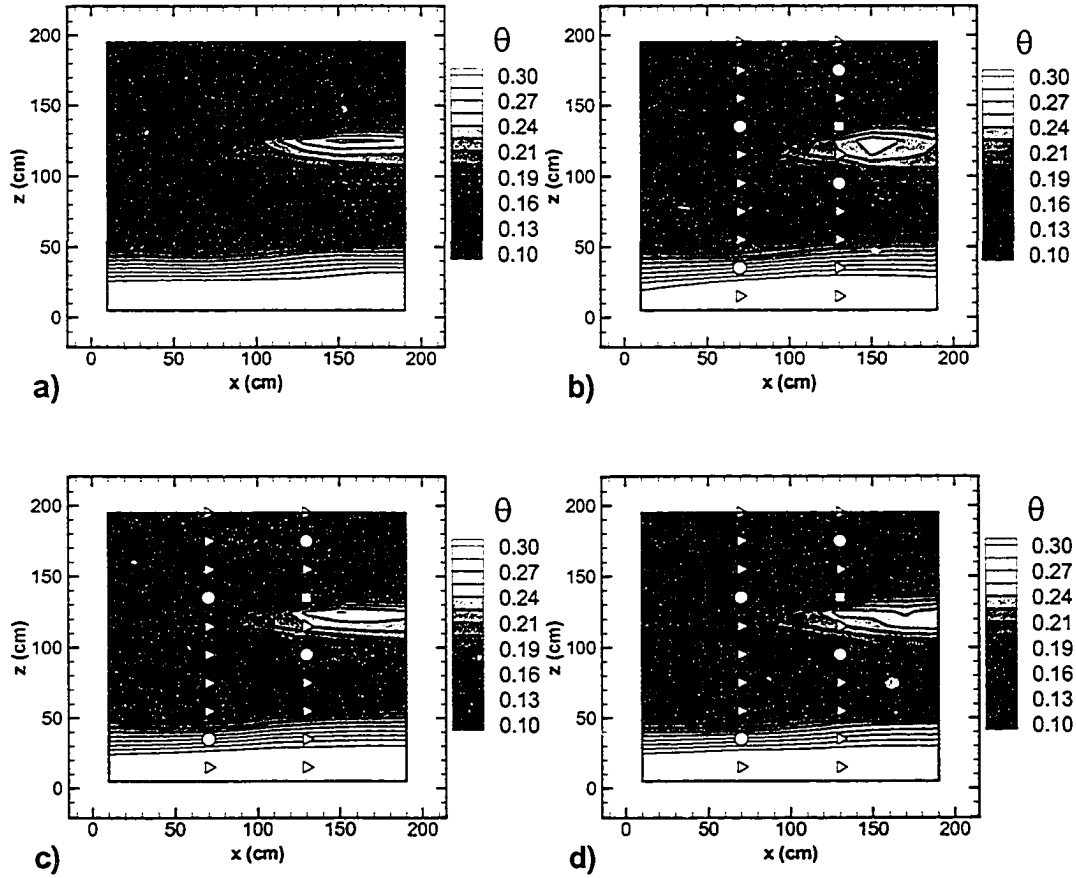


Figure 5. a) True water content distribution; b) estimated water content distribution assuming water content has a geometric mean and exponential covariance function; c) estimated water content distribution assuming water content has a true mean and exponential covariance function; d) estimated water content distribution assuming a true mean and computed covariance function. Circles indicate current source locations, right triangles indicate voltage measurement locations and square indicates the water content measurement location.

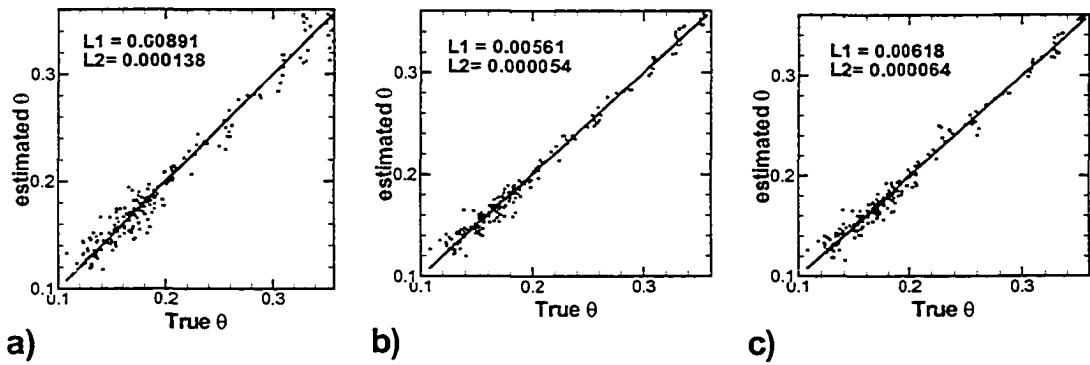


Figure 6. a) Scatter plot corresponding to Figure 5b; b) Scatter plot corresponding to Figure 5c; c) Scatter plot corresponding to Figure 5d.

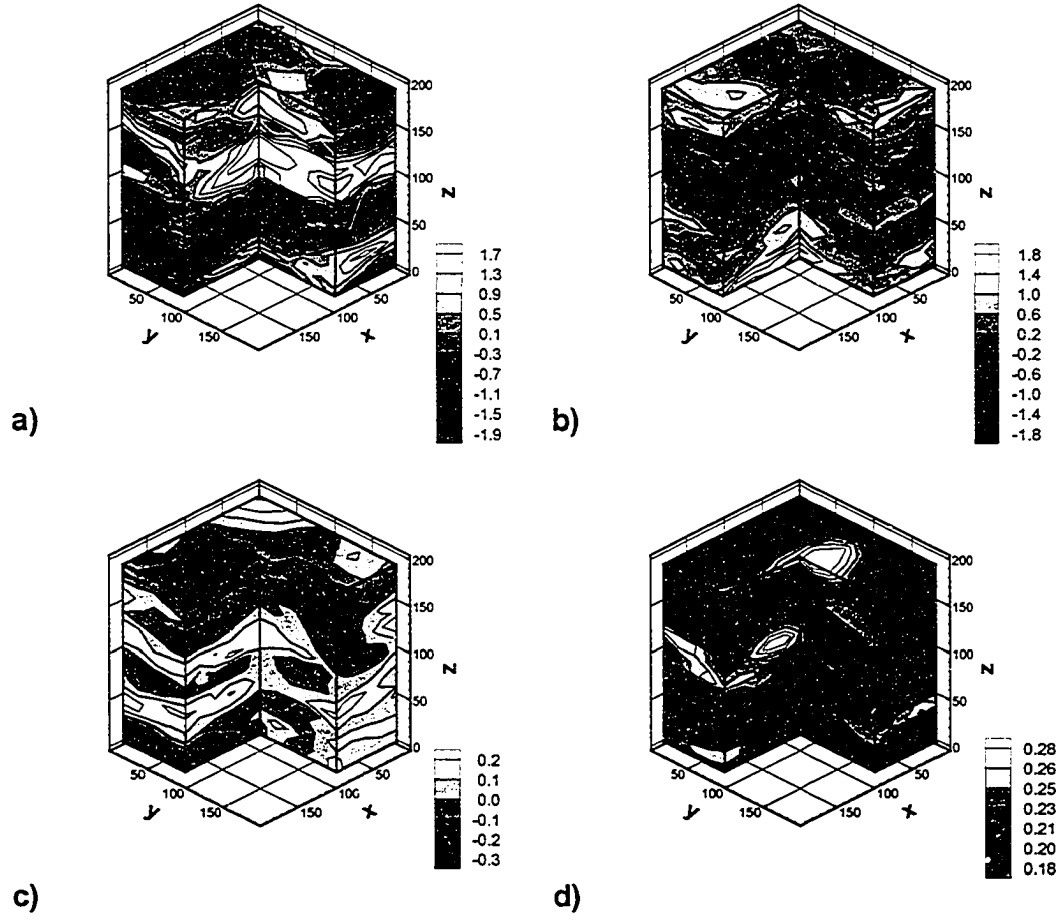


Figure 7. a) Generated log Ks field with mean of 0.043 cm/min, $\sigma^2_{\log K_s} = 0.893$, $\lambda_x = \lambda_y = 80$ cm, and $\lambda_z = 20$ cm; b) Generated log α field with mean of 0.067/cm, $\sigma^2_{\log \alpha} = 0.631$, $\lambda_x = \lambda_y = 80$ cm, and $\lambda_z = 20$ cm; c) Generated log n field with mean of 1.811, $\sigma^2_{\log n} = 0.015$, $\lambda_x = \lambda_y = 80$ cm, and $\lambda_z = 20$ cm; d) True water content field at t=1,000 minutes.

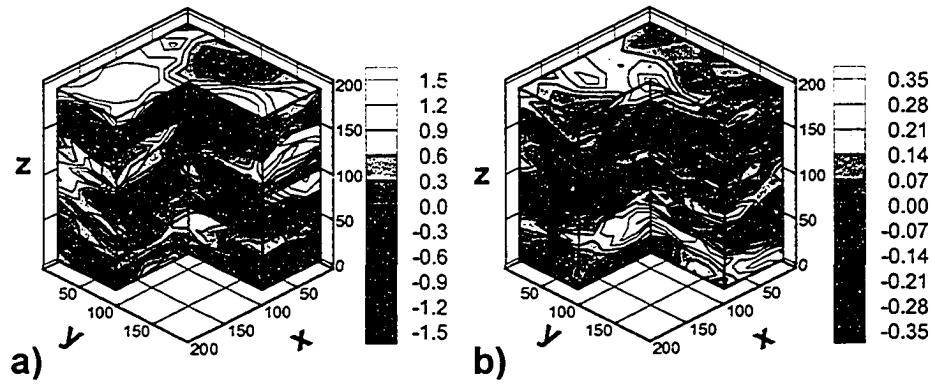


Figure 8. a) Generated true $\log \rho_0$ field; b) Generated true $\log m$ field.

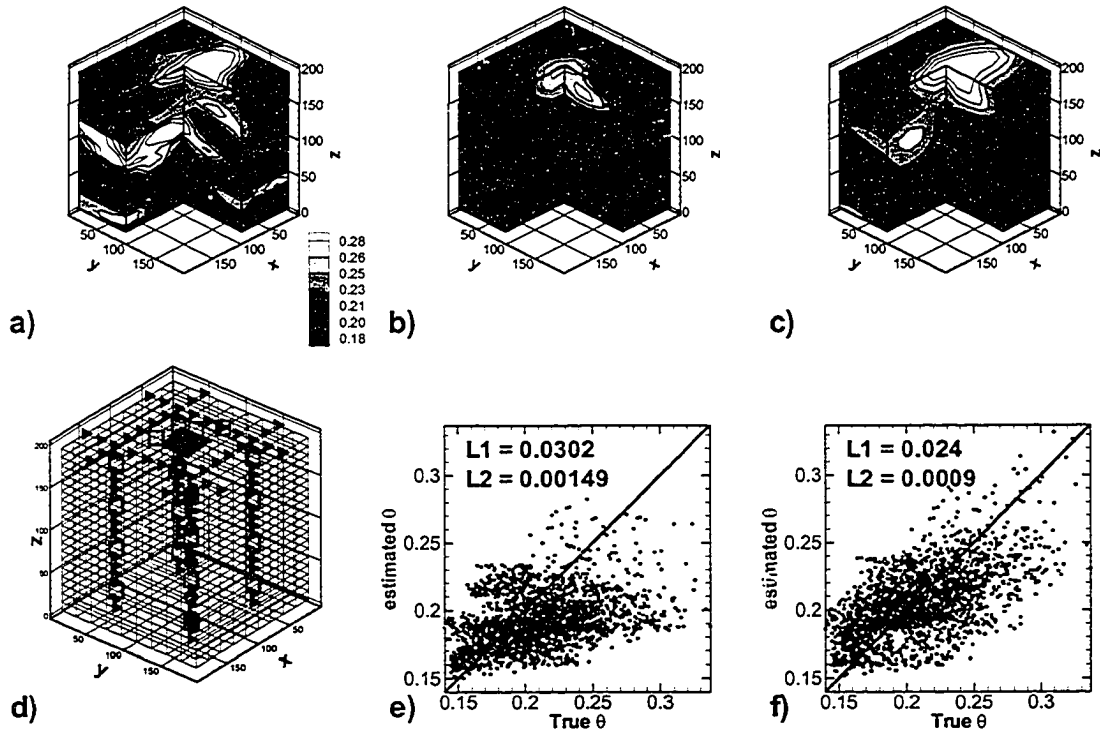


Figure 9. a) True water content θ at $t = 50,000$ minutes; b) Estimated θ at $t = 50,000$ minutes without θ measurements; c) Estimated θ at $t = 50,000$ minutes with 20 θ measurements; d) Schematic diagram for 3-D ERT experiments, top center square indicates the infiltration area, right triangles indicate voltage measurement locations, circles show current source locations, and squares show the locations of 20 θ measurements; e) The scatter plot corresponding to b); f) The scatter plot corresponding to c).

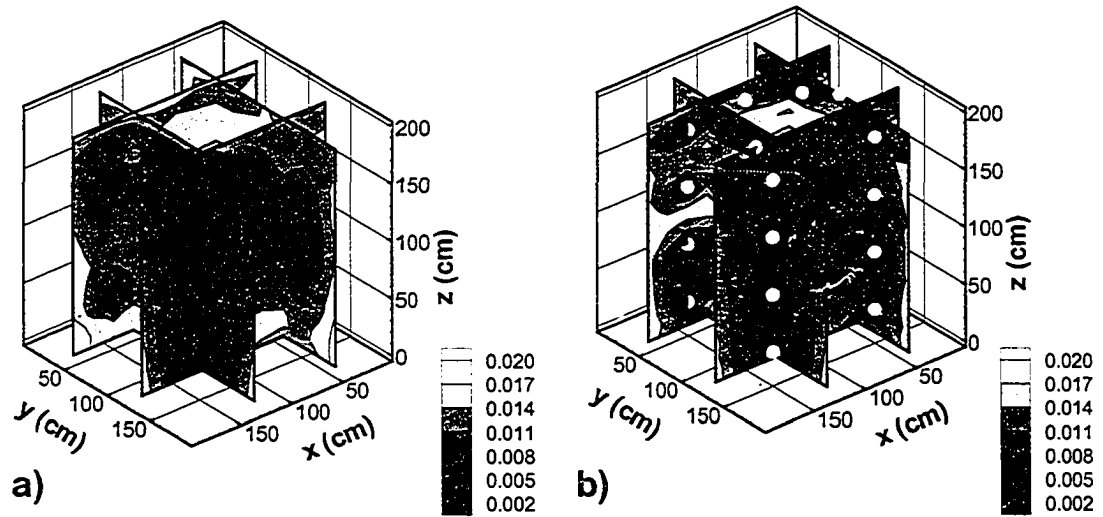


Figure 10. a) Conditional variance when no θ measurements are used at $t = 50,000$ minutes; b) Conditional variance when 20 θ measurements are used at $t = 50,000$ minutes. Circles indicate θ measurement locations

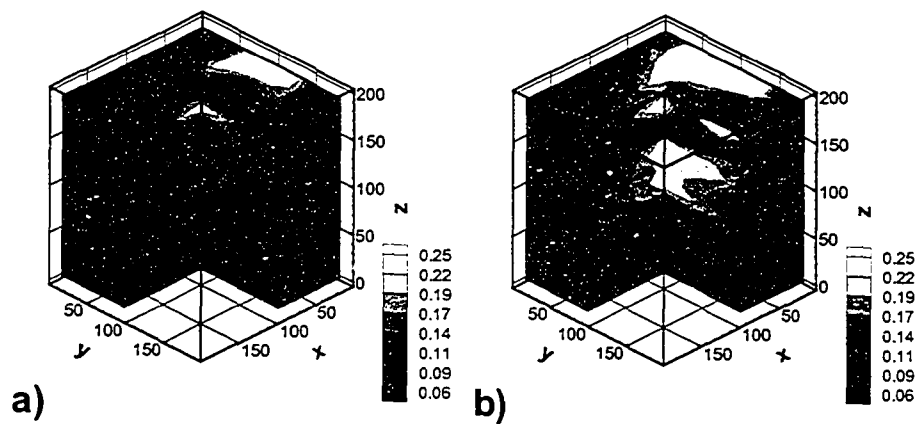


Figure 11. a) True $\Delta \log \theta$ from 1,000 minutes to 5,000 minutes; b) Estimated $\Delta \log \rho$ from 1,000 minutes to 50,000 minutes.